FACULTY OF SCIENCE
UNIVERSITY OF COPENHAGEN

Master thesis in geophysics

Oceanographic variability at a boulder reef in the Kattegat and surrounding waters

Lea Kamille Drescher Sørensen

Academic advisors:
Peter Ditlevsen, Niels Bohr Institute, University of Copenhagen
Christian Mohn, Department of Bioscience, Aarhus University
Kristine Skovgaard Madsen, Danish Meteorological Institute
Submitted: June 6, 2012

Master thesis in geophysics

Title: Oceanographic variability at a boulder reef in the Kattegat and surrounding waters

Danish title: Oceanografiske variation på et stenrev i Kattegat og omkringliggende farvande

Front page picture reference: Karsten Dahl, Steffen Lundsteen & Stig Asger Helmig (2003), *Stenrev – havbundens oaser*, 1. udgave, 1. oplag 2003, Gads Forlag, København K, Danmark.

Author: Lea Kamille Drescher Sørensen

E-mail: leakamille@gmail.com

ECTS points: 60

Supervisor: Peter Ditlevsen, Niels Bohr Institute, University of Copenhagen

External supervisor: Christian Mohn, Department of Bioscience, Aarhus University

External supervisor: Kristine Skovgaard Madsen, Danish Meteorological Institute

Abstract

In this thesis, an analysis of long-term time series of temperature and salinity in the Kattegat and Belt Sea is carried out. This analysis provides a picture of the stratification between the dense waters from the North Sea and the lighter waters from the Baltic Sea. The long-term analysis gives an overview of the region surrounding the area of interest, the boulder reef Hatter Barn. The research shows a year to year variation and a linear trend with increasing temperature in the bottom waters of 1.46°C over the 20 year observation period.

Hatter Barn is enclosed by very busy conventional shipping routes with 26000 ships above 300 tons passing the area in 2010. The physical environment at the Hatter Barn reef is exposed to a combination of tidal flow, local weather conditions and large-scale currents regularly affecting the whole water column due to shallow water depths not exceeding 20 m. A study of three months high temporal resolution observations of salinity and temperature was carried out. The results show great mixing events both over longer and shorter periods with large temperature and salinity fluctuations. The tidal oscillation and wind impact are analyzed. A critical wind speed threshold of about 10 m/s appeared as the major forcing mechanism of strong mixing events. Model data are compared with observations to learn about the connections of the observed temperature and salinity variability with the flow pattern in the area. Underwater noise data were used to analyze potential effects from passing ships on short-term temperature and salinity variability. There is some indication of a possible correlation which may explain the large fluctuations within minutes observed in the temperature and salinity data.

Dansk resumé

I dette speciale udføres en analyse af langsigtede tidsserier af temperatur og salinitet i Kattegat og Bælthavet. Denne analyse giver et billede af lagdelingen imellem det tunge vand fra Nordsøen og det lettere vand fra Østersøen. Den langsigtede analyse giver et overblik af området omkring fokusområdet nemlig stenrevet Hatter Barn. Forskningen viser en år til år variation og en lineær trend med stigende temperaturer i bundvande på 1,46^{o}C over den 20 årige observationsperiode.
Hatter Barn er omsluttet af travle skibsruter og i 2010 passerede 26.000 skibe over 300 tons området. Det fysiske miljø ved stenrevet Hatter Barn bliver udsat for en kombination af tidevand, lokale vejrforhold og globale vandstrømme, der regelmæssigt påvirker hele vandsøjlen pga. den lave vandstand, der ikke overstiger 20 m.
Et studie af tre måneders observationer, med høj tidslig opløsning, af salinitet og temperaturen blev udført. Resultaterne viser store blandingsbegivenheder både over korte og længere perioder, med store temperatur og salinitets udsving. Tidevands svingning og vindens effekt bliver analyseret. En kritisk vindhastighed ved 10 m/s fremstår som den største årsag til stærke blandings begivenheder. Modeldata bliver sammenlignet med de observerede data for bedre at forstå sammenhængen imellem den observerede temperatur og salinitet med strømningsmønstret i området. Undervandsstøjsmålinger blev brugt til at analysere en potentiel påvirkning fra passerende skibe mht. en kortsigtet variation i temperatur og salinitet. Der er indikation af en mulig korrelation som kan forklare de store udsving indenfor minutter observeret i både temperatur og salinite.

Acknowledgment

I am very grateful to all the people who have helped me through my study; my friends, family and supervisors: Peter Ditlevsen, University of Copenhagen, Christian Mohn, Aarhus University, Kristine Skovgaard Madsen, Danish Meteorological Institute.
Thanks to Christian Mohn and Kristine for coming up with this exciting project and Karsten Dahl for talking and helping when I have been at the department at Roskilde.
A thanks to MyOcean.eu, Danish Meteorological Institute and Department of Bioscience, Aarhus University for providing data.
I would especially like to thank my supervisor Christian Mohn for our cooperation, always helping me, being a great support and even come to Copenhagen to meet. I am very thankful for that and have appreciated it a great deal.

Contents

1 Introduction

This study is designed as a case study to investigate major properties and variability patterns of important oceanographic parameters at individual locations in the Kattegat and the Danish straits at different temporal scales. The study is composed of an analysis of water properties of (1) decadal time series at selected monitoring stations in the Kattegat and Danish straits and (2) short-term time series at a boulder reef in the Kattegat to address the question of the possible impact of ship traffic on ocean mixing in relation to natural forcing. Study areas include selected monitoring stations in the Kattegat and Danish straits, as well as Hatter Barn, a boulder reef in the Great Belt designated as a Natura 2000 area, which is flanked by very busy conventional shipping routes. The working hypothesis is that ocean mixing and ultimately passive tracer dispersal may be locally affected by ship traffic. The study involves the analysis of existing data from previous observations (in the case of the Kattegat/Danish straits) and the analysis of new data. This data was collected between May and September 2010 at Hatter Barn and include 3 months of temperature, salinity, and some underwater noise data close to the reef top and the reef base. The data are used to identify the major variability and energy signatures and to examine possible correlations with oceanographic motions generated by passing ships in comparison to natural forcing components such as wind and tides. Another aspect of this study is to estimate the level of conflict between commercial use of a marine area and nature preservation. The major tasks of the study include:

- A review of relevant literature references.
- Analysis of the large-scale and long-term variability patterns of temperature and salinity throughout the Kattegat and Danish straits based on multi-year in-situ monitoring data.
- Analysis of physical data (temperature T, salinity S) from in-situ recordings (3 months time series) at two locations at Hatter Barn. This includes the analysis of the major physical characteristics and signatures, as well as the assessment of the potential correlation between the observed frequency of passing ships and corresponding T-S signatures.
- Peak events in the T-S characteristics are quantified and the relative importance of anthropogenic forcing (e.g. wave induced mixing from ships) in comparison with natural forcing factors (e.g. wind, tides) is assessed together with the level of pressure they may impose to the local ecosystem.

2 Background

2.1 Kattegat and Danish straits

The North Sea and the Baltic Sea are communicating through the Skagerrak and Kattegat with the Great Belt, Little Belt, and Oresund as the main connecting belts and straits between Kattegat and the Baltic Sea. The division of the Danish waters are shown in Figure 1a.

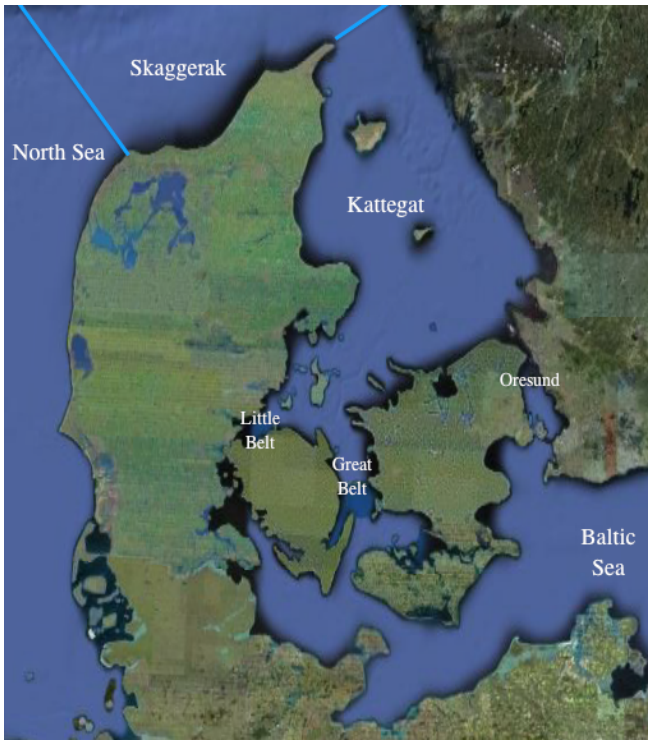

(a) The North Sea, Skagerrak, Kattegat and the Baltic Sea with the three connecting belts and straits.

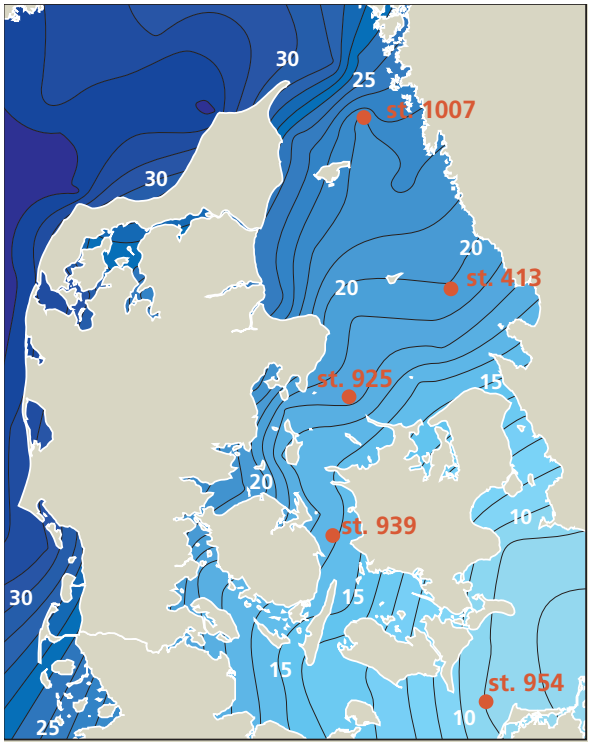

(b) The yearly average salinity in the surface layer. Red dots are mesurment stations not used her. The figure is taken from [Dahl et al. (2003)].

Figure 1: The separation and salinity diversity of the Danish waters.

The Kattegat is an interesting area because it constitutes an important mixing area between the waters from the North- and Baltic Sea. Some of the physical conditions for the Kattegat and the Belt Sea compared to the North Sea and Baltic Sea are listed in Table 1. It clearly shows that the Kattegat and Belt Sea regions are a lot smaller in surface area, volume and the depth of the water column than the surrounding waters, thus allowing for intensified mixing of the different water masses. The waters in the North Sea and Skagerrak have a high salinity around 30 PSU in the surface layer, but waters in the Baltic Sea are less saline and have a salinity around 10 PSU when entering the Danish straits, resulting in a difference of approximately 20 PSU as shown in Figure 1b. Because of this large salinity difference, a strong frontal system is formed in the inner Danish waters. This salinity frontal system plays an important role for the local marine vegetation

Sea areas	Mean depth [m]	Surface [km^2]	Volume [km^3]
North Sea (incl. Skagerrak)	94	575000	54000
Skagerrak	210	32300	6780
Kattegat	22	21100	455
Belt Sea	14	20350	291
Baltic Sea	56	372700	20920

Table 1: Water volumes, areas and mean depths [Aarup (1994)].

and fauna. The amount of different species of plants and animals shows a positive relationship with salinity. The higher the salinity, the higher is the number of different species, e.g. there are significantly less seaweed species near Bornholm than there are in the Kattegat (see Figure 2).

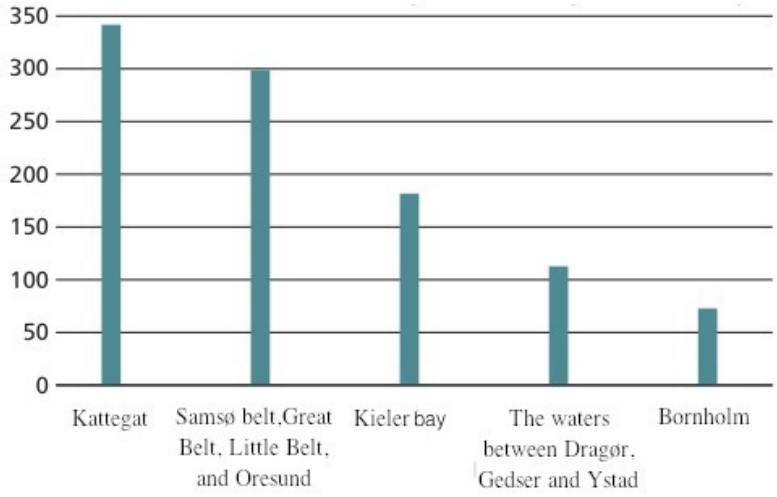

Figure 2: Species numbers of red, brown and green algae, as observed in the Kattegat, Belt Sea area and near Bornholm. The figure is from [Dahl et al. (2003)], but has been translated to English.

The Baltic Sea has once been a freshwater lake after glaciation retreated from the Baltic Sea region at the end of the Pleistocene (ended approximately 12000 years BP). During that epoch it has been covered with ice over extended periods. The most recent time the Baltic Sea region was completely covered with ice was 16000 - 17000 years BP, when the ice also covered most of Denmark. Subsequent deglaciation and ice retreat started shaping the Baltic Sea landscape into the form as we know it today. At this point, the Skagerrak was free of glacier ice, whereas the Kattegat was covered with sea ice. The ice covering the Baltic Sea was loosened at the bottom and started flowing over the eastern part of Denmark. Because of continuous melting of ice, the sea level rose and the sea penetrated further into the Oresund, ultimately causing the Baltic Sea to get connected to the Kattegat due to uplifting of the sea surface and sub-surface soil

[Houmark-Nielsen et al. (2005)]. The ice retreat and opening of the western Baltic Sea are shown in Figure 3.

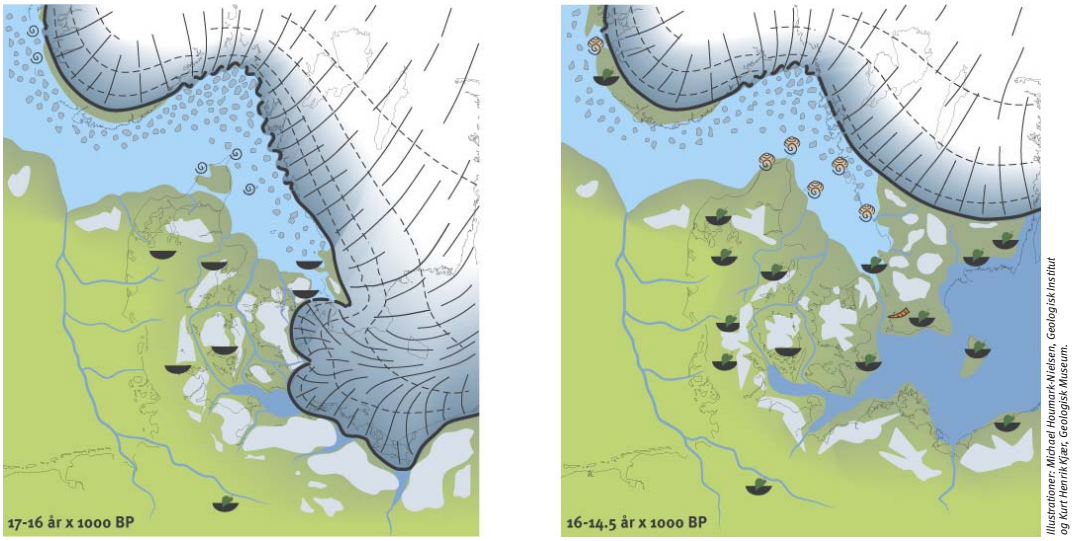

Figure 3: Ice cover in the western Baltic from 14500 to 17000 years BP [Houmark-Nielsen et al. (2005)].

The present day salinity variability and the depth of the halocline in the Kattegat is controlled by an interaction between the amount of rainfall carried into the Baltic Sea through rivers and streams from the surrounding land areas, evaporation and precipitation, wind conditions and sea surface temperatures [Dahl et al. (2003)]. The amount of freshwater inflow to the Baltic Sea is approximately 470 km^3 per year and the amount of precipitation and evaporation are broadly equal resulting in a flow of freshwater through the Skagerrak and Kattegat into the North Sea of approximately 470 km^3 per year. The total water flow from the North Sea to the Baltic Sea is approximately 1190 km^3 per year whereas the outflow from the Baltic Sea to the North Sea is approximately 1660 km^3 per year [Lund-Hansen et al. (1994)]. Water masses of low salinity and water masses of high temperature have lower density than a water mass with higher salinity and lower temperature. Because of these conditions the water masses flowing from the Baltic Sea into the Kattegat are located in the top of the water column, more saline water from the North Sea will flow along the near-bottom layer of the Kattegat. The two water mass types are separated in layers, but there is continuous mixing of the two water masses because of wind. The separation between the top and bottom layers is enhanced in the summer where the sun heats the surface layer and a strong stratification is established through a sharp thermocline. In the winter, the surface waters are cooled and become colder than the bottom waters. At one point, the difference in the water mass densities become so small that convective overturning in combination with increased storm activity leads to a greater mixing of the water column [Dahl et al. (2003)].

2.2 Wind and density controlled water transport

As mentioned in the previous section, the salinity variability in the Kattegat is controlled by an interaction between the amount of freshwater inflow, wind conditions, summer warming and winter cooling, and the depth of the halocline. The spatial salinity variability can also say something about the water transport which essentially is controlled by the same factors, i.e. wind forcing, horizontal density and resulting pressure differences.
One of the major circulation components is the wind driven advection, which is important for the movement of the frontal system. The circulation is driven by the alternating water level difference between the Skagerrak and the southwestern part of the Baltic Sea. Inflow to the Baltic Sea is favoured by strong west winds over the Kattegat. In such situations the wind over the North Sea is usually from the northwest, creating high sea level in the southeastern part of the North Sea and in the Skagerrak. At the same time the winds blow from a southwesterly direction over the Baltic Sea, this makes the water level fall inside the Danish straits. If the wind instead is from the east, the outflow from the Baltic Sea is enhanced [Rodhe (1998)].
The wind is a source of energy that is gradually moved further down the water column. The wind-driven flow in the surface layer is named the Ekman drift. If we eliminate the fluctuations of the flow with time periods shorter than a day, the near-surface current moves theoretically at an 45^o angle to the wind direction (this is shown in Figure 5a) and becomes weaker with depth (see Figure 4).

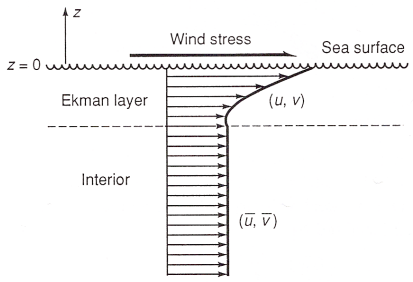

Figure 4: The surface Ekman layer generated by wind stress, the wind is blowing in to the paper with an angle of 45^o. The figure is taken from [Cushman-Roisin (1994)].

There is a direct relationship between the wind stress, τ, and the depth-integrated flow. The magnitude of the Ekman flow M_e is given by:

$$\mid M_e \mid = \left| \frac{\tau}{f} \right| \tag{1}$$

M_e is the mass transport generated by the wind in unit $[kg * m^{-1} * s^{-1}]$ and f is the Coriolis parameter [Tomczak et al. (1994)].
This generation of flow is named the Ekman drift. From equation (1) we see that variations of the Ekman transport are mainly influenced by two factors, the change of Coriolis parameter with

latitude and the structure of the wind stress field (see Figure 5). The combined effect of the Coriolis force and internal friction causes the near-surface flow to respond to wind forcing in the form of an Ekman spiral. The surface flow deviates at a 45^o angle from the wind. In deeper layers, the angle of the flow to the wind increases, while the flow velocity decreases exponentially. The Ekman layer depth is defined as the water depth where the flow direction is directed opposite to the surface flow. The depth-integrated Ekman transport is directed at right angles (90^o) from the wind [Cushman-Roisin (1994)].

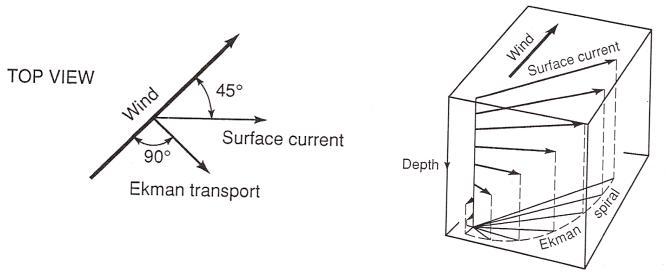

(a) (b)

Figure 5: Wind driven currents. (a) Top view and (b) 3D view of the theoretical direction of the wind, surface current and the Ekman transport. In the northern Hemisphere (f > 0) the deflection of the flow will be to the right of the surface wind stress. The figure is taken from [Cushman-Roisin (1994)].

Circular wind fields create an important forcing known as wind stress curl. Cyclonic winds generate net divergence and upwelling or Ekman pumping (Figure 6b), while anti-cyclonic winds cause net convergence and downwelling or Ekman suction (Figure 6a). The Ekman pumping (upwelling) is oriented negative, whereas Ekman suction (downwelling) is oriented positive (see Figure 6).

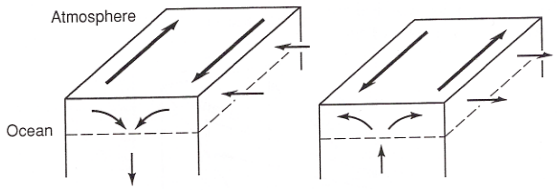

(a) (b)

Figure 6: Wind conditions for (a) up- and (b) downwelling. The figure is taken from [Cushman-Roisin (1994)].

The vertical velocity of the flow, w, is given by the divergence of the Ekman transport:

$$-\rho_0 w = \frac{\partial M_e^x}{\partial x} + \frac{\partial M_e^y}{\partial y} \tag{2}$$

x indicates the direction towards east and y towards north. If we look at it in terms of wind stress:

$$-\rho_0 w = \frac{\partial(\tau_y/f)}{\partial x} - \frac{\partial(\tau_x/f)}{\partial y} \tag{3}$$

ρ_0 is the average water density.
This relation between Ekman pumping and wind stress curl is shown in Figure 7. Here we can see that Ekman pumping only occurs when there is rotation in the atmosphere [Tomczak et al. (1994)].

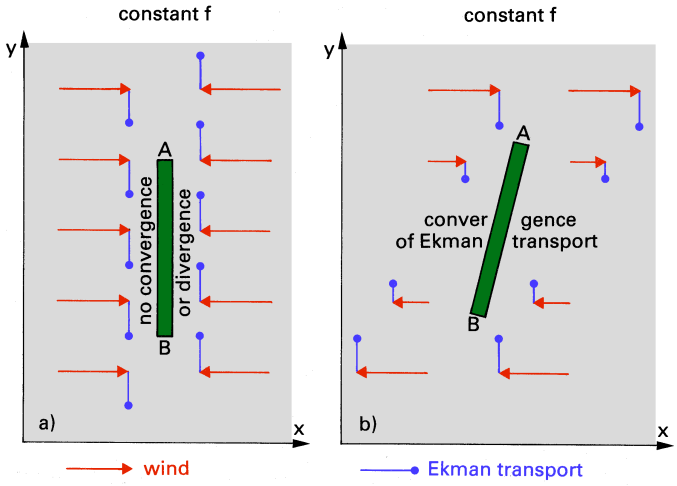

Figure 7: : Wind field and the related Ekman transport. (a) No wind stress curl, (b) with wind stress curl. The figure is taken from [Tomczak et al. (2003)].

The coastal circulation is influenced by the shoreline geometry and the offshore topography, with some areas being dominated by wide and shallow continental shelfs and others by the total absence of shallow water areas. The runoff of fresh water from the continents also add an aspect to the circulation in coastal areas. But the biggest disturbance in many coastal zones is generated by tidal activity and related currents, as tidal currents increase with decreasing water depth. This can be described by the maximum horizontal particle speed of a shallow water wave:

$$u = a\sqrt{\frac{g}{h}} \tag{4}$$

so even if the wave amplitude, a, is constant the tidal current will increase as the water depth, h, decreases. There are places where the bottom topography is so irregular that this rule does not work. Tidal currents in shallow coastal areas are 5 to 10 times stronger compared to those found in the deep ocean [Knauss (1997)].
As runoff from continents effects the coastal areas, the upwelling of open oceanic waters may also have a big influence. The upwelling is strongest when wind is blowing parallel to the shore [Sørensen (2010)]. The upwelling of deeper oceanic waters plays an important role for mixing of

the different water masses also in the Kattegat.
Density differences (differences in temperature and salinity) in combination with the acting Coriolis force are also an important driver of the circulation in the Kattegat. When the dense, high saline water from the North Sea meets the lighter Baltic Sea water it will sink below the lighter water and the less dense Baltic Sea water is forced to flow over and spread out. If we look at situations where we have a density gradient over a distance $y > 0$ and constant atmospheric pressure, we get a flow u defined as:

$$fu = -\frac{1}{\rho}\frac{\partial \rho}{\partial y} \tag{5}$$

$$fu = -\frac{g}{\rho}\left((\eta - z)\frac{\partial \rho}{\partial y} + \rho\frac{\partial \eta}{\partial y}\right) \tag{6}$$

here hydrostatic equilibrium is assumed and η is the water level. If we assume no flow at the bottom, $u = 0$ at $z = -h$ the density gradients influence will be:

$$u = \frac{g}{\rho f}(z + h)\frac{\partial \rho}{\partial y} \tag{7}$$

This gives rise to a flow across the gradient. The flow is a result of the balance between the Coriolis parameter and the density gradient.
The depth-integrated flow $\langle u \rangle$ is defined as:

$$\langle u \rangle = \frac{gh}{2\rho f}\frac{\partial \rho}{\partial y} \tag{8}$$

This transport is strongest in the Kattegat where the density differences are largest. There are four mechanisms to induce currents in the Kattegat: wind stress at the sea surface, sea surface tilt, thermohaline horizontal gradient of density, and tidal forces. Currents are also steered by Coriolis acceleration (as seen above), topography, and friction. Because of the small size of the Kattegat and Belt Sea, friction caused by the bottom and shores damps the currents [Leppäranta & Myrberg (2009)]. The transport is also depending on the season. In autumn and winter, when strong winds cause enhanced water mixing, the transport due to the gradient is smaller. Seasonal variations in temperature and salinity (enhanced evaporation and surface warming in summer in contrast to higher precipitation and surface cooling in winter) also contributes to the variations in water transport [Nielsen (1999)].

2.3 MATLAB modeling theory

To analyze the data MATLAB was used. The following section will explain some of the principles behind the functions and methods used in the data modeling process.

2.3.1 Interpolation

A method designed to solve an interpolation/extrapolation problem was used to handle scattered data points. Because it is unknown which points are near each other in advance, operations to determine this data point connectivity are carried out. The best and simplest solution is to use a Delaunay triangulation.
The approach for approximating values for the temperature and salinity is as follows. First a triangulation of P(a planar region containing a set of data points) are determined so that any point to be interpolated inside the convex hull of the data must lie inside exactly one non overlapping triangle. Then a linear interpolation within each triangle of the triangulation moves each sample point to its correct value, thereby mapping every triangle in the triangulation to a contour maps [Berg et al. (2008)].

2.3.2 Moving average

A filter function named RUNMEAN is used to calculate a moving average to look at different aspects in the data. For a vector, the running mean Y= RUNMEAN(X,M) is computed on the elements of the vector X. It uses a window of 2*M+1 data points, where M is an positive integer defining (half) the size of the filter window. In pseudo code:

```
1 Y(i) = sum(X(j)) / (2*M+1), for j = (i-M):(i+M), and i=1:length(X)
```

[Matlab Central 2012]

2.3.3 Fast Fourier transform

Time series of temperature and salinity are analyzed by calculating individual power spectra. This calculation involves the application of a fast Fourier transformation (fft). The functions Y = fft(x) and y = ifft(X) implement the transform and inverse transform pair given for vectors of length N by:

$$X(k) = \sum_{j=1}^{N} x(j)\omega_N^{(j-1)(k-1)} \tag{9}$$

$$x(j) = (\frac{1}{N}) \sum_{k=1}^{N} X(k)\omega_N^{-(j-1)(k-1)} \tag{10}$$

where $\omega_N = e^{(-2\pi i)/N}$ is an N^{th} root of unity.
Y = fft(x) returns the discrete Fourier transform of vector x, computed with a fast Fourier transform algorithm [MathWorks 2012].

2.4 Boulder reefs and area of interest, Hatter Barn

The boulder reefs in the Danish waters were formed during the ice age. The glaciers brought large quantities of material with them and when the ice melted the material was released. The boulder reefs are not found in many other places in the world ocean and are therefore a unique and ecologically distinct feature. There is an estimated stone reef area of approximately 1200 km^2 reefs in the Danish waters. The boulder reefs are important areas to study biomass and biodiversity in the ocean, because of their role as biological hotspots. Danish boulder reefs are habitats for many different plant and animal species [Dahl et al. (2003)]. In many places, the ocean bottom looks like a desert with muddy or sandy bottom that can go on for many kilometers. Within this marine landscape, the reefs are like an oasis on the seabed providing a unique physical environment for both animals and plants. Studies have shown that there are up to 10 times more fish on boulder reefs than on the surrounding sandy bottom. Therefore boulder and stone reefs also have attracted fisheries activity for many years. Between approximately 1930 and 1990 the reefs' stones and boulders were a major resource to build harbor piers and coastal scour protection against ocean forces. A total area of 40 km^2 of rock surface from reefs has been removed as a result of harbor building, coastal protection measures and commercial fishing [Dahl et al. (2003)]. Two different kinds of reefs can be distinguished, i.e. soft and hard bottom reefs, with stone reefs falling under the hard bottom reef category. The definition of a hard bottom reef is vague, because there are different possible varieties depending on the actual stone and boulder size, shape, density and concentration. The challenge is to decide whether a small stone or seashell is too small and is moved too often to be an integral part of the hard bottom reef. This largely depends on the area where the object is placed and how waves and currents are impacting on a certain location. Other definitions consider on the amount of hard substrate which must be present, before a reef can be characterized as a hard bottom reef. [Dahl et al. (2003)] provide one of most comprehensive hard bottom reef definitions and categories (see also Figure 8):

A hard bottomed reef is an area that rises from the surrounding sea floor. The hard substrate, whether it is stone, rock, or of biogenic origin have to cover at least 5% of the sea bottom and the area must have a size of at least 10 m^2. If the reef is subdivided into smaller banks, i.e. reefs divided into smaller collections of rocks, the reef is defined by a line around all banks, each of which meeting the requirements of size and coverage. If the reef is sharply or gradually changing into a sandy or gravel dominated seabed, the border of the reef is defined with the requirement of at least 5% coverage of hard substrate

The area of interest is a boulder reef named Hatter Barn which is located within the Kattegat near the island Samsø. Hatter Barn covers an area of approximately 6.3 km^2 consisting of small and well preserved hard bottomed reefs. It has a bank structure with large sandy areas between hard substrate as shown in Figure 8c. The stones on the reef is estimated to cover an area of 4.8 km^2 [Naturstyrelsen]. Hatter Barn is a highly diverse marine habitat with a heavily used shipping route on both sides, a deep fairway which meanders west and north of the reef and a shallower

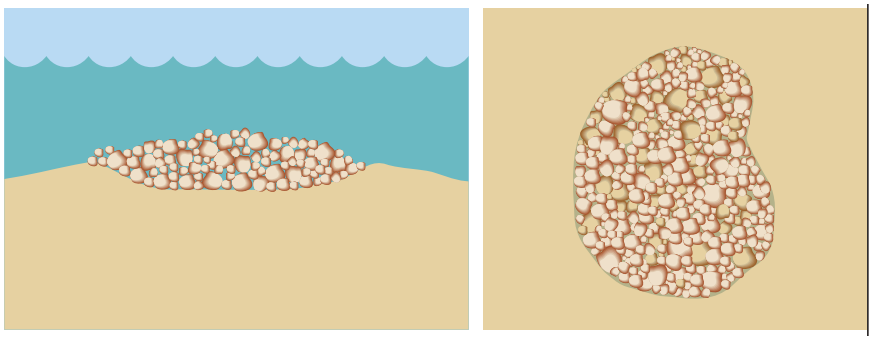

(a) Reef with sharp borders to the surrounding bottom of sand and gravel.

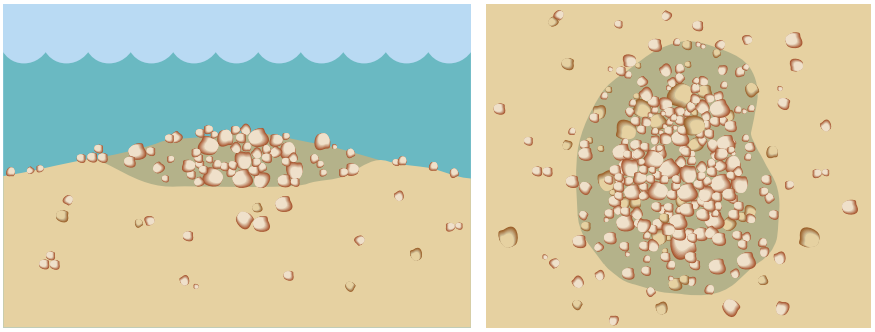

(b) Reef with a gradual transition to the surrounding bottom of sand, gravel and mud. The reef ends where hard sub- strate covers less than 5% of the bottom.

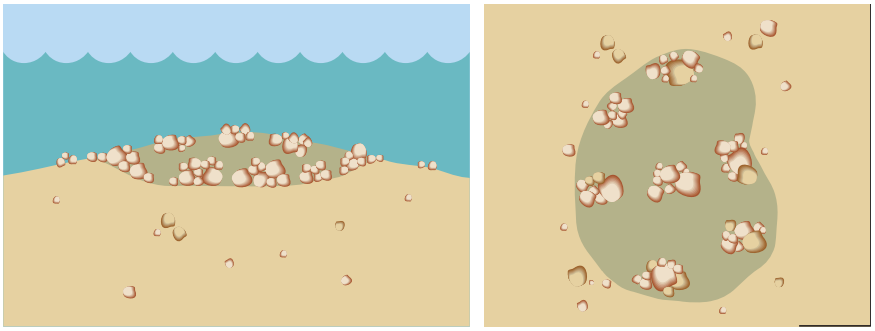

(c) Reef with bank structure.

Figure 8: Definition of reefs and sketch of different reef types and their borders to other types of seabed habitats. The left column shows a side view and the right column shows a top view of the reef, from [Dahl et al. (2003)].

route to the southeast, see Figure 9.

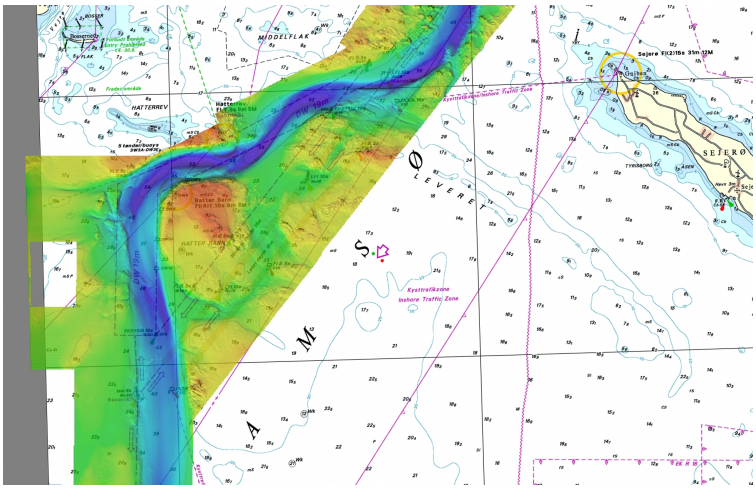

Figure 9: The area of Hatter Barn. Nautical chart with color coded bathymetry. The deep and shallow water shipping routes surrounding the reef are indicated by narrow lines. From farvandsvæsenet with modifications [Dahl et al. (2012)]

The ecological setting of Hatter Barn is related to the concept of "blue corridors" [Martin et al. (2006)]. Blue corridors describe non-random dispersal of particles (e.g. eggs, larvae and plankton) which are driven by physical factors (currents, hydrography) or biological mechanisms (route of choice, food locations). The dispersal of particles is depending on the water mass characteristics in the initial particle release areas. The halocline acts as an important barrier for exchange between the surface and bottom waters. Dispersal routes from an area above the halocline will face a barrier to distribute particles towards an area below the halocline. This is not the case the other way around, as it can be seen from Figure 10a. Due to the barrier in the water column, the spreading of particles in Danish waters may look like in Figure 10b. Figure 10b is adapted from a model study by [Bendtsen et al. (2007)] where a specific tracer is released from each location on the map corresponding to the location of major reefs. Red circles indicate reef areas with a mean water depth above the halocline, blue circles indicate areas with a mean water depth around the halocline (13-16 m) and green circles indicate areas with a mean water depth below the halocline. Diameters of the circles are scaled proportionally to average tracer concentration in the bottom layer [Bendtsen et al. (2007)].

The model results showed that the different reefs play different roles in the distribution of particles. Kim's Top is a major particle supplier (donor area) at depths around the halocline. Other reefs work as particle carriers to southern areas above the halocline (green areas and arrows in Figure 10b). Hatter Barn lies within this southerly distribution route and can be regarded as a stepping stone. This means that Kattegat exports larvae and propagules, thereby helping to maintain population and biodiversity in adjacent areas.

There is a conflict of use between human activities and ecosystem preservation, as it can be

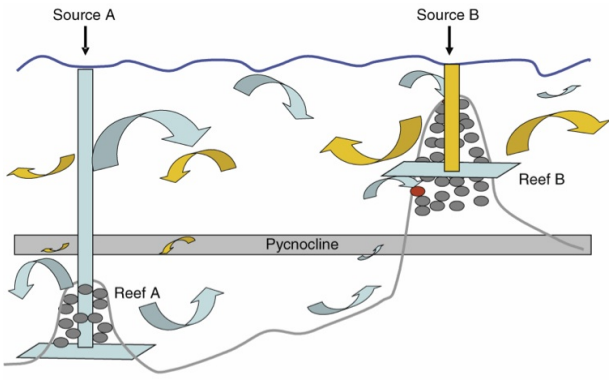

(a) Sketch showing the spreading of particles in the water column. Particles can move from A to B but not the other way, due to the halocline barrier [Bendtsen et al. (2007)].

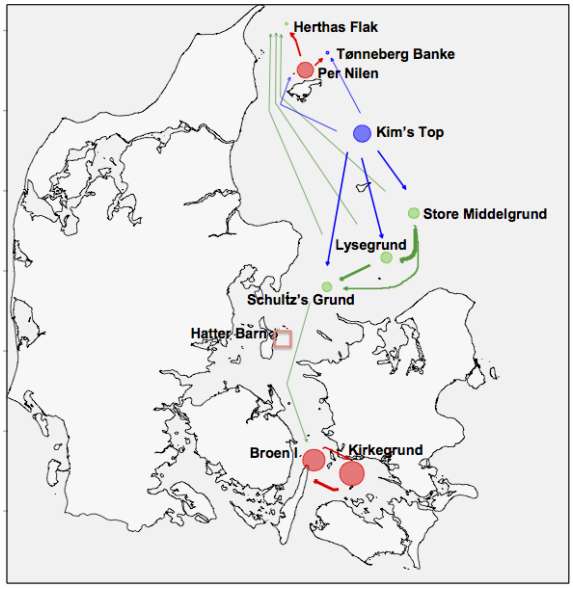

(b) Particle source areas, boulder reef locations and major particle dispersal routes based on the connectivity study by [Bendtsen et al. (2007)]. The figure was slightly modified. For color codes see text.

Figure 10: Particle connectivity study in Danish waters [Bendtsen et al. (2007)].

seen from the two maps in Figure 9 and 10b. Protection of important stepping stone areas and habitats acting as donor or nursing areas during a life cycle of a certain species is an obvious way to protect or restore biodiversity in a highly exposed and exploited area like Hatter Barn [Bendtsen et al. (2007)].

There are many animals living on the reefs. The main grazers of macroalgae (seaweed and kelp) in the deeper, more saline parts of the boulder reefs in the Kattegat are sea urchins. Especially two species of sea urchins must be considered primarily responsible for feeding on the macroalgae vegetation on parts of the reef, thus putting a severe grazing pressure on reef vegetation. The large urchin (Echinus esculentus) is found in the northern part of Kattegat, and the green sea urchin (Strongylocentrotus droebachiensis) is most common in the southern parts. Both species are omnivorous, and with their sharp teeth they can clear the hard bottom reefs of large part of their vegetation leaving behind barren grounds [Norderhaug & Christie (2009)]. Sea urchins prefer a higher salinity physical environment with salinities typically 24 PSU [Sameoto & Metaxas (2008)]. Therefore, the green sea urchin is normally restricted to water depths at or below the halocline in the Kattegat. Vertical mixing events associated with upwelling of high salinity bottom waters would however allow sea urchins to move up to surface waters and graze on reef top seaweed forests. In addition, sporadic horizontal shifts in the Kattegat's salinity frontal system might extend the sea urchin's favorable salinity levels further to south [Dahl et al. (2003)].

3 Data analysis of the Kattegat and Danish straits

In this chapter, long-term variations of the main water mass properties are analyzed based on temperature and salinity data from monitoring stations in the Kattegat and Danish straits over a period of 20 years. The analysis considers both, temporal and spatial variations of surface and bottom waters. Inter-annual variations in both layers are analyzed by a time series analysis, whereby the seasonal variability is excluded through pre-processing of the data with a 12 month moving average.

3.1 Water properties and their variability in the Kattegat and Great Belt

The goal of this analysis is to give a detailed picture of the long-term variations and their dominant patterns both over time and within the water column.
The raw data was taken from the Department of Bioscience, Aarhus University, database MArint Data System (MADS) [MADS database - a] and represents the salinity and temperature conditions across the main transition area between the Baltic Sea and Skagerrak/North Sea. The geographical positions and the corresponding observation periods for the four selected stations are given in Table 2 and Figure 11.

Stations	Coordinats	Period: From/To	Days
Gniben	$11^o09'6E$ $56^o07'9N$	14. Feb. 1989 21. Jan. 2009	7281
Asnæs	$10^o45'7E$ $55^o39'3N$	15. Feb. 1989 21. Jan. 2009	7280
Halsskov Rev	$11^o00'E$ $55^o22'6N$	15. Feb. 1989 20. Jan. 2009	7279
Langelans bælt	$11^o02'E$ $55^o03'N$	15. Feb. 1989 20. Jan. 2009	7279

Table 2: Positions and data collection periods of the analyzed MADS monitoring stations.

In the data from MADS, the temperature and salinity are available at different depths and with different sampling intervals over each year. There are approximately 9 measurements per year over the whole time series, but the sampling periods differ from year to year. From 1989-1997 there are measurements almost every month, after 1997 there are only 4 to 5 measurements per year and not spread across the year with one measurement in February and three from August to November. The observation times can be seen in Figure 12. The sampling depths are more consistent throughout the time series. At Gniben measurements were taken 1, 5, 10, 15, 20, 25, 30, 40 meters and one at the bottom which varies between 40 and 49 meters depending on the exact location, water level and flow. The same depths were used at Asnæs with bottom values

(a) (b)

Figure 11: Geographical location of the four stations in the Kattegat and the Great Belt. (a) Overview, (b) Zoom.

between 40 and 52.6 meters. At Halsskov Rev and Langelands Bælt the salinity and temperature are measured at depths of 1, 5, 10, 15, 20, 25, 30 meters with a bottom sample between 30 to 39 and 30 to 39.7 meters respectively. The depths of these measurements are also shown in Figure 12. The parameters are derived from measurements with a CTD profiler, which measures conductiv-

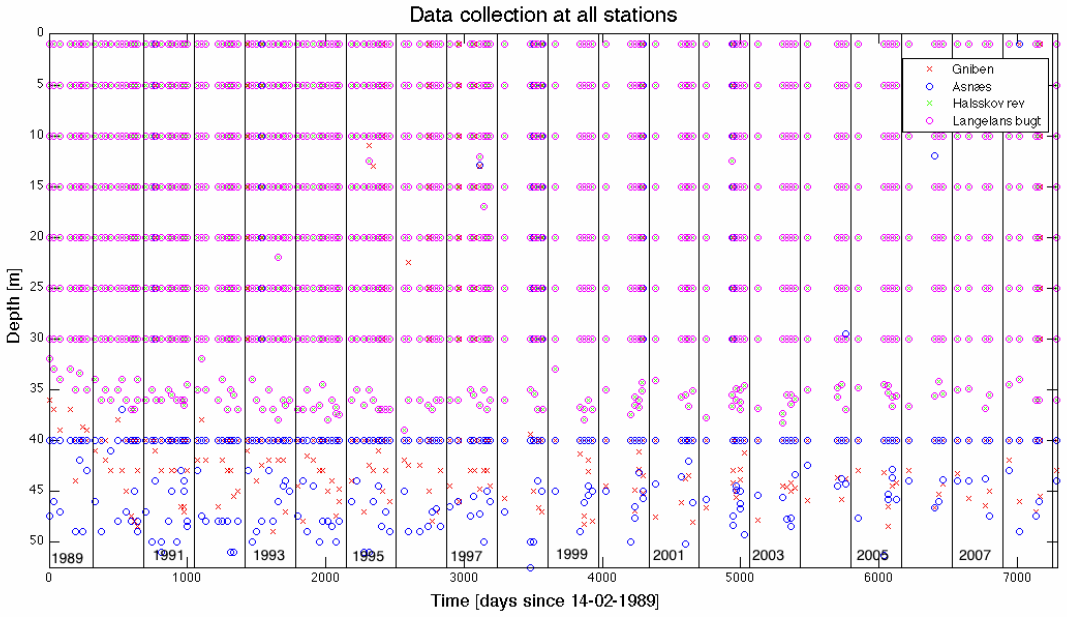

Figure 12: Data coverage, data gaps and depth of all stations.

ity, temperature, pressure, oxygen and fluorescence. The depth is calculated from pressure and the salinity is calculated from pressure, conductivity and temperature.

3.1.1 Contour maps of temperature and salinity

I have created contour plots to analyse the time-depth relationship of temperature and salinity at each station during the observational periods. Because of the interpolation method used the lowest bottom values are very questionable. I will start with the analysis of temperature, followed by salinity. This first analysis of the data provides useful information on the major spatial and temporal signals and properties as a background for a more detailed study of the major variability patterns and forcing mechanisms. The time line on the x-axis is the same on all the figures, starting with day 1 at the 14. February 1989 and ending at day 7281 which is the 21. January 2009. Figure 13 shows the depth-time distribution of temperature at the four monitoring stations. The temperature time series are dominated by the seasonal summer heating and winter cooling cycle, reflecting the seasonal and inter-annual variations of the vertical heat flux due to solar radiation. There are significant year to year changes in both the maximum summer temperatures and depth of the thermocline, i.e. the subsurface layer where temperature changes occur more rapidly with depth in comparison with the layers above and below. The number of summer seasons with maximum temperatures $>18^oC$ continuously decreases from north to south. Another prominent feature are extended periods of low winter temperatures extending from the surface to the bottom, possibly representing years of strong convective mixing followed by years of weaker winter mixing.
Figure 14 shows the corresponding salinity distribution at the selected monitoring stations. The most prominent signal at all stations is the two water layer system consisting of the salty bottom layer originating from the North Sea and the fresher water in the top layer from the Baltic Sea. Sub-surface salinities >26 PSU can only be found at the two northernmost monitoring stations Gniben and Asnæs, (see Figure 14a and 14b). Salinities quickly decrease in the southern Great Belt with increasing distance from the North Sea source waters (see Figure 14c and 14d). This indicates the possible importance of the Great Belt as a potential hot spot of lateral mixing. The time series do not show a consistent inter-annual periodicity or clear seasonal cycle when compared to temperature. Salinity is not directly depending on seasonal variations of atmospheric forcing at high latitudes such as solar radiation. Temporal salinity variability is more affected by wind and associated mixing events, as well as large-scale and long-term variations of the inflow of high saline waters from the North Sea. However, salinity variability is an import ecological factor in the Kattegat area. The green sea urchin (Strongylocentrotus droebachiensis) is an example of particular importance. The green sea urchin can occur on hard-bottom habitats in the Kattegat and Great Belt in massive numbers, causing destructive grazing of seaweed forests in shallow waters and strongly reduced species diversity as a consequence. Green sea urchins are very sensitive and adaptive to the salinity conditions. Salinities of >24 PSU have been found to be a suitable habitat

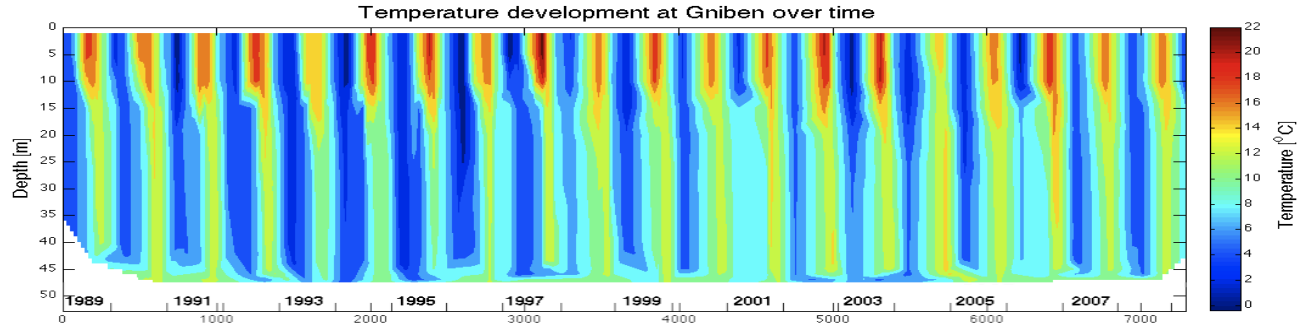

(a) Gniben

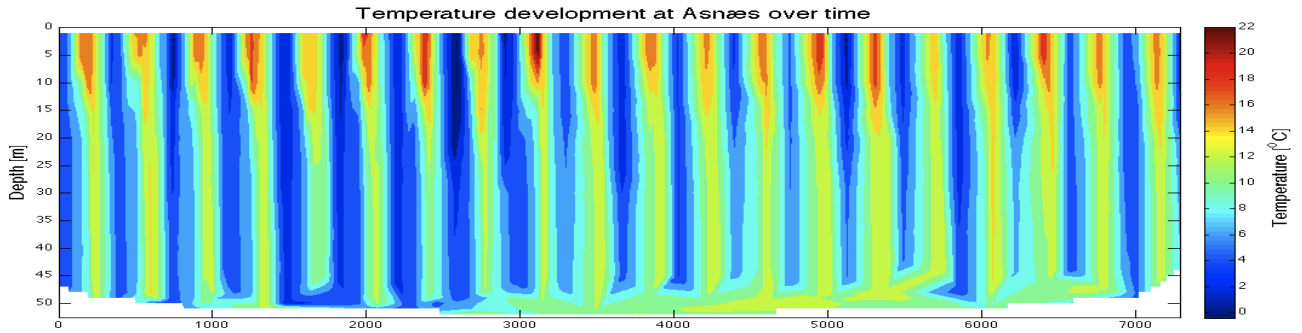

(b) Asnæs

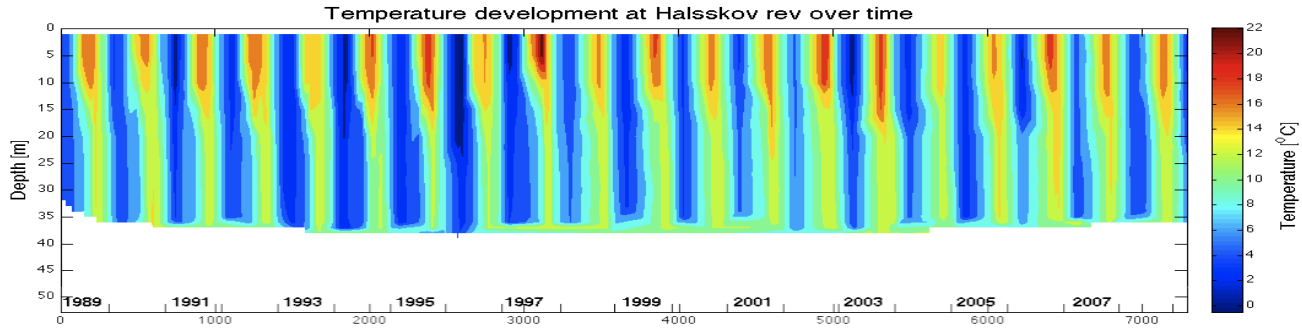

(c) Halsskov Rev

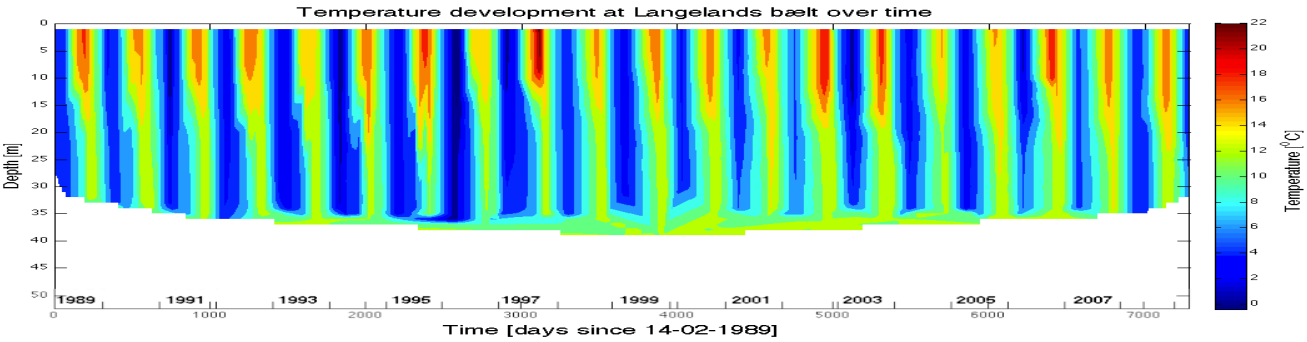

(d) Langelands bælt

Figure 13: Contour plot of the temperature of all four stations.

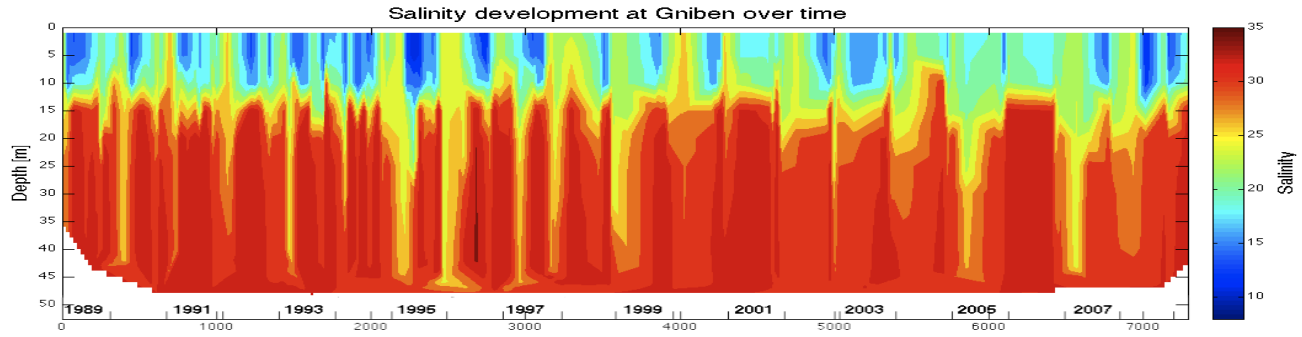

(a) Gniben

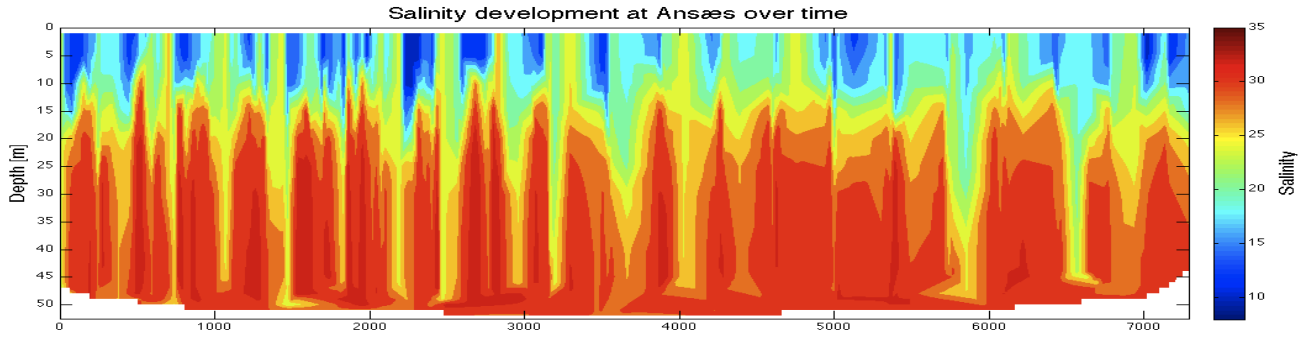

(b) Asnæs

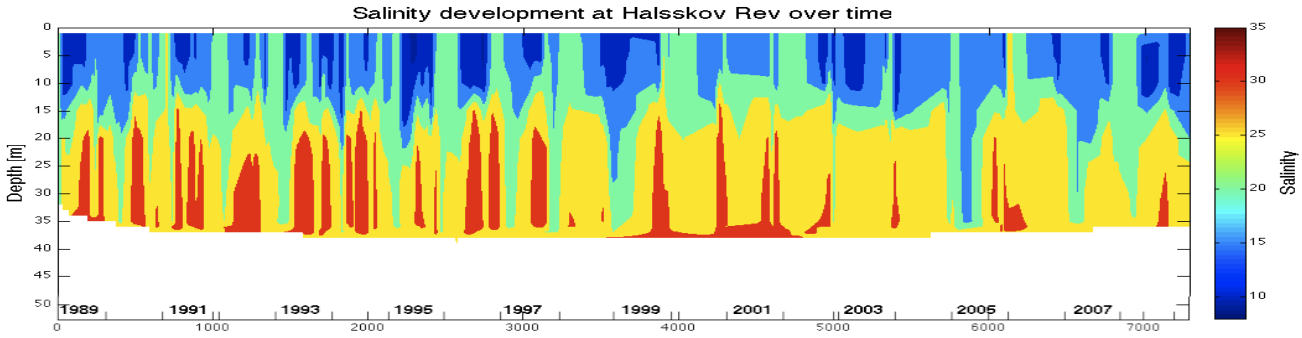

(c) Halsskov Rev

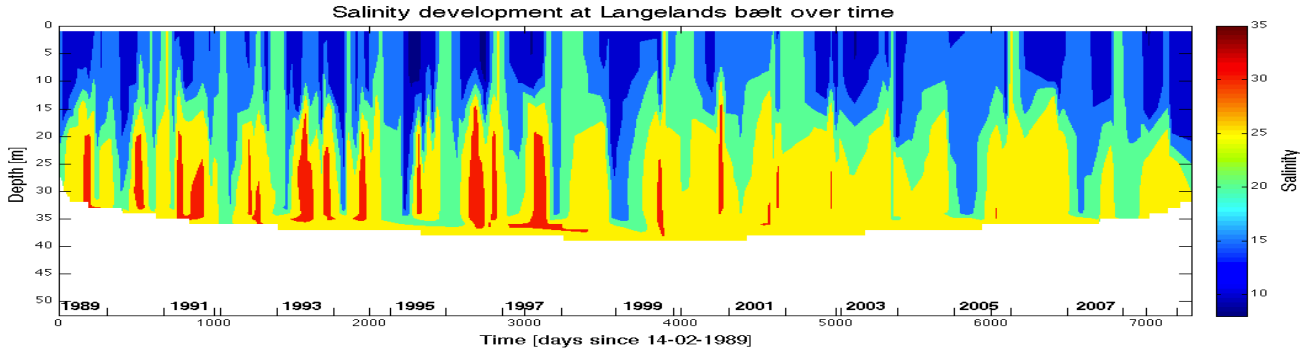

(d) Langelands bælt

Figure 14: Contour plot of the salinity of all four stations.

(see Section 2.4).

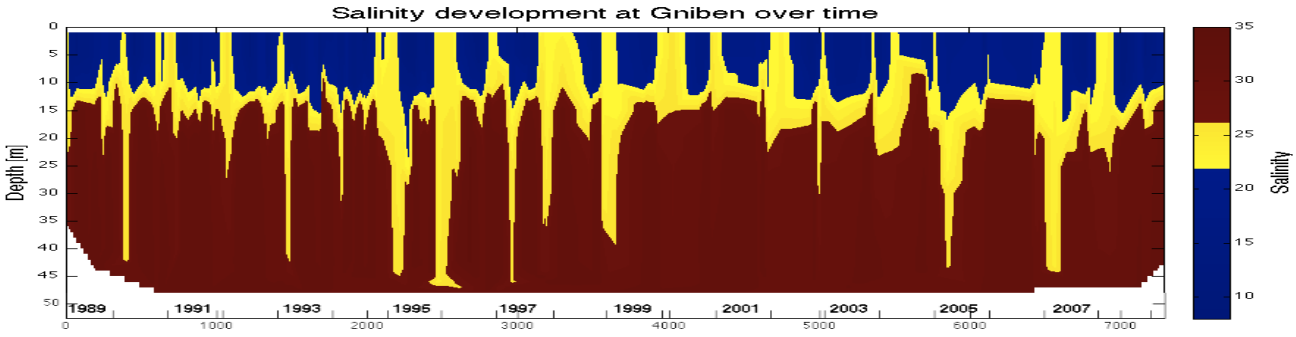

(a) Gniben

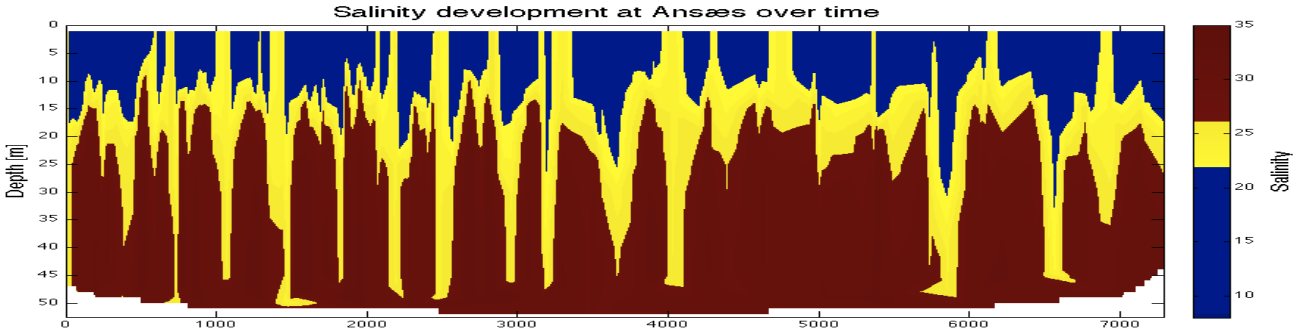

(b) Asnæs

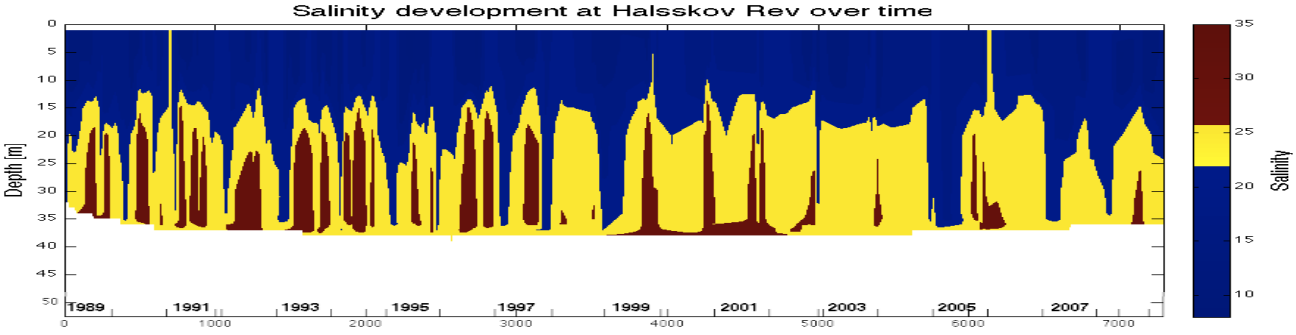

(c) Halsskov Rev

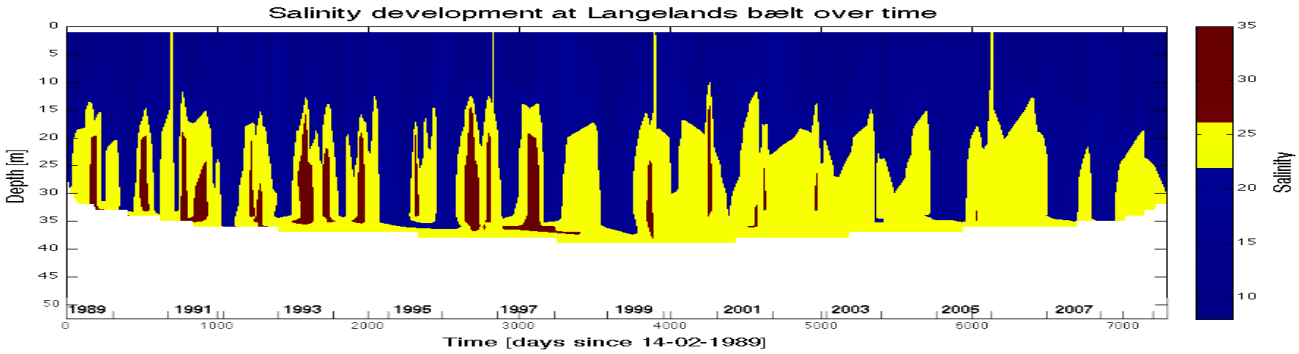

(d) Langelands bælt

Figure 15: Contour plot of the critical values of the salinity of all four stations.

Figure 15 shows the salinity time series sub-divided into three salinity classes: (a) Salinities > 26 PSU (deep and bottom layers), (b) salinities in the range 22-26 PSU centered around the halocline, and (c) salinities < 22 PSU in the surface layer. At the two northernmost stations Gniben (Figure 15a) and Asnæs (Figure 15b) regular events of high salinity water (22-26 PSU) injections into the surface layers can be observed.

3.1.2 Differences between the top and bottom layer

In this subsection, the temperature and salinity differences between the top and bottom layer at each monitoring station are presented. The top and bottom layer were chosen because it is there where the biggest variations and the largest differences can be expected. Prior to the analysis, the temperature and salinity time series were linearly interpolated in both depth and time. The time interval is 5 days and the depth interval is 5 meter. An interpolation period of 5 days seams to be a reasonable compromise between periods of good data coverage and periods of large data gaps. The surface layer values were defined at 5 m depth and the bottom layer values were taken at the deepest observed depth level at each station and time. Large data gaps were replaced by interpolated values from the nearest available observed data points. Because of the interpolation the figures now start at the 1. February 1989.

3.1.2.1 Temperature

Figure 16 shows the time series and power spectra of the surface (red) and bottom (blue) temperatures at each monitoring station. The power spectral density is the frequency response of a periodic signal and is often used in signal processing to identify the energy distribution of periodic signals in a time series, i.e. at which periods the most energetic signals can be found.
The dominant signal in all four time series is the seasonal cycle. Temperatures in the surface layer typically vary between winter minima of approximately 4^oC and summer maxima of 17^oC. Bottom layer minimum temperatures are close to the surface layer values, but never exceed 14^oC in summer. There is generally little variation in both temperature ranges and seasonal extrema across the Kattegat and the Danish straits. The spectral analysis also confirms that the surface is the layer of the most energetic temperature fluctuations. The most energetic signals at all stations, both in the surface and bottom layer, appear at a period of approximately 365 days, thus representing the seasonal warming/cooling cycle. The spectral analysis also confirms the surface as the layer of the most energetic temperature fluctuations. Interannual changes are evident in the individual time series, but they are weak compared to the seasonal changes and do not produce a significant signal in the power spectra.

To study the long-term variations in the top and bottom layer I have calculated the running mean, RM, of the temperature time series data. In signal processing, a moving average is used as a form of a low-pass filter to filter out short-term fluctuations in time series data in order to highlight long-term trends or periodic cycles. To remove the seasonal cycle and to emphasize the low frequency variability, I have therefore put the running mean threshold to 365 days. Figure 17 shows the effect of the running mean on the original temperature data together with a more detailed comparison of the resulting long-term surface and bottom layer temperatures.
In Appendix A.1 the power spectra of the running mean of the temperature are presented. The energy of the periodic signals is weak, but there is indication of a variation with a period of 5 and

(a) The stations

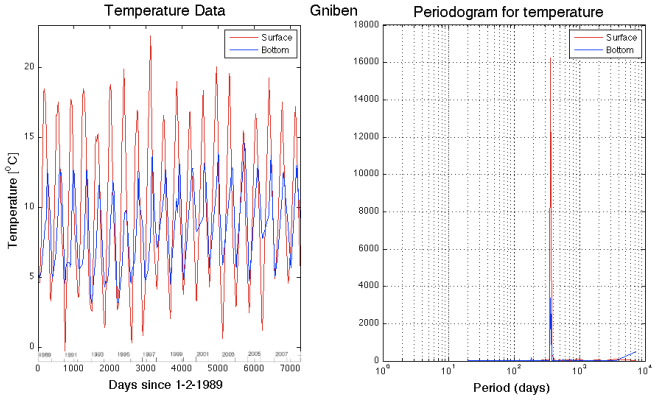

(b) Gniben

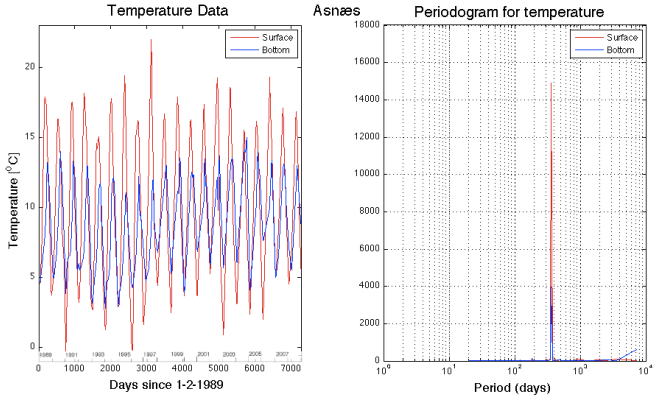

(c) Asnæs

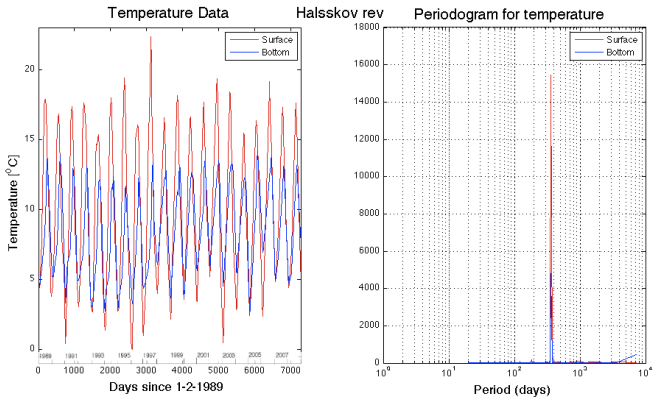

(d) Halsskov Rev

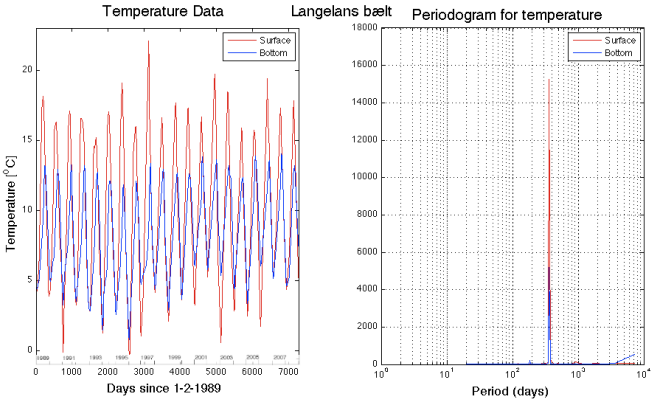

(e) Langelands bælt

Figure 16: Time series and power spectra of the temperature for the top (red) and bottom layer (blue) of the four stations.

10 years.

Figure 18 presents a summary of the running averages in the surface (a) and bottom layer (b) . The goal of this analysis is to illustrate the main long-term variability patterns at the individual monitoring stations relative to each other.

The surface layer temperature variability beyond the seasonal cycle is dominated by significant

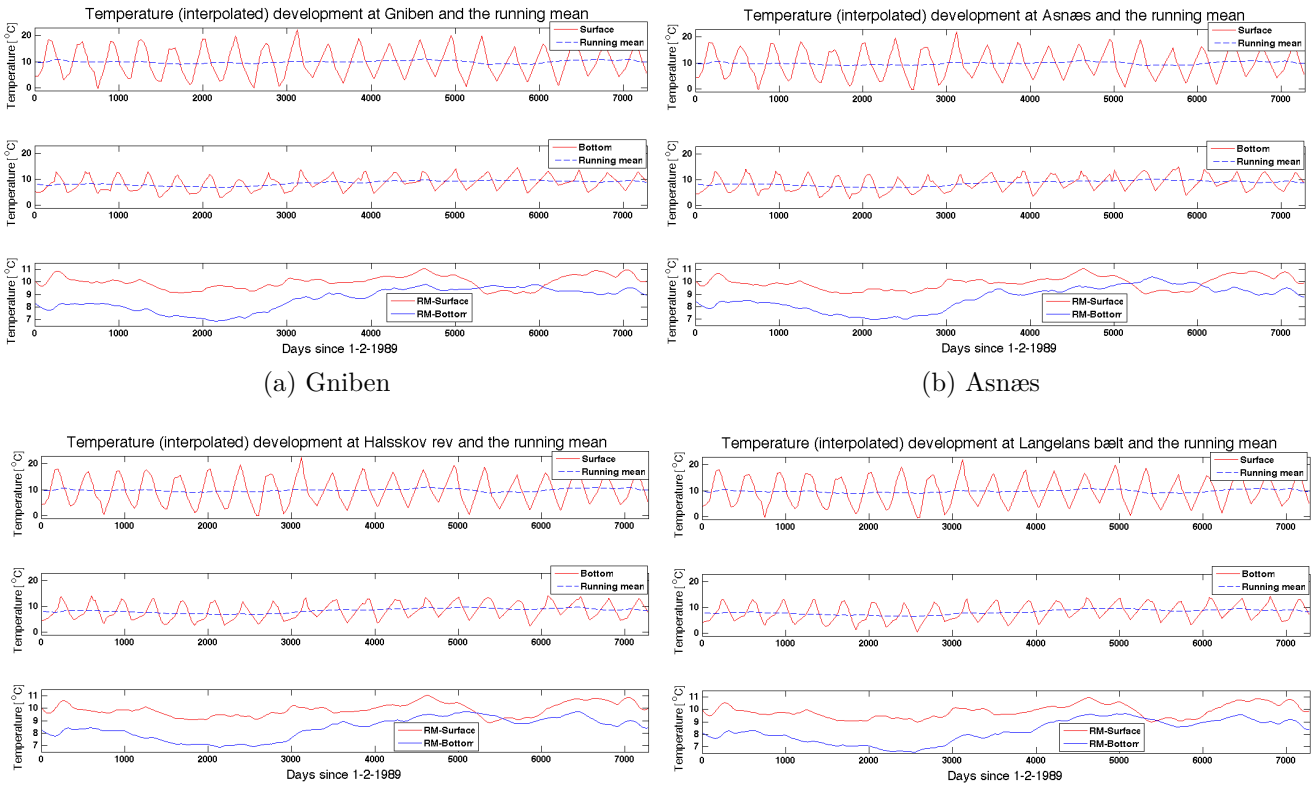

(a) Gniben (b) Asnæs

(c) Halsskov rev (d) Langelands bugt

Figure 17: Comparison of the original, interpolated temperature time series in the surface (top) and bottom (middle) layer and the corresponding one year running averages (bottom) at the four monitoring stations.

long-term changes over different periods. The surface temperatures appear at consistent levels until around (year 1992) 1300 days since the beginning of the time series. Thereafter, the values drop by approximately 1^oC over a period of 500 days and remain at low levels for next 800 days with a minimum at year 1997. Temperatures increase again by 1.5^oC to a maximum over the next 2000 days (year 2001), followed by a decrease of about 2^oC between day 5000 and 6400 (2003 - 2006). Long-term temperature changes at all stations largely follow the same pattern with little variation between them. The bottom temperature variability largely follows the observed surface pattern with decreasing temperatures until 1997 at the same magnitude (1^oC), followed by a similar warming period. During this period, temperatures increase by approximately 3^oC until 2003. The prominent cooling period observed in the surface layer after 2003 is much weaker in the bottom layer and entirely absent at the two northernmost stations Gniben and Asnæs. At these stations, bottom temperatures occasionally exceed the surface values.

As a next step, the long-term variations in the temperature data were analysed for existing continous trends by applying a linear regression to the running averages. The results of this trend analysis are presented in Figure 19 which shows the regression lines and running averages of sur-

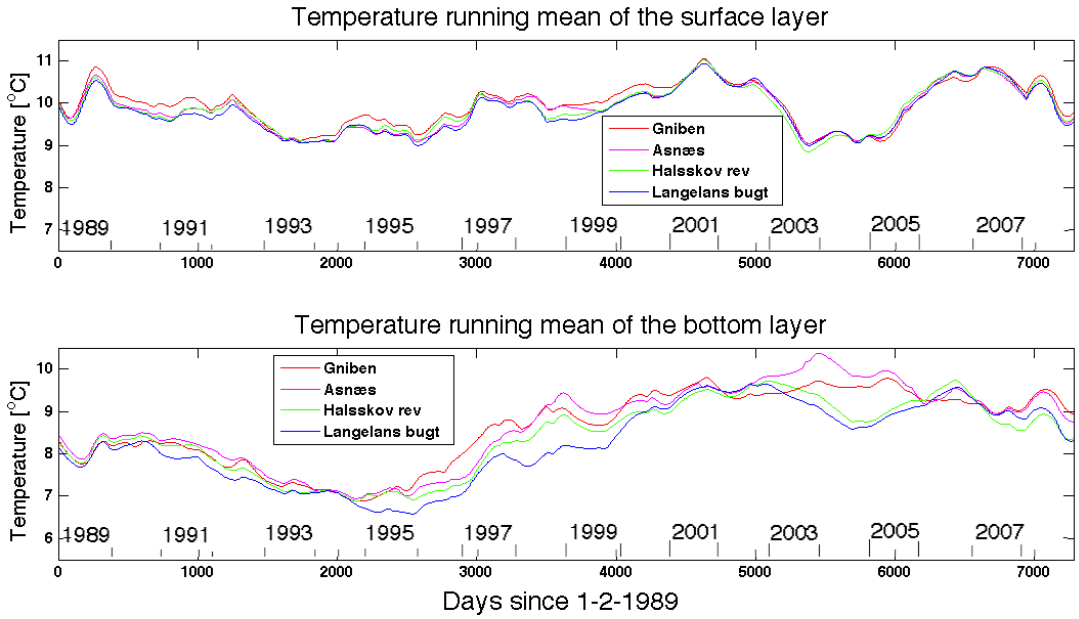

Figure 18: 12 month running means of surface (a) and bottom layer (b) temperatures at all stations.

face and bottom temperatures for all stations.

Each picture contains the measure of goodness-of-fit, R^2, for each linear regression. R_a^2 refers to the linear regression of the running mean of the surface layer and R_b^2 to the running mean of bottom layer.

The regression analysis did not reveal a statistically significant linear trend over time for the surface layer data all stations. The goodness-of-fit never exceeds 17%. However, there is a statistically more reliable linear trend in the bottom layer time series. With a goodness-of-fit between 46-59%, there is a clear trend towards higher bottom temperatures with an average increase of 1.46^{o}C at all station between 1989 and 2009.

(a) The stations

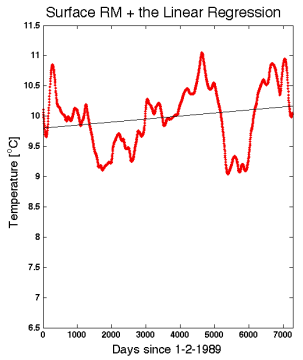

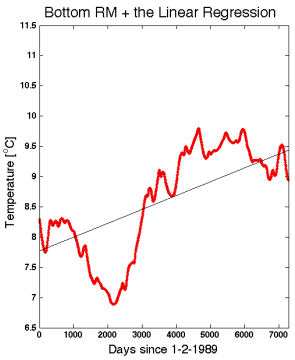

(b) Gniben: R_a^2=0.066 R_b^2=0.587

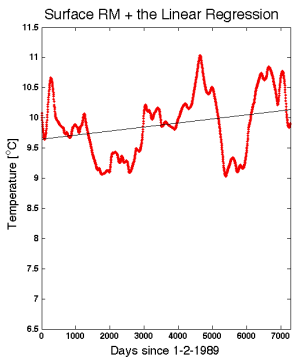

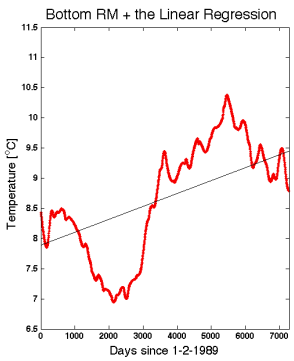

(c) Asnæs: R_a^2=0.124, R_b^2=0.516

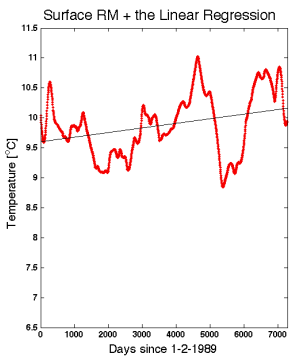

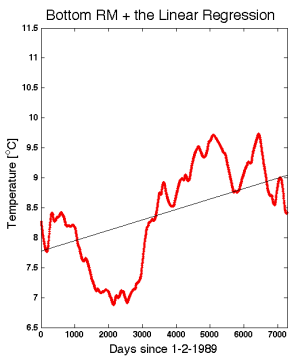

(d) Halsskov Rev: R_a^2=0.128, R_b^2=0.468

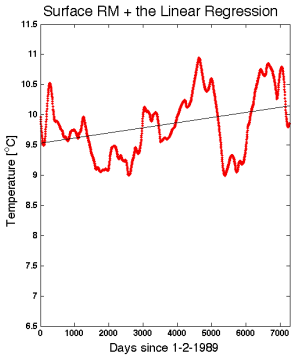

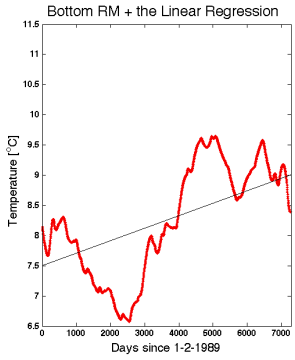

(e) Langelands bælt: R_a^2=0.166, R_b^2=0.502

Figure 19: The temperature surface and bottom layers running mean (RM) with a linear regression.

3.1.2.2 Salinity

The spectral analysis was also carried out for salinity.

(a) The stations

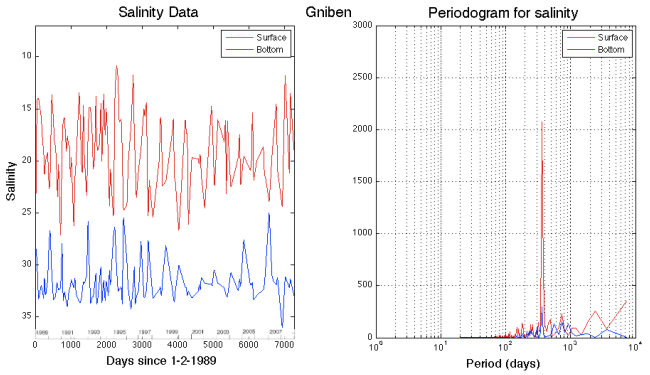

(b) Gniben

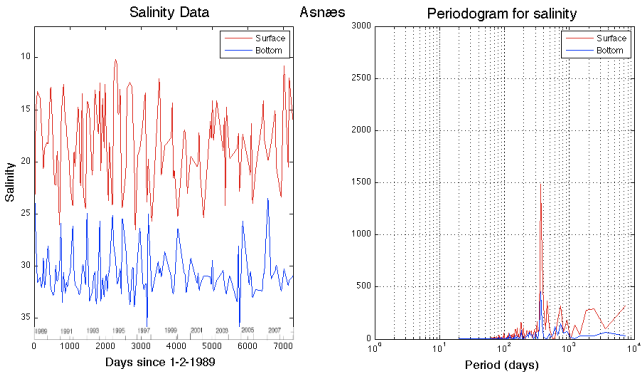

(c) Asnæs

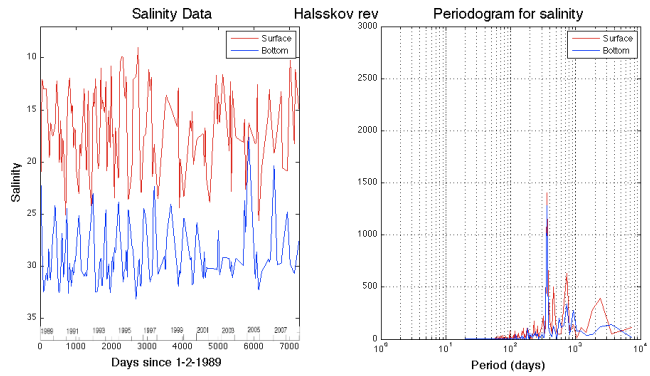

(d) Halsskov Rev

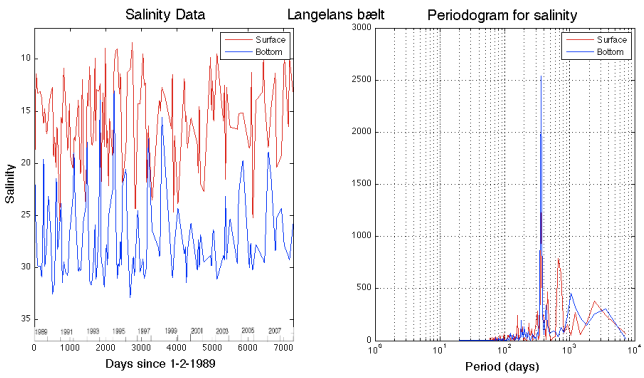

(e) Langelands bælt

Figure 20: Time series and power spectra of the salinity for the top (red) and bottom layer (blue) of the four stations.

Figure 20 shows the time series and power spectra of the surface (red) and bottom (blue) salinities at each monitoring station. The main patterns of salinity variability are more complicated when compared to temperature. The salinity variability at the two northernmost stations (Gniben and Asnæs) is again dominated by a clear seasonal cycle in the surface layer. The seasonal cycle is also visible at stations further south (Halsskov Rev and Langelands Bælt), but significantly less

energetic. In addition, the southern regions exhibit other significant surface salinity spectral peaks at 455 days (1 year and 3 months), 730 days (2 years) and approx. 2400 days (6.6 years). In contrast, the salinity variability in the respective bottom layers indicates an inverse pattern. The seasonal bottom salinity cycle becomes more energetic at the southern stations. An interesting feature in the bottom salinity time series is a substantial weakening of salinity fluctuations between year 2000 (day 4000) and year 2004 (day 5500). This period is not only marked by lower bottom salinity extrema, but also by a generally lower salinity range. A similar attenuation period is also visible in the surface salinity, but to a much lesser extent.
I have again calculated the 365 day running mean to further examine any existing long-term variations in the salinity top and bottom layer data. Figure 21 again shows the effect of applying a 1 year running mean to the original salinity data.

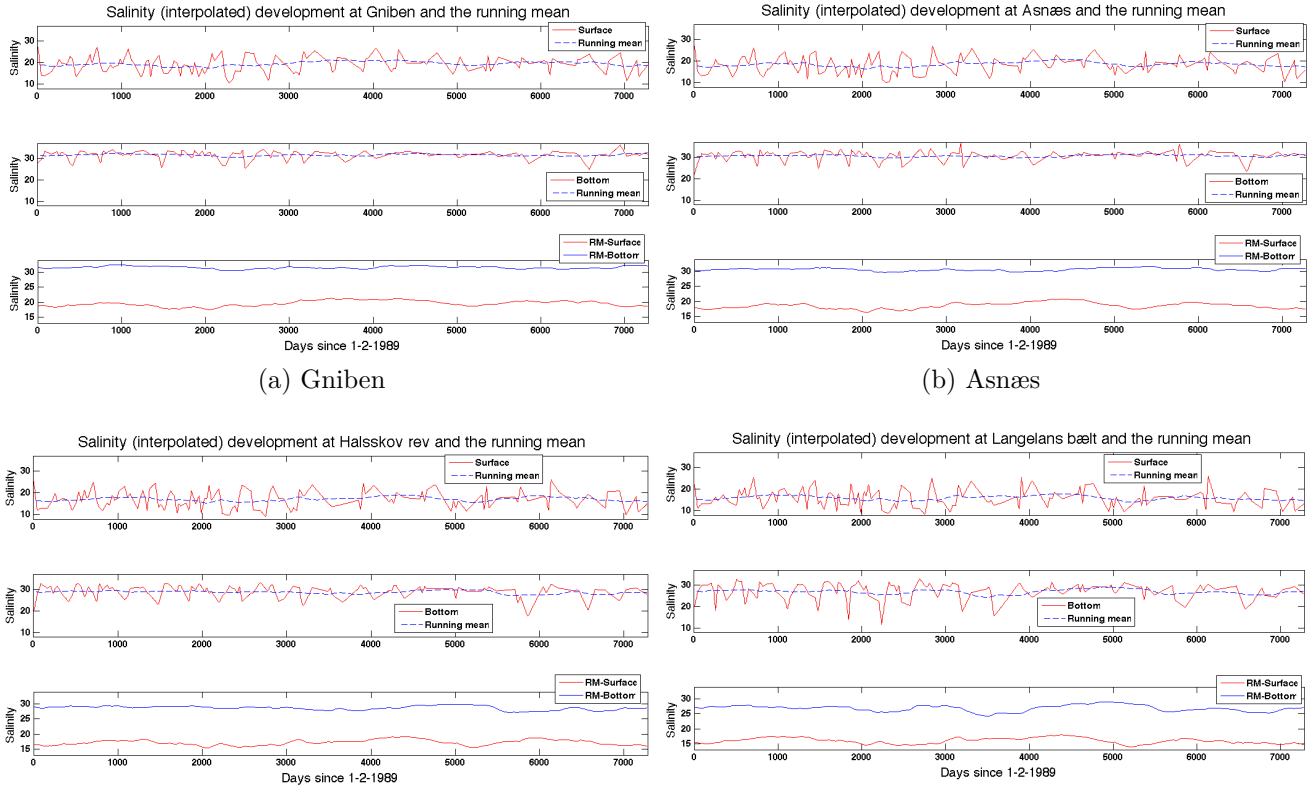

(a) Gniben (b) Asnæs

(c) Halsskov rev (d) Langelands bugt

Figure 21: Comparison of the original, interpolated salinity time series in the surface (top) and bottom (middle) layer and the corresponding one year running averages (bottom) at the four monitoring stations.

A more detailed summary for all stations at each respective layer is shown in Figure 22.
The most prominent long-term signal at all stations is a salinity cycle with a period of approximately 7 years. There are clear regional differences both in absolute salinities associated with the typical North-South salinity gradient and the temporal evolution of peak values. However, the

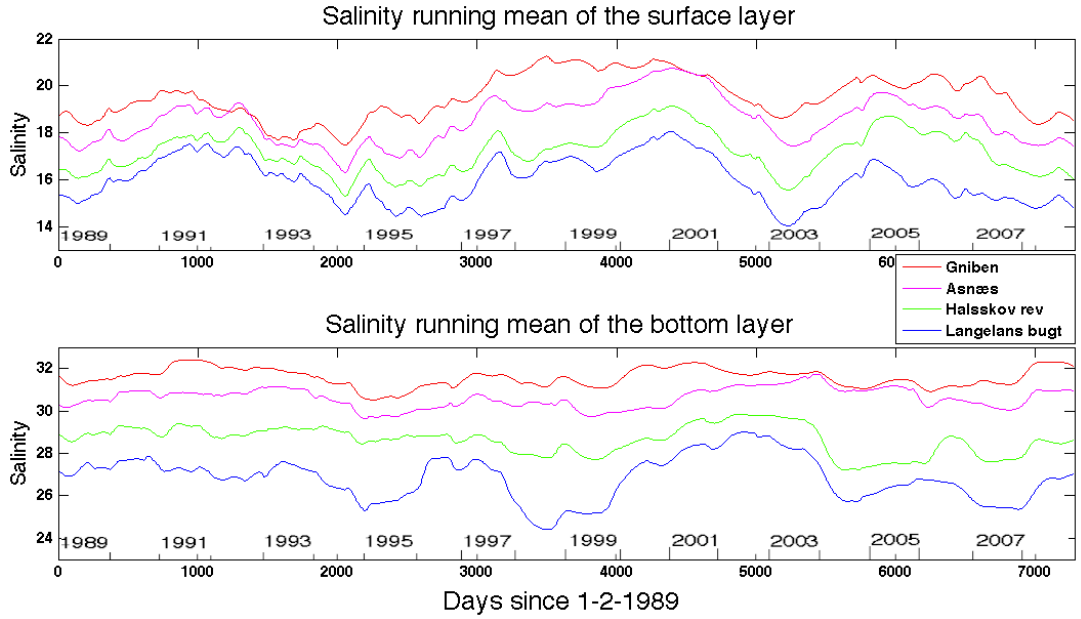

Figure 22: The running mean of the salinity of all stations

oscillation pattern is spatially independent, i.e. salinity fluctuations are in phase at all stations over the full observation period. A similar spatially consistent oscillation pattern is not seen in the bottom salinities. In fact, there are strong station to station differences with the largest bottom salinity variations observed at the southernmost stations. A fast increase in the surface layers of 1.25 PSU over a 200 day period appears around day 2000 to 2200 (in the years 1994-1995), thereafter decreases again over the same number of days. A similar pattern appears again from day 3000 to 3150 (1997-1998), when salinity increases by 1.5 PSU and drops again over the next ∼150days. There are also a change in horizontal gradient or the offset between the station eg. the variations between the stations are smaller in the surface in the years 1992-1993 than from 1998-2008.

As for temperature, I have carried out a linear trend analysis for both surface and bottom salinity time series. The result is shown in Figure 23.

The linear regression of the salinity shows no clear general trend in combination with a poor goodness-of-fit throughout the time series. At all stations, less than 13% of the variability can be explained by a general linear trend. In addition, the calculated trends are inconsistent. In the surface layer, salinities increase over the 20 years at three of the stations by 0.66 PSU (Gniben), 0.3 PSU (Asnæs), 0.2 PSU (Halsskov Rev), and decreases by 0.9 PSU (Langelands Bælt). In the bottom layer, the regression analysis predicts no significant linear salinity trend at Gniben and Asnæs, but a significant decrease of 1.0 PSU over the 20 year observation period at both Halsskov Rev and Langelands Bælt. As a result it can be concluded that either (i) there is no significant long-term trend in salinity, (ii) a linear regression is not a suitable tool to identify trends due to the symmetric oscillatory structure of the data or, (iii) it is actually significant, and the horizontal gradient has become stronger.

(a) The stations

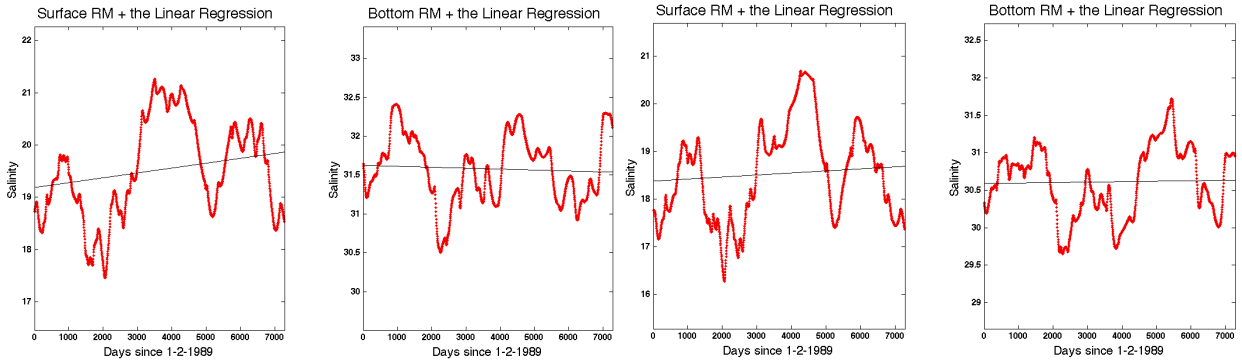

(b) Gniben: R_a^2=0.128, R_b^2=0.002 (c) Asnæs: R_a^2=0.063, R_b^2=0.023

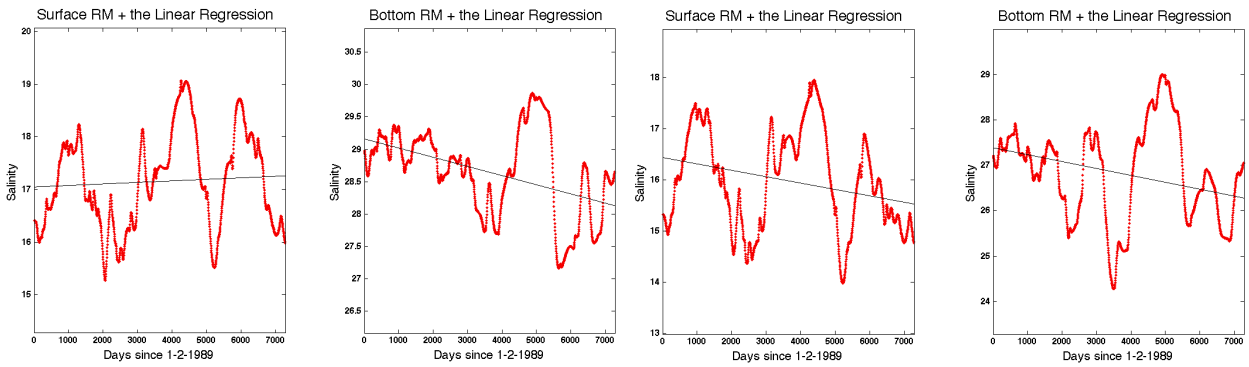

(d) Halsskov Rev: R_a^2=0.037, R_b^2=0.164 (e) Langelands bælt: R_a^2=0.042, R_b^2=0.023

Figure 23: The salinity surface and bottom layers running mean (RM) with a linear regression.

4 Data analysis of Hatter Barn

In this chapter, short-term variations of temperature and salinity at two locations at Hatter Barn are analyzed based on in-situ observations over a period of three months in 2010. The physical environment at the Hatter Barn reef is exposed to a combination of tidal flow, local weather conditions and large-scale currents regularly affecting the whole water column due to shallow water depths not exceeding 20 m. In addition, Hatter Barn is surrounded by one of the most heavily used shipping routes worldwide, with 26000 ships above 300 tons passing the area in 2010 [Mortensen et al. (2011)], [HELCOM]. Ship generated waves and associated currents may have a secondary influence on the local hydrodynamics at the reef by adding high-frequency variations of temperature, salinity and sea level [Davis et al. (2009)]. These variations correspond to an artificially increased and transient vertical mixing. Ship signatures in the temperature and salinity time series are analyzed and compared with underwater noise measurements at Hatter Barn from the same period [Mortensen et al. (2011)].

4.1 Hatter Barn in-situ observations

Two Seabird MicroCAT profilers, measuring temperature and conductivity, were deployed by the Department of Bioscience, Aarhus University, from May 2010 to September 2010 at the newly discovered boulder reef Hatter Barn. The measurements were of the activities within the EU INTERREG BaltSeaPlan project (www.baltseaplan.eu). Each profiler was mounted on a mooring line and anchored two meters above the seabed at the fixed positions listed in Tabel 3 and shown in Figure 24.

Stations	Coordinats	Period: From/To	Depth
Hatter Barn 1	$10^o49'43.92"E$ $55^o52'17.85"N$	27. May. 2010 28. Aug. 2010	13 [m]
Hatter Barn 2	$10^o49'38.40"E$ $55^o52'17.82"N$	27. May. 2010 28. Aug. 2010	15.5 [m]

Table 3: Positions, collection periods and depth from two sampling locations at Hatter Barn.

The two mooring stations had a distance of approximately 100 m from each other and data was collected every minute. The MicroCAT profilers were located at different depths (as listed in Tabel 3) in order to sample a shallow and deeper part of the reef. The initial accuracy of these profilers is 0.0003 S/m (0.003 mS/cm) for the conductivity and 0.002^oC for the temperature [MicroCAT 2011]. After the recovery, a post-cruise calibration of the sensors was carried out to determine possible a sensor drift and the data was corrected accordingly.
The observed data were later compared with tidal data. Information on high and low tide from the port at Aarhus was obtained from the Danish Maritime Safety Administration [DaMSA]. Data from Aarhus was chosen, because it was the closest location to the observed sampling sites at

Figure 24: Geographical location of the two Hattar Barn stations in the Kattegat.

Hatter Barn. Potential impacts arising from atmospheric conditions were analyzed using wind observations from the Danish Meteorological Institute (DMI). DMI operates a weather station named Gniben at the following location: $56^o00'0"N$ and $11^o16'8"E$ (see Figure 25 for map illustration) and the data are collected every hour.

Figure 25: Location of the Hatter Barn moorings and the weather station Gniben.

4.2 Results of the Hatter Barn observations

From conductivity, temperature and pressure, the salinity was calculated (practical salinity, PSU). The time series of salinity and temperature at the two stations at Hatter Barn (HB1 and HB2 in the figures) are plotted in Figure 26.

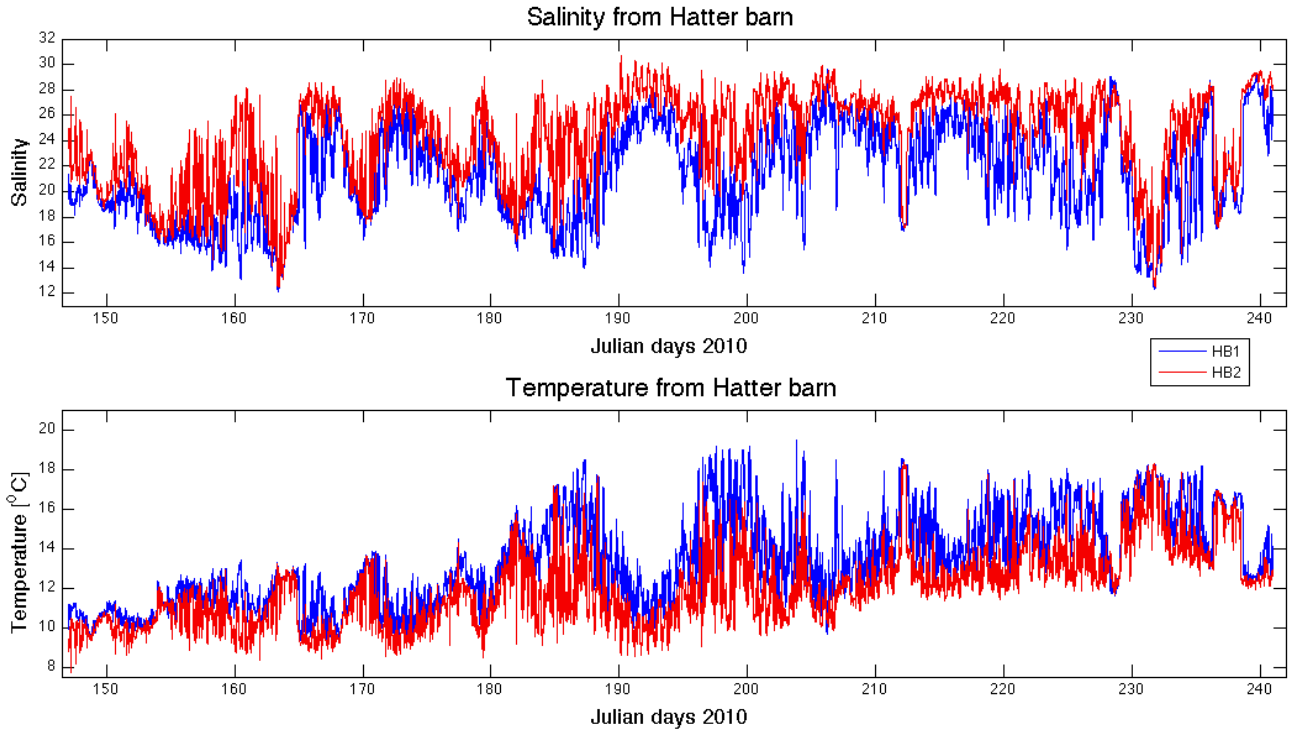

Figure 26: Salinity and temperature from Hatter Barn from Julian day 147 to 241 (27^{th} May to 28^{th} August 2010).

A first comparison of the two Hatter Barn data sets reveals an offset in both temperature and salinity. This offset results in generally higher temperature (average 1.58^{o}C) and lower salinity (average 3.25 PSU) at the shallower station HB1. This large temperature and salinity offset between the two stations develops as a consequence of the difference in water depth (2.5 m) in combination with the strong vertical gradients of both parameters within the thermocline and halocline in the Kattegat (see for example Figures 13, 14 a and b in Section 3.1.1).
The fluctuations within each time series are very large and some occur over a relatively short period of time. The minimum and maximum values for salinity over the observed 94 days at the two stations are $HB1_{min}$=12.2 PSU, $HB1_{max}$=29.6 PSU, $HB2_{min}$=12.5 PSU and $HB2_{max}$=30.7 PSU. The temperature shows a significant seasonal signal rising towards a summer maximum. The net increase of temperature at both stations is 4.9^{o}C over the full sampling period. The strongest changes in both salinity and temperature can be observed at day 188 (7^{th} July 2010) where the temperature drops by 9^{o}C over a period of two and a half days, afterwards increasing again by the same amount over the next 6 days. In the same period, salinity changes of ± 12 PSU

can be observed.
Temperature and salinity fluctuations can also develop much faster as it can be seen in Figure 27. The figure presents a short period of 2 days. Here the salinity changes by ± 10 PSU within a period of several minutes around day 165.5 (noon 14^{th} June 2010) at the HB1 time series. The

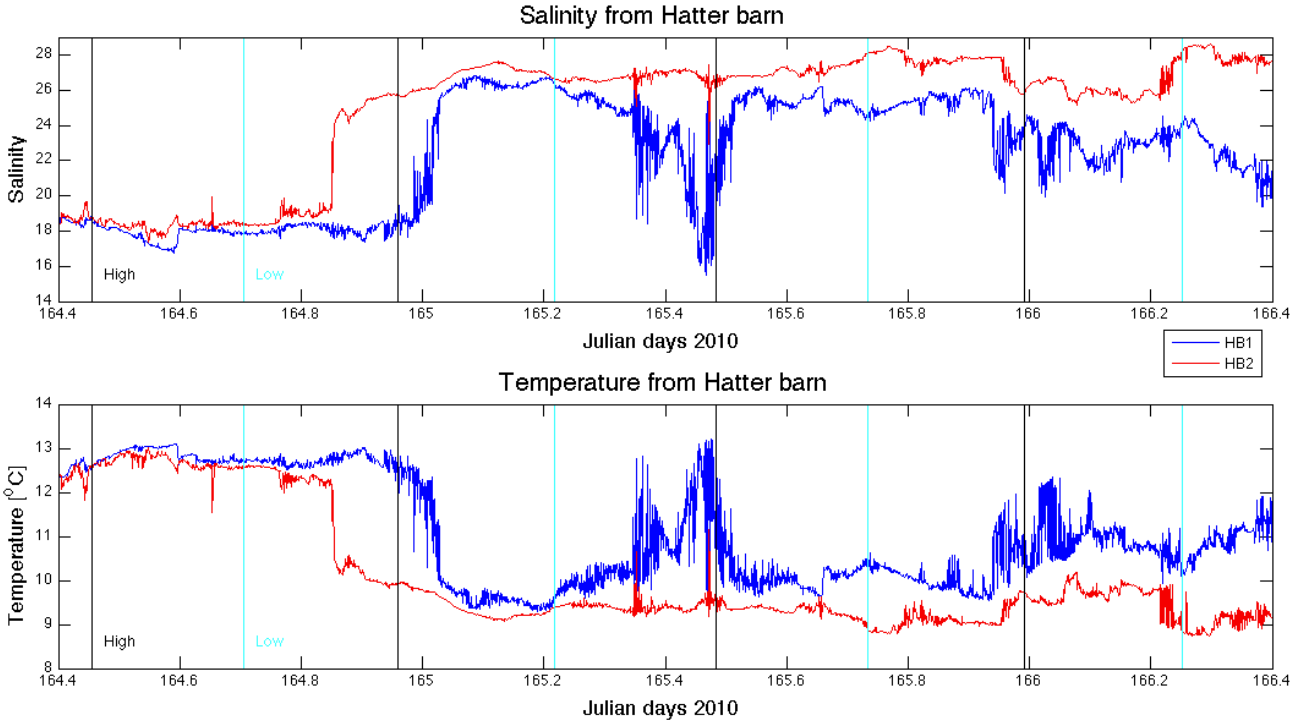

Figure 27: Salinity and temperature from Hatter Barn, extracted for the period Julian day 164.4 to 166.4 (noon on the 13^{th} June 2010 to noon 15^{th} June 2010).

extracted 2 day period also shows that such events are not necessarily happening at the same time and magnitude at both mooring locations. Another event is visible at the beginning of the 14^{th} June 2010 (Julian day 165) with an increase in salinity of around 8 PSU in the data from station HB1. A corresponding salinity signal at station HB2 can be found at around 21:00 of the 13^{th} June 2010 (Julian day 164.8). A decrease of 2-3^{o}C is visible in the temperature time series at the same time. In this 2 day plot the salinity and temperature fluctuations at station HB1 are generally much larger than the changes at the deeper station HB2.
However, this is not the case during other periods in time series. In Figure 27, the times of the high and low tide at Aarhus harbour [DaMSA] are presented (vertical lines in Figure 27, black = high tide, blue = low tide) to show that there are no temperature and salinity variations due to tides in this particular period. In contrast, temperature and salinity fluctuations with a semi-diurnal period are clearly visible in Figure 28 at both stations HB1 and HB2 between the 4^{th} July 2010 (Julian day 185) and the 7^{th} July 2010 (Julian day 189). Periodic salinity oscillations of approximately ± 5 PSU were observed (Figure 28).
These changes are most likely generated by the dominant semi-diurnal tide at this period in the

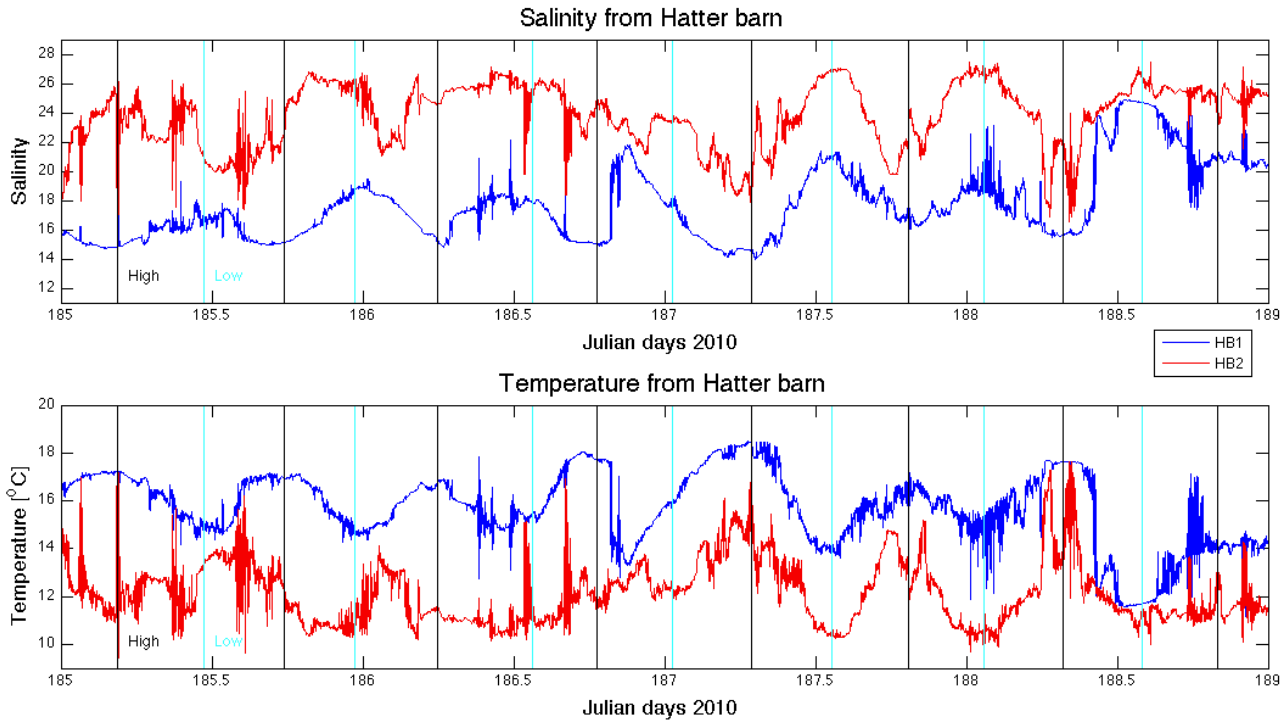

Figure 28: Salinity and temperature from Hatter Barn, extracted for the period Julian day 185 to 189 (4^{th} July 2010 to 7^{th} July 2010).

Hatter Barn area. Changes in tidal height at Aarhus harbour are only 0.1-0.3 meters in magnitude, but tidal currents at Hatter Barn may increase with decreasing water depth. This is confirmed by Equation (4) in Section 2.2 which demonstrates that the tidal current will increase with decreasing water depth, even if the amplitude of the tidal wave stays constant. Short-term, high frequency events (as seen in Figure 27) are also visible in Figure 28 and are superimposed to the longer period tidal oscillations. The tidally induced oscillations at stations HB1 and HB2 appear almost depth independent in magnitude and phase. However, the short-term fluctuations are spatially and temporally inconsistent which was also observed at other periods (see Figure 27).

4.2.1 Wind impact

To analyze the observed fluctuations at Hatter Barn in more detail, a comparison with local wind conditions was carried out. The wind observations are at one hour intervals and were taken from DMI's weather station Gniben (see Figure 25). The wind observations are shown together with the salinity time series from the Hatter Barn stations in Figure 29. Only the salinity is shown here, because the temperature follows the same variability pattern.
A comparison of wind speed and salinity indicates that an increase of wind speeds to values ≥ 10 m/s (represented by the red horizontal line in Figure 29 c) at the Gniben station is connected with a decrease in salinity at Hatter Barn. This seems to be a consistent pattern throughout the whole

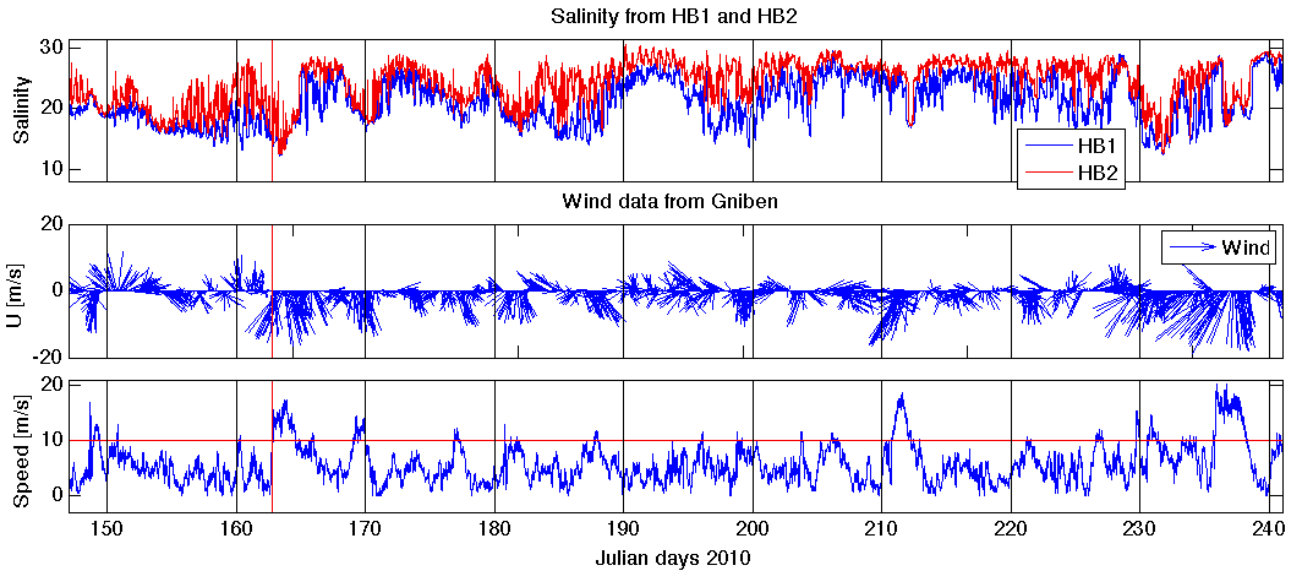

Figure 29: (a) Salinity from both Hatter Barn stations, (b) stick plot of the wind, shown as a combination of wind direction and speed, (c) wind speed. The horizontal red line in (c) indicates a wind speed of 10 m/s. The vertical red lines at Julian day 163 indicate the onset of a strong wind event.

observation period. There are two possible mechanisms to explain this connection. First, salinity decreases as a consequence of local wind induced vertical mixing of low saline surface waters into the water column. Secondly, the wind field influences the near surface currents to bring more saline surface waters from the Kattegat southward to Hatter Barn through wind induced horizontal advection events. This second aspect is discussed in more detail in the next section. Therefore, wind speed can explain most of the longer period fluctuations in the observed salinity data. In contrast, there is no clear evidence that the wind direction has a comparable direct impact on the salinity levels. The strong change in salinity seen around day 188 does not appear to be controlled directly by wind direction, as the wind direction is very variable in the period between Julian day 188 and 195 (see Figure 29 b). Nor can the wind observations explain the high frequent peaks e.g. at day 165 (Figure 27).

4.3 Currents

Currents in the area surrounding Hatter Barn were investigated by using data from a three-dimensional ocean circulation model for the Baltic Sea. Temperature and salinity time series of model data were first compared with the observed data to determine the model skill. Modeled currents were then used to describe the flow conditions in the Hatter Barn area during the observation period.

4.3.1 Model description

Direct measurements of currents in combination with the MicroCAT temperature and salinity survey at Hatter Barn were not carried out due to the absence of instrumentation. In order to compare the observed variability patterns in the Hatter Barn temperature and salinity time series with variations in the flow field, it was therefore necessary to extract such data from available hydrodynamic models. The EU FP7 project MyOcean (www.myocean.eu) provides hydrodynamic model and remote sensing data products for all European Seas including the Baltic Sea, Skagerrak, Kattegat and the Belt Sea. The main purpose of MyOcean is to support the scientific community with important and well tested environmental data on temperature, salinity, currents, sea level, sea ice and primary ecosystem characteristics for the purpose of marine safety, seasonal and climate forecasting, and studying the coastal and marine environment. Data are available from the starting period of the project (2009) and are updated regularly. MyOcean modeling data are created by different hydrodynamic models for different European Seas. The Baltic Sea physical model is based on the Baltic Sea community model code HBM (HIROMB-BOOS Model, see [Funkquist & Kleine (2007)] for further details). The DMI version of the HBM model is forced with meteorological data from the DMI-HIRLAM S05 atmospheric model with a horizontal resolution of 5 km. Boundary forcing is provided through surge models and climatologies for temperature and salinity. River runoff data is provided by the operational hydrological model of SMHI [Bergström (1992)]. The V0 version of the MyOcean Baltic Sea product of the model is used here which covers the period from 08/2009 to 09/2011. The horizontal resolution is approximately 3 nautical miles (0.0833 degrees) and the temporal resolution is every hour. The V0 Baltic Sea model product offers data at five vertical depth levels (4m, 9m, 51m, 96m and 175m) [MyOcean]. To compare the model data with the observations at Hatter Barn, I extracted the modeled temperature, salinity and currents from the 9m depth level within an array of 5 model grid points closest to Hatter Barn (see Figure 30 and Table 4).

(a) (b)

Figure 30: Geographical location of the two Hatter Barn and five MyOcean model grid points in the Kattegat. (a) The Hatter Barn stations (green) and MyOcean points (yellow), (b) zoomed.

Grid points	Coordinates
MyO1	$10^o52'50"E$ $55^o55'5"N$
MyO2	$10^o57'49.80"E$ $55^o55'5"N$
MyO3	$10^o47'50.20"E$ $55^o52'5"N$
MyO4	$10^o52'5"E$ $55^o52'5N$
MyO5	$10^o47'18.15"E$ $55^o49'5"N$

Table 4: Positions and name of the five MyOcean grid points.

The 9m depth level is the best available match to the MicroCAT sampling depths (13m and 15.5m) at Hatter Barn.

4.3.2 Model-data comparison

The modeled temperature and salinity data were used for validating the time series of the model in comparison with the observations (shown in Figure 31). Only one station from the Hatter Barn observations (HB1) and two MyOcean stations are compared for a better clarity. The two chosen data sets from the MyOcean model are MyO3 and MyO4 which are located next to the Hatter Barn sampling stations.

The model data and the observed data are largely following the same variability pattern. There is a clear offset of 6.3 PSU and 2.5^{o}C in average between model and observations which, for the most part, can be explained by the depth differences. The absolute and daily variations in temperature and salinity are higher in the observed than the modeled data. The model does not reproduce some of the strong peaks visible in the observations. As an example, the strong salinity increase during the 2 day period from day 164.4 to 166.4 is clearly underestimated by the model (Figure 32). At Julian day 165, the modeled salinity also shows a moderate increase of approximately 4 PSU, but it is not able to reproduce the observed magnitude of 10 PSU. Both modeled and observed salinities show reduced tidal influence in this period when compared to other periods (see for example Figure 33). It is also important to note, that the modeled salinity does not show the strong short-period salinity fluctuations between Julian days 165.3 and 165.6 and elsewhere, partly because of the differences in temporal resolution. In the 4 day period between Julian days 185 and 189 (Figure 33), model and data show a good agreement in the phase of the tidal signal and in the relative changes of the tidal oscillations.

The absolute changes of tidal fluctuations are again higher in the observed data which again can partly be explained by the presence of stronger temperature and salinity gradients at the depth of the observations. The observed short-period fluctuations, superimposed to the tidal signal, are

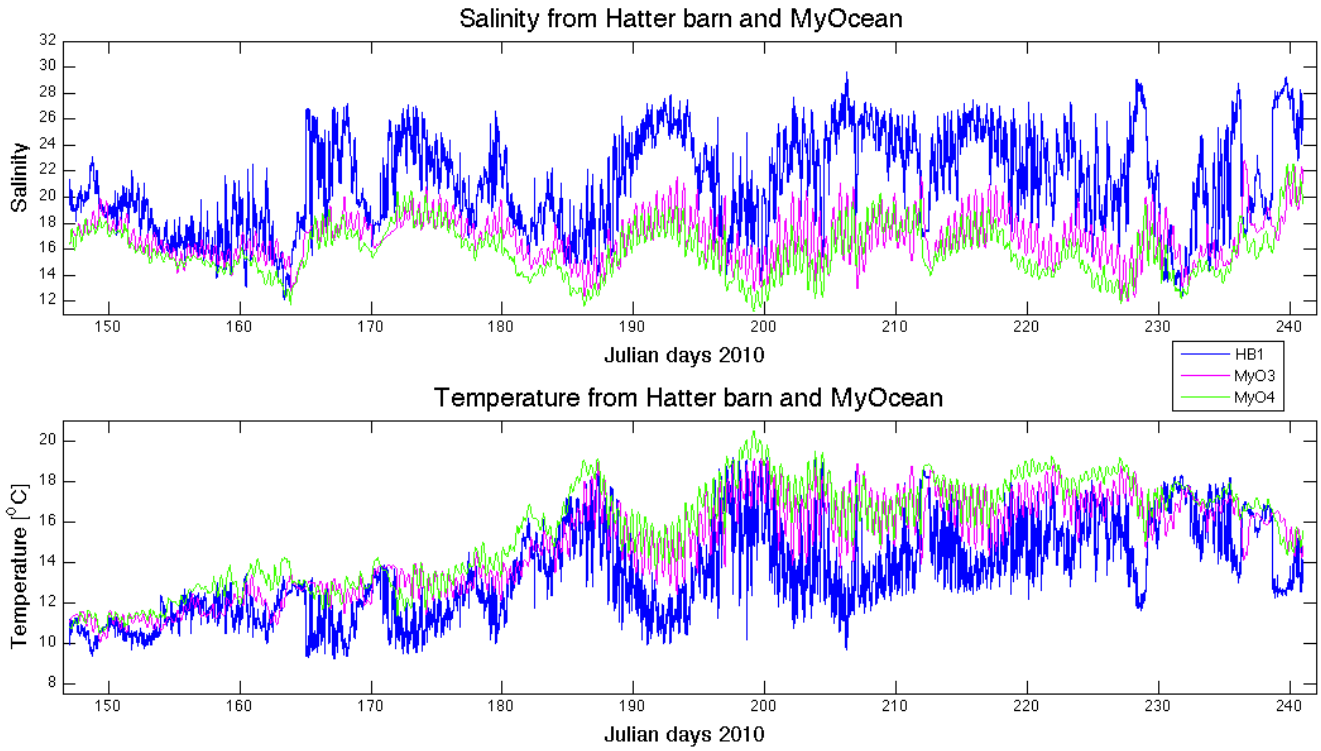

Figure 31: Salinity and temperature from Hatter Barn and two MyOcean locations.

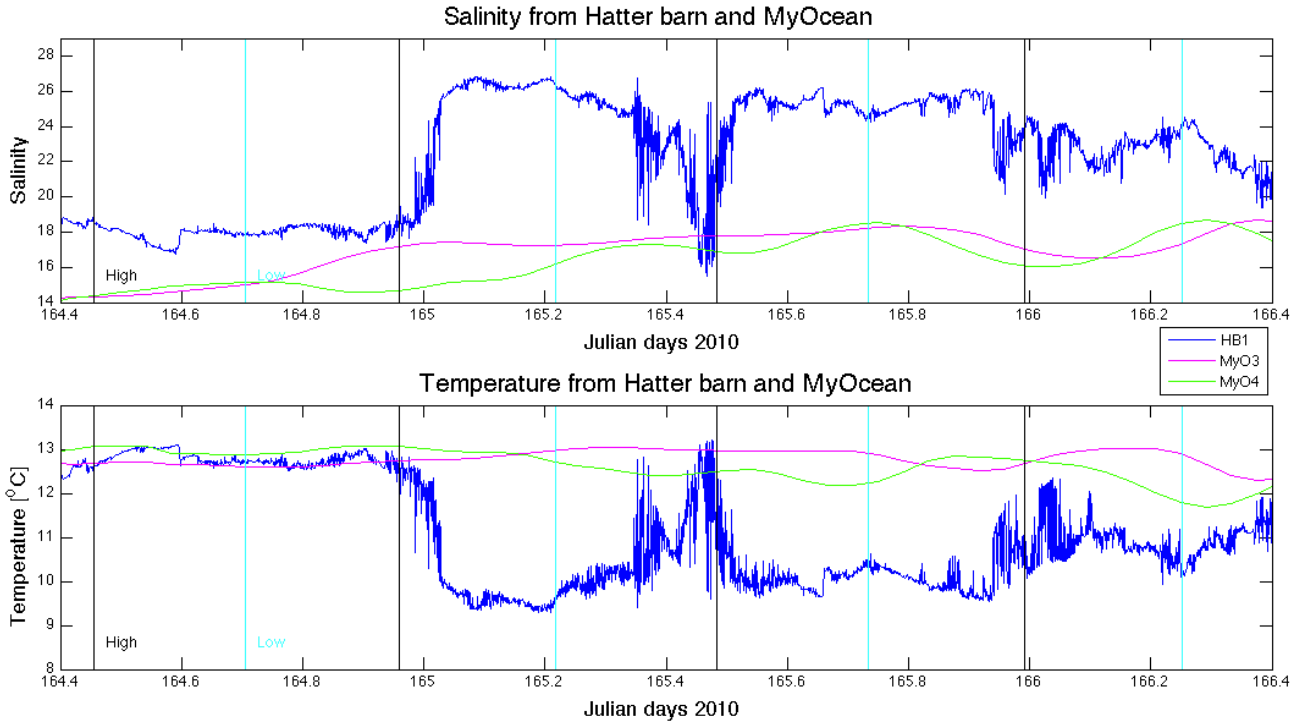

Figure 32: Salinity and temperature from Hatter Barn and MyOcean, extracted for the 2 day period Julian day 164.4 to 166.4 (starting at the 13^{th} June 2010).

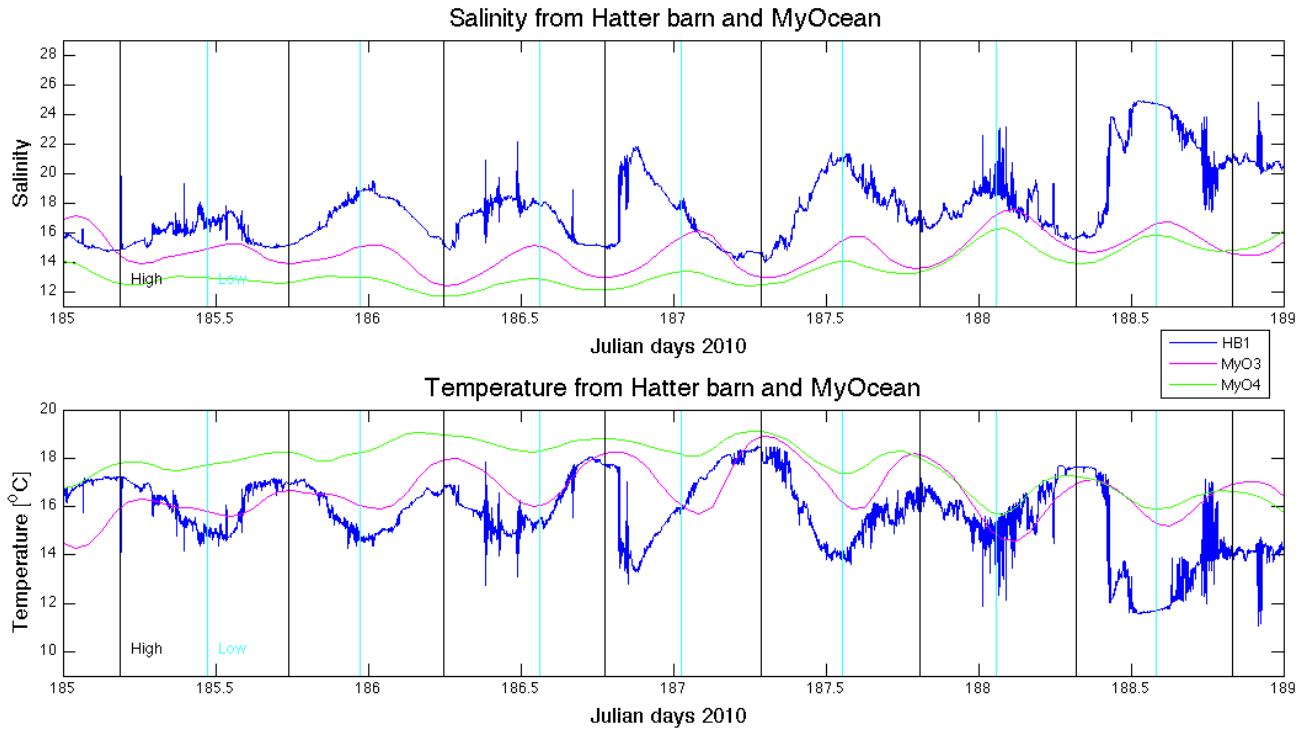

Figure 33: Salinity and temperature from Hatter Barn and MyOcean, extracted for the 4 day period Julian day 185 to 189 (starting at the 4^{th} July 2010).

again not reproduced by the model. This might be a consequence of the lower temporal resolution of the model output of one hour compared to one minute in the observations.
In Figure 46 in Appendix C a period from day 160 to 172 is shown to demonstrate the presence weak or almost absent tidal effects. In the period from Julian day 160 to 172 there are two events with small or no tidal effects, both lasting approximately two days. There are 4-5 periods in the observed 94 days where weak tidal effects can be observed. Figure 47 in Appendix C shows that there also are times when tidal activity causes major fluctuations in the salinity and temperature. In this period temperature shifts of 7^oC and salinity shifts of 7.25 PSU over one tidal cycle can be found. In summary, the model-data comparison showed fair qualitative similarity on longer time scales between model and observations considering the available depth levels. It is therefore justified, to use the model results for an interpretation of currents and potential forcing mechanisms.

4.3.3 Description of currents and potential forcing mechanisms

The currents from the MyOcean model locations at 9 m depth are shown in Figure 34. The near-surface circulation close to Hatter Barn is dominated by north- and northeastward flow contributing to the mean outflow of Kattegat surface water (e.g. [Danielssen et al. (1997)]). The periods of northward flow are occasionally interrupted by extended periods of reversed flow to the

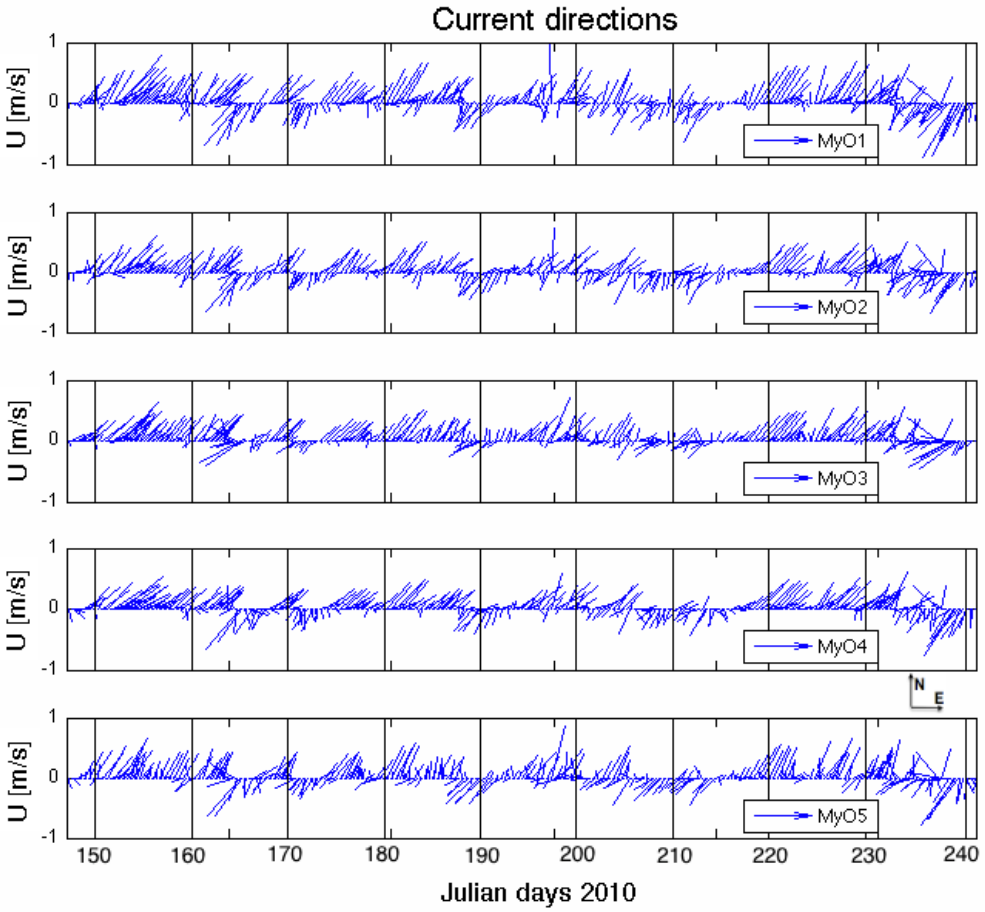

Figure 34: Stick plot of modeled currents at 9 m depth at each MyOcean station..

southwest. Changes in flow magnitude and direction between the five locations appear to be small suggesting little spatial variation in areas surrounding Hatter Barn.

However, if the Eulerian time series are used to simulate a Lagrangian flow, spatial differences become more obvious. The Eulerian view describes the flow at specific location as a function of time, whereas the Lagrangian view describes the flow of an individual fluid parcel as a function of space and time. This was done by constructing progressive vector diagrams (PVDs) from the individual time series at each location.

The current vector components (u,v) are used to calculate the distance of each current vector relative to each other in a Cartesian grid and are converted to space units (km). Each vector starts at the end of the previous one. The transformation into space units is calculated for each velocity component according to $\Delta X = U * \Delta T$, where ΔX is the travel distance of a water particle, $U(u, v)$ is the speed in each direction, ΔT is the measurement interval. The resulting PVD shows the movement of a water particle under the assumption that the current does not change wherever the water particle is moving. Figure 35 shows the PVDs for the five MyOcean

stations indicating how a water particle would travel from each of the five stations. The three most

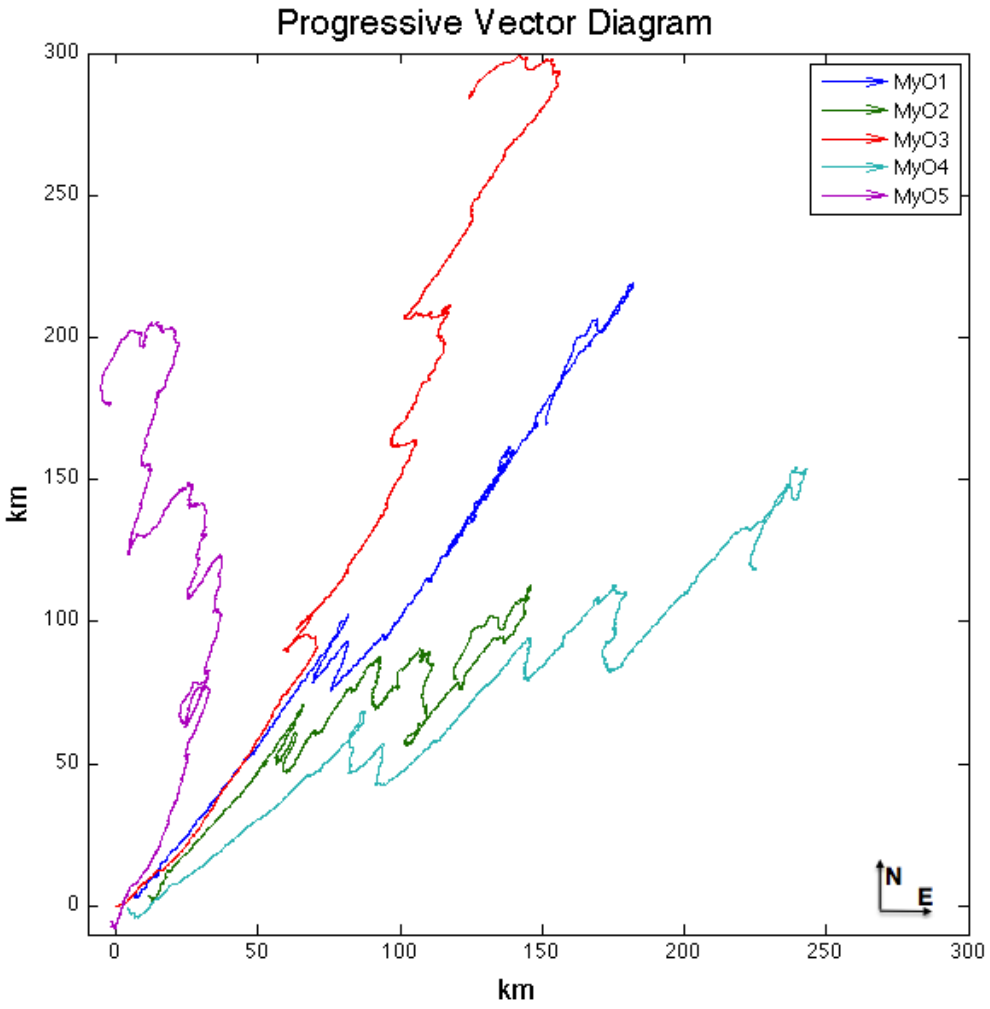

Figure 35: Progressive vector diagrams (PVDs), showing the simulated flow pattern of an individual water particle at each MyOcean station (Lagrangian view).

westerly stations MyO1, MyO3, and MyO5 are located close or within the deep water shipping channel which passes Hatter Barn to the west and northwest (see Figure 9 for an overview). At these stations, the flow shows a stronger tendency to move northward, especially at station MyO3. In contrast, the flow at the stations east of Hatter Barn (MyO2, MyO4) is directed more eastward. It also shows more frequent flow reversals suggesting longer residence times of near surface waters in this area. The differences between the areas west and east of Hatter Barn might be a result of topographic steering of the flow west of Hatter Barn as a result of the steeper topographic slope acting as a barrier and flow guide for waters impinging at Hatter Barn from the west. The shallower stations east of Hatter Barn show a stronger variability, because they are more exposed to wind and surface mixing.

A comparison of model currents at MyO4 with observed temperature and salinity from the Hatter Barn measurements is shown in Figure 36.

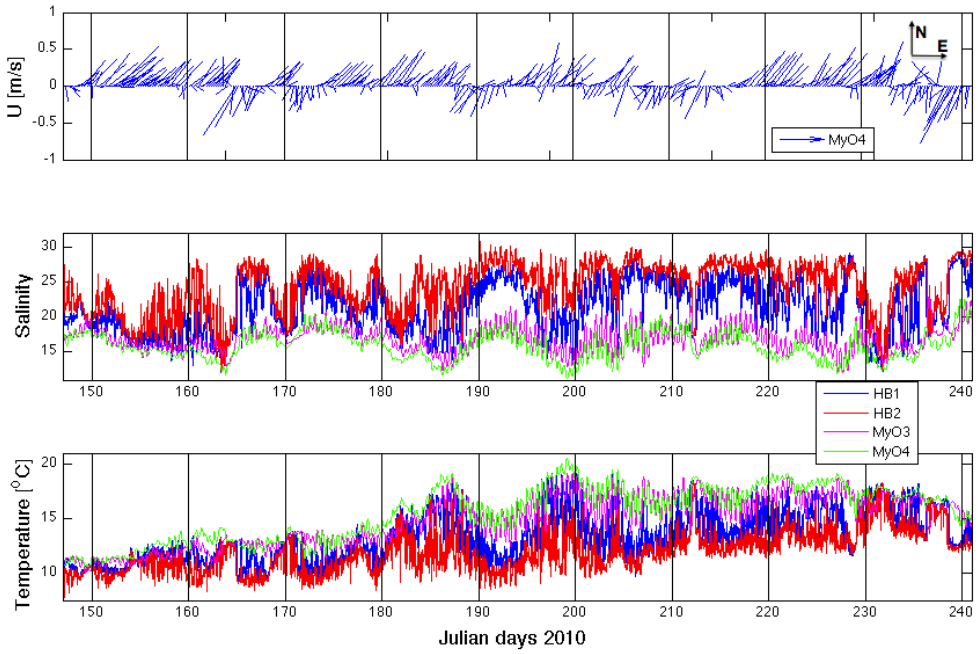

Figure 36: Comparison of modelled flow with observed salinity and temperature at Hatter Barn. (a) Modelled currents at 9 m depth from the MyO4 model station. (b+c) Observed (blue, red) from Hatter Barn 1 and 2 and modelled (magenta, green) from MyO 3 and 4.

A comparison of model currents at MyO4 with observed temperature and salinity from the Hatter Barn measurements is shown in Figure 36. MyO4 was chosen, because it is the nearest model station with a comparable water depth to Hatter Barn. Figure 36 shows that events of flow reversal from northeastward to southwestward flow coincide with a transition from low to high salinity. This is particularly the case in the periods from Julian day 165 to 168 and 187 to 193 (Figure 36 a and b). It is interesting to note that these events are also visible in the modelled salinities, but with a much smaller response in salinity partly due to the shallower water depth of the model time series. These events of occasional flow reversal can also be seen at other MyOcean stations further north. This indicates that waters of increased salinity at Hatter Barn might have their source in waters further north during periods of flow reversal, rather than being only or mostly driven by local wind effects.

4.4 Sound observations

A study of possible detrimental effects of man-made underwater noise on marine ecosystems was conducted between 4^{th} December 2009 and 24^{th} August 2010 as part of the EU INTERREG project BaltSeaPlan (www.baltseaplan.eu). The ship noise was measured in five areas along the main shipping route through the Great Belt close to Hatter Barn and along fast ferry lanes across the Great Belt (Figure 37). Five stations were established in each area, with each station containing a DSG noise logger (Loggerhead Instruments, Sarasota, Florida) for recording noise and a T-POD version 5 (Chelonia Limited, U.K.) recording harbour porpoise vocalisation.

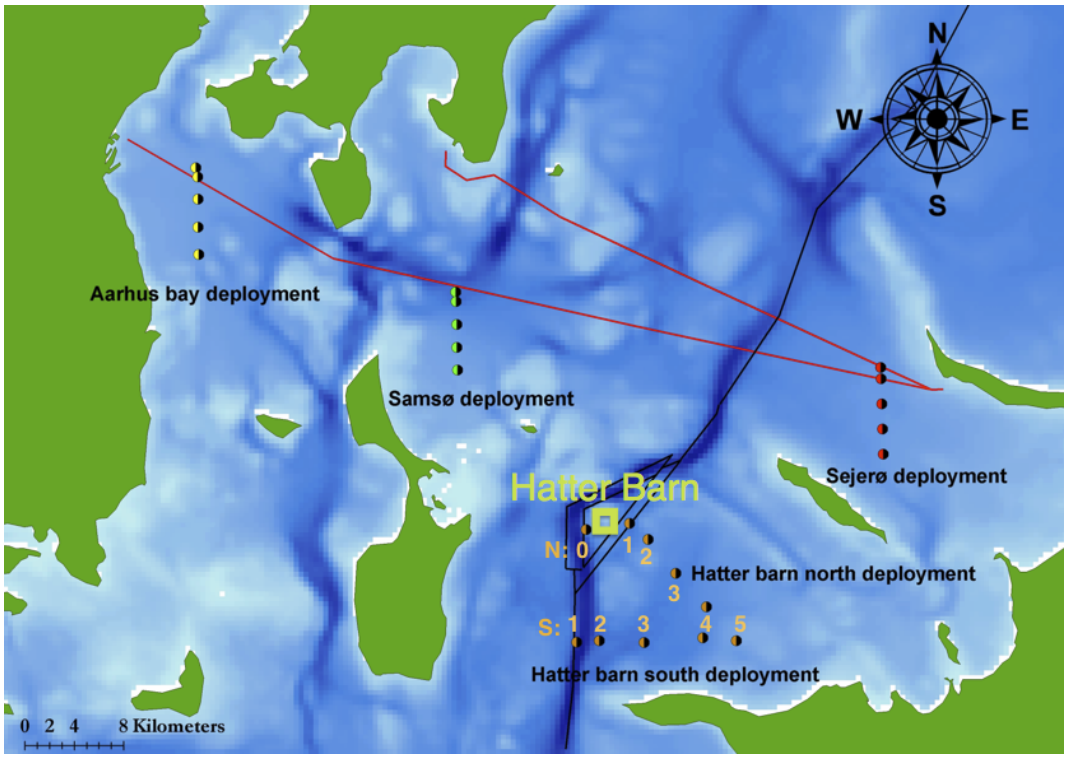

Figure 37: Map showing deployment sights (dots), fast ferry route (red line), the Hatter barn area of the T-route (black line), Hatter Barn temperature and salinity observations (green box) The figure is from [Mortensen et al. (2011)], but with modifications.

The experimental setup is described in detail in [Mortensen et al. (2011)]. Each area contains one station in the center of the shipping lane. The remaining stations were deployed along a line perpendicular to the shipping lane. Underwater noise was measured by DSG-dataloggers. The DSG logger system consists of a sensitive hydrophone and a data acquisition facility operating at sampling frequency of 50.000 Hz. The logger operates within the frequency band 25 Hz to 16 kHz, there are measured 10 seconds every 2 minutes throughout the day [Mortensen et al. (2011)].
The peak energy from underwater shipping noise is typically at low frequencies within the band 63 Hz to 125 Hz in this area. Due to the large amount of noise recordings, sound data were not continuously available over the whole time period of the Hatter Barn temperature and salinity

observations. Salinity and temperature data from Hatter Barn were compared with sound observations at two stations close to Hatter Barn, N0 and N2 (see Figure 37) to look for wave indused mixing. N0 covered the period from Julian day 209 to 218 (28^{th} July - 6^{th} August 2010), station N1 did not collect any useful data during the study period and N2 recorded data from Julian day 209 to 230 (28^{th} July-18^{th} August 2010). The rest of the stations were not analyzed, because they were too far away from the reef. In Figure 38, the underwater noise levels at stations N0 and N2 are presented together with temperature records from Hatter Barn and wind data from the Gniben station for the period from Julian day 209-211. Only noise measurements in the frequency band from 25 Hz-630 Hz are presented. The black horizontal lines in the noise level contour maps are encompassing the 63 Hz and 125 Hz frequencies, where the strongest signal from commercial ships can be expected. The units of the noise level is in decibel (dB), but due to the physical differences between air and water, noise level in water is not comparable to conditions in air and can therefore only be used as a relative measure. A visual comparison of noise events from shipping activity with the temperature records from Hatter Barn indicates that there is a connection between ship traffic and the occurrence of high-frequency fluctuations in temperature and salinity (see Figures 32 and 38). Typical periods of such oscillations are below 10 minutes. The strongest continuous period of shipping activity and potential temperature response can be seen between Julian day 210.4 and 211 with typical temperature oscillation amplitudes of 2^oC (Figure 38). Figure 39 shows the temperature and noise distribution over next two days (211-213). In this period, strong wind conditions dominate the oceanic regime and short-term temperature oscillations are weak or entirely absent. The remaining noise data from the N0 and N2 stations are shown in Figure 48-56 Appendix D. This first visual examination of possible effects of shipping activity on oceanic variability demonstrates the potential importance of artificial, i.e. man-made mixing for this particular area. A more systematic approach is required, however, to obtain a more robust picture of the oceanic response to ship traffic and ecological implications. Some of the challenges and difficulties of such a systematic comparison are discussed in Chapter 5.2.1.

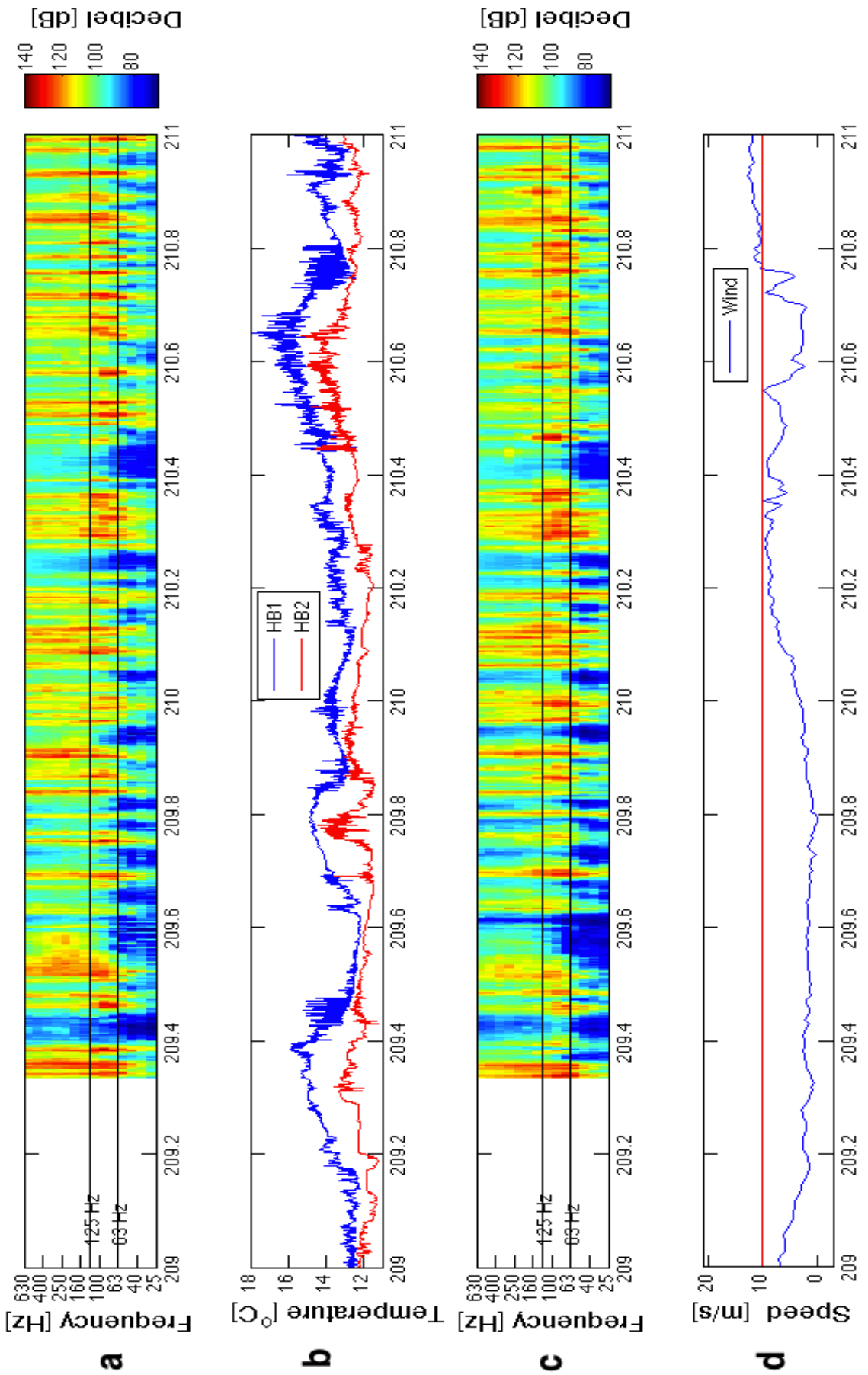

Figure 38: Observations from Julian day 209-211: (a) Underwater noise levels at sound station N0, (b) temperature from Hatter Barn, (c) underwater noise levels at sound station N2 and (d) wind observations at the Gniben station.

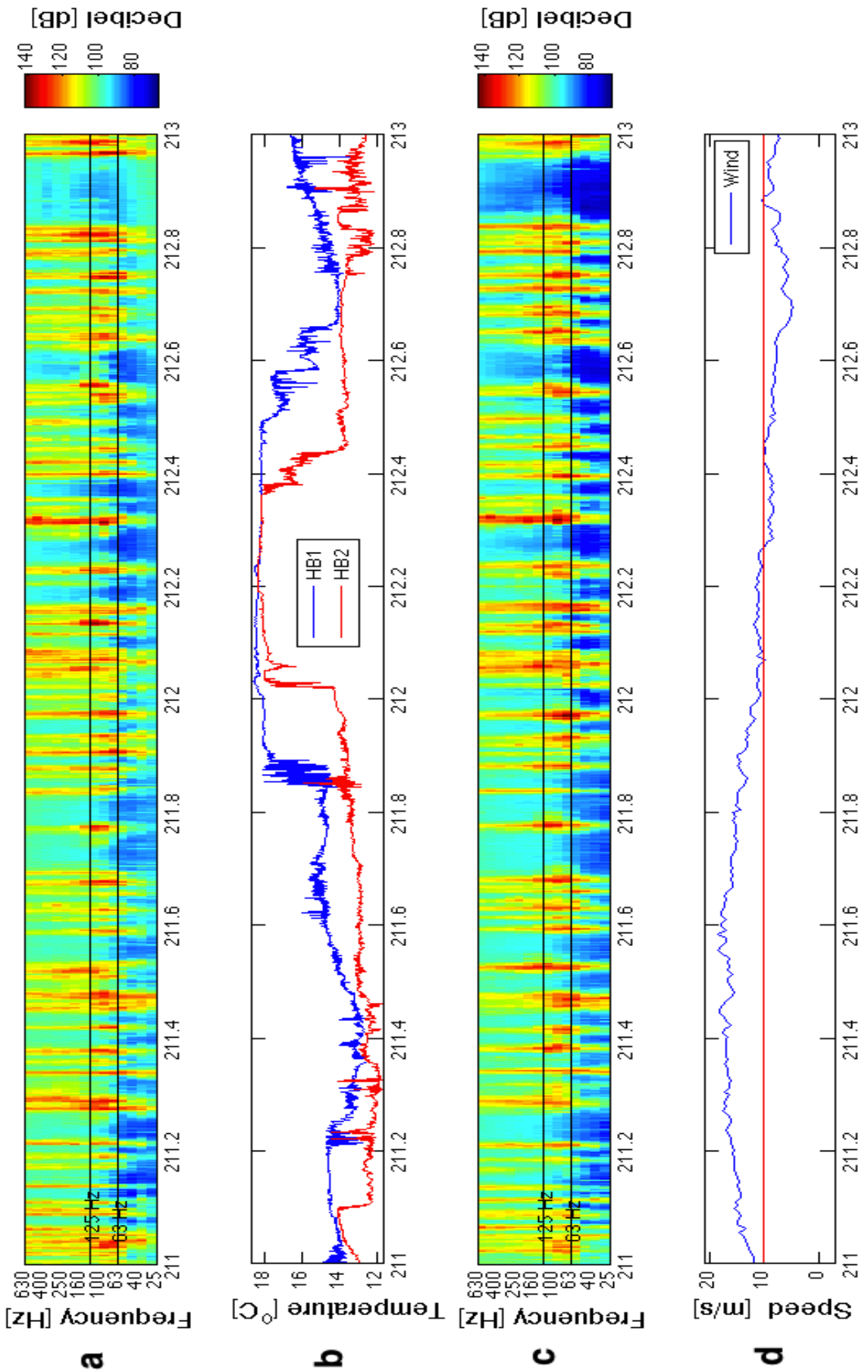

Figure 39: Observations from Julian day 211-213: (a) Underwater noise levels at sound station N0, (b) temperature from Hatter Barn, (c) underwater noise levels at sound station N2 and (d) wind observations at the Gniben station.

5 Discussion

5.1 Temperature and salinity variability in Danish waters

5.1.1 Contour plots

The time-depth relationship of temperature and salinity in Figures 13 and 14 clearly shows a seasonal signal, but also inter-annual and changes from station to station. The vertical gradients of temperature and salinity are more pronounced at the northern stations due to often higher summer temperature maxima (Figure 13) and generally higher near-bottom salinities (Figure 14). This stratification pattern reflects the separation of the Baltic Sea surface water from bottom waters originating in the North Sea and Skagerrak [Leppäranta & Myrberg (2009)]. Figure 13 can also be used to identify warm and cool summers. In the summer of 1997, there is very warm summer temperature peak at all stations. This warm summer peak fits well with atmospheric data from the Danish Meteorological Institute (DMI) where the record for the warmest summer is also found in 1997. The average summer air temperature in this year was 17.7^{o}C, whereas average summer temperatures in Denmark were 15.2^{o}C, calculated from 1961 to 1990 for the months June, July and August. It can also be observed that 1993 was a very cold year, which again corresponds very well with DMI data which shows that the summer of 1993 was the fourth coldest summer since 1920 with an average temperature of 14^{o}C [DMI - a]. The winter of 1995-1996 also produced a strong and cold temperature signal, strongest in the south and slightly decreasing towards the northern stations, where the stratification is more pronounced. The contour plot for the temperature cannot always be used as a clear indicator of climate conditions in Denmark, e.g. the summer of 2004 was relatively warm, but this cannot be seen in Figure 13, where only a weak summer peak is present. This is mainly due to the reduced availability of data in some years. In 2004 for example, measurements were only conducted in February, September, October and November. As a consequence, interpolation across this summer gap results in a weaker or underestimated summer peak. According to DMI [DMI - c], the year 1990 was also a warm year, but again no strong summer peak is visible in the contour plots shown in Figure 13. In this particular year, however, the data coverage was good with data from all months except for April and December. The seasonal and inter-annual temperature and salinity variability patterns between 1997 and 2009 are strongly biased by the large data gaps mostly beginning from 1997 (see Figure 12). The example of 1990 shows that even in years of good data coverage (1989-1997) the data have to be interpreted carefully.

The salinity contour plots in Figure 14 show a clear signature of the halocline. The halocline is much more pronounced at the stations in the northern part of the Kattegat as a result of the strong south to north increase of near-bottom salinities. This fits well with the general knowledge of the salinity frontal system in Danish waters [Leppäranta & Myrberg (2009)]. Figure 15 shows occasional injections of high salinity water (22-26 PSU) into the surface layer. Such injections are

most likely caused by upwelling events or horizontal advection triggered by strong storms. Two of these events can be found at all stations in January 1991 and at the end of the year 1999. In January 1991, the high surface salinity peak could be caused by a hurricane like storm on the 9^{th} January 1991 with wind speeds >28.5 m/s. In the salinity contour plots another peak is visible in the end of the year 1999, when Denmark was hit by the hurricane 'Anatol' (3^{th} December 1999) with wind speeds of 38 m/s [DMI - b]. The stations in the northern part of Kattegat generally show more frequent events of high salinity water injections into the surface layer than the stations in the southern parts of the study area (see Figure 15 a and b in comparison with Figure 15 c and d). This is most likely because these stations are closer to the more saline North Sea source waters in combination with a shallower halocline depth. The southward deepening of the halocline can also be clearly seen in Figure 45 of Appendix B.

5.1.2 The differences between the top and bottom layer

The characteristic peak at a period of 365 days in the power spectra for the temperature and salinity data correspond to the seasonal variability of the summer heating and winter cooling cycle. The peaks in the interpolated temperature data (Figure 16) are more energetic in the top layer than in the bottom layer. This can be expected, because the surface layer is mostly affected by meteorological forcing and solar heating. The yearly peaks in the power spectra of the salinity data (Figure 20) are less energetic, because seasonal salinity changes are weaker than temperature changes and less controlled by summer heating and winter cooling. In contrast to temperature, the salinity data also shows energetic peaks at different periods longer than one year, particularly at the two southernmost stations (Figure 20). Here, one of the other energetic peaks in the salinity power spectra has a period of 2 years representing inter-annual variations, most likely driven by changes in freshwater inflow. The range of inter-annual variations of river discharge, for example, can be very large in some basins of the Baltic Sea and can be higher than seasonal variations [Bergström et al. (2001)].

A more detailed analysis of the inter-annual temperature and salinity variability by applying a one year running mean (Figures 18 and 22) shows some interesting long-term variations. The pronounced drop in surface temperatures in the years 2002-2004 (day 5000-5900) cannot be explained by the atmospheric conditions in Denmark or on a global scale. All these years were warmer than the average air temperature and therefore this decrease is probably an artifact due to the interpolation with a lack of summer data. It is interesting to note that this drop is also visible in the bottom temperatures of the two southernmost stations, but not at the Gniben and Asnæs stations further north (Figure 18). The bottom salinity layers at the Langelands Bælt and Halsskov Rev stations (Figure 22) show several periods of strong salinity increase and decrease which were not found at the two northern stations. This is probably due to the generally weaker stratification and deeper halocline in these areas. Some events are now discussed in more detail.

The period 1994-1995 (day 2050 to 2200 in Figure 22) is characterized by a strong increase in surface salinity of 1.25 PSU over 200 days. This increase can be attributed to very warm and dry years. The summer of 1994 was very sunny leading to increased evaporation and the year 1995 was very dry with reduced precipitation [DMI - c]. Another event is visible in 1997, when the surface salinity increased by 1.5 PSU over a period of 150 days (day 3000 to 3150 in Figure 22). This year is also reported to be dryer than normal [DMI - c]. The combination of low precipitation and high evaporation over the entire baltic sea basin leads to less freshwater inflow and an increase in the surface salinity. The drop in the surface salinity of about 3.5 PSU from 2001 to mid-2003 (day 4400 to 5200 in Figure 22) could be the result of a very high amount of precipitation in the winter of 2001-2002, where the precipitation was 258 mm compared to an average of 161 mm [DMI - d]. The subsequent surface salinity increase of 1 PSU from 2003-2005 (day 5200 to 5800 in Figure 22) can not be explained by anomalies in the local atmospheric system. It is more likely a response to restore a steady state after an anomalous event. The running mean salinity in the bottom layer is more stable. The occasional steep increases, as discussed above, can also be detected in the bottom layer, but at a much lower magnitude. The largest long-term variations are found in the two stations furthest south, Halsskov Rev and Langelands Bugt. This could indicate that long-term variations are more important in the southern part of Kattegat and that the salinity frontal system is stronger affected in this area. Due to the large variations both in the temperature and salinity, it is not easy to say what the normal conditions typical for each area really are. To give a better picture a larger time series of data is necessary.

The linear trend line for the surface temperature is weak (see Figure 19). The main reason for this is due to the fact that the surface temperature is more dominated by short-term atmospheric disturbances and fluctuations, whereas the bottom temperatures are more affected by the advection of water masses from the North Sea, thus showing a statistically more significant linear trend. The increase of approximately 1.46^oC in the bottom temperature over the whole 20 year time series compared with the fact that the yearly mean air temperature in Denmark has increased around 1^oC from 1980-2009 [DMI - e], could have a connection. The trend line for the salinity does not show a significant linear trend in both the surface and bottom layer, and is therefore not a useful tool to describe long-term salinity changes. A study of salinity trends in the Baltic Sea over a 98 year period from 1902-2000 showed a very weakly increasing trend in the salinity but a very clear increase in deep-water temperature during the 20^{th} century [Fonselius et al. (2003)]. Another study shows that North Sea temperatures have increased with a rate of about 1–2^oC over the past 25 years [OSPAR]. This confirms the observed weak trend seen in the salinity and that the increase in the temperature also is observed in the Baltic and North Sea.

A third study shows that the temperature was relatively steady in the period from 1905-1985, from 1985 the temperature started to rise. The temperature was approximately 0.6^oC higher in 1989 where this long-term study was stated than the average temperature from 1905-1985. This rise is shown in Figure 40.

This indicates that the increasing trend started a couple of year before this study started but also

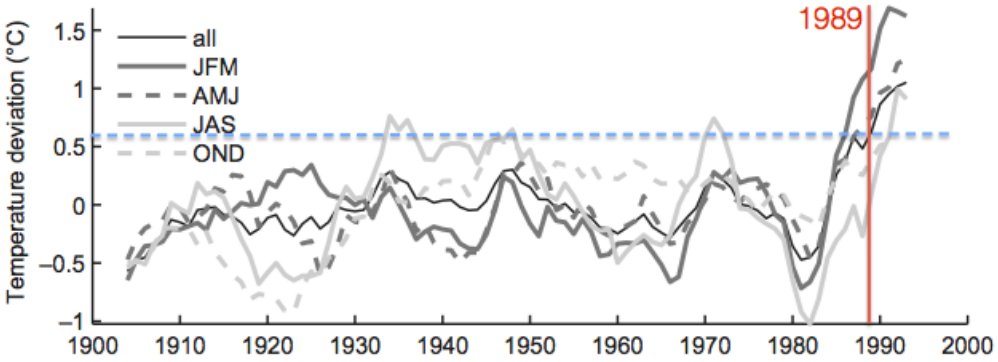

Figure 40: 10 year running mean of seasonal surface temperatures from Drogden measurement station (January– march, april–June, July– september, and october– December), deviations from seasonal mean. Blue dashed line show temp increase in 1989. The figure is from [Madsen & Højerslev (2009)], but with modifications.

shows that there was no or little increasing trend before 1985 [Madsen & Højerslev (2009)].
A correlation with wind data was performed, but the wind data only goes back to 1999 for the stations close to the salinity and temperature observations. Because of the big gaps in the observed salinity and temperature data after 1997, the correlation analysis does not show anything useful.

5.2 Hatter Barn

5.2.1 Forcing factors

Natural forcing factors such as solar radiation, tidal oscillations and wind mixing are visible in the observed salinity and temperature data. The tidal changes are present at both stations HB1 and HB2. Relatively weak tidal height changes of 0.1-0.3 meters in magnitude, observed at Aarhus harbor, can cause temperature and salinity changes of up to 7^o C and 7.5 PSU over one tidal cycle. These large fluctuations are developing as a result of the strong stratification and steep vertical gradients in connection with the depths of the thermocline and halocline in the waters at or close to Hatter Barn. Many of the changes in the observed data are controlled by wind events. A wind speed of approximately 10 m/s was found to be the critical threshold for wind induced mixing of low salinity and higher temperature surface waters to greater depths. Similar events were described in a study by [Guihen et al. (2012)], conducted on Tisler reef, a cold water coral reef in the Skagerrak. Here, the temperature records showed several rapid increases of approximately 4^oC within a 24 hour period at two occasions in the autumn months of 2006 and 2008. These events were also closely linked to strong wind conditions [Guihen et al. (2012)]. Periods of strong winds with wind speeds greater than a critical threshold of > 10 m/s fall together with periods of weak or absent tidal activity. Throughout the whole Hatter Barn time series, there are 4-5 periods where such a situation occurs, both in the observed and modelled data.
Progressive Vector diagrams (PVDs) of modelled currents at five locations were used to describe the flow and its variability in waters surrounding Hatter Barn. The model is forced by atmospheric conditions and is generally reproducing the major variability patterns of the observed temperature and salinity distributions. The remaining differences between model and observations are most likely due to the limitation of available model depth layers for a comparison with the observations. The temporal resolution of the model data is one hour and is therefore not sufficient to resolve processes at time scales less than one hour. The PVDs provide a Lagrangian view of the flow under idealized assumptions. For example, the topography of a water particle at its new position is not taken into account. Nevertheless, the PVDs give some useful indications about the flow close to Hatter Barn (see Figure 35). The general tendency of the near-surface flow is northward, but there is a clear difference between stations located at shallower water depths east of the reef and stations located close to the deep water shipping lane to the west. At the deep water stations, the flow seems more controlled by topographic steering showing a northward tendency and only occasional flow reversals. In contrast, the flow at the eastern stations has a more eastward tendency and more frequent flow reversals.
The very fast changes in the observed data from Hatter Barn (as seen for example in Figures 32 and 33) cannot be explained by the analyzed natural forcing. The most likely reason is due to regular wave-like disturbances caused by ship traffic passing Hatter Barn. The underwater noise data reveals frequent ship traffic in the area as expected from the heavily used shipping lanes on each side of the reef. Some of the noise signals seen at station N2 (Figure 39 and Figures 48-

56 Appendix D) are not visible at station N0. This difference in noise signatures are probably caused by ships using the shallower lane on the eastern side of the reef. The noise observations are difficult to correlate directly with the observed temperature data, because the ships may generate a spectrum of waves depending on speed, weight, shape and sailing direction. In addition, a strong noise signal is not necessarily caused by large and heavy ships. Noise levels are influenced by the ship engine technology, ship speed, propellers and the age of each ship, amongst others. The wave propagation and wave damping also depends on natural factors, such as current direction and speed, as well as wind direction and speed. For example, fast ferries are not heavy, but they operate at greater speeds.
[Dahl & Kofoed-Hansen (2003)] conducted a study within an area close to the island of Læsø to investigate the impact of ship-generated waves and currents 60 m away from a fast-ferry route on gravel seabeds and the associated vegetation. The results of this study showed that ship-generated waves and currents penetrate the water column to a depth of 10 meters with a horizontal velocity of approximately 0.4 m/s at normal operational ferry speeds. As a result, small stones and gravel with a weight of up to 650 g were moved out their initial positions. In addition, algae leaves were covered by sandy sediments [Dahl & Kofoed-Hansen (2003)]. The study has a number of uncertainties, but it confirms the potential of ship induced mixing effects at shallow reefs near sailing routes.
The temperature and salinity fluctuations seen in the data are large because of the strong gradients of these parameters in the upper water column at the reef. Longer noise data time series would be helpful in the future to allow for a more robust statistical analysis of the connection between ship traffic and related oceanic mixing. Other sources of information, such as ship AIS (Automatic Identification System) data would also be useful to provide additional information on ship specifications, e.g. ship speed, weight, shape and distance to the area of interest.

5.2.2 Ecological implications

Many of the changes in the salinity and temperature could have an impact on the reef's ecosystem. Sudden shifts to higher temperature have been found to be followed by a mass mortality of sponges at Tisler Reef in the Skagerrak [Guihen et al. (2012)]. The observed summer warming at Hatter Barn is a slow change in temperature allowing the vegetation to adapt over the 3 month period. Hatter Barn, like other boulder reefs in the Kattegat, is a natural habitat for macroalgae vegetation, in particular seaweeds. Seaweeds have a limited tolerance to changes in salinity and adapt to salinity changes by regulating cell processes to keep an osmotic balance [Luening (1990)]. Sudden and frequent osmotic pressures imposed by large short-term salinity fluctuations, as observed at Hatter Barn, can be dangerous for seaweed, because its shape and growth depends on a constant osmotic pressure [Luening (1990)]. The observed changes over time scales of minutes and days together with large fluctuations in salinity could therefore make it unsuitable for seaweeds to live on reef areas where salinity disturbances are largest. Another danger to the macroalgae

vegetation is imposed by grazing pressure through green sea urchins. The distribution of green sea urchins in the Kattegat is constrained by salinity. [Sameoto & Metaxas (2008)] have shown that the most suitable environment for green sea urchins is at salinity levels of 24 PSU or higher. Figure 41 illustrates potentially suitable habitats for green sea urchins varying with the depth of the 24 PSU isoline between the Kattegat and the southern Belt Sea.

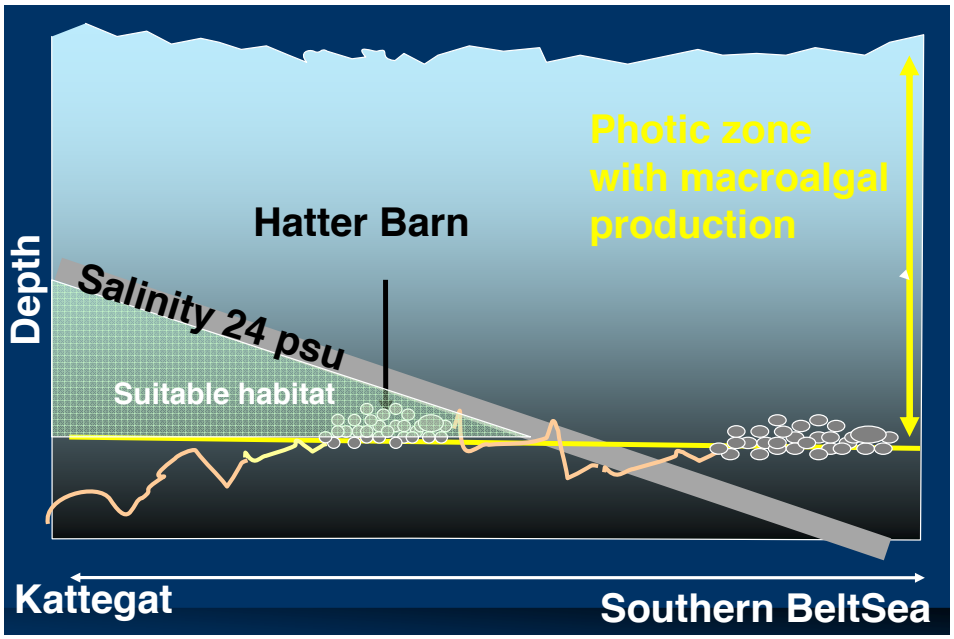

Figure 41: Schematic illustration of potentially suitable habitats for the green sea urchin in Danish waters (Karsten Dahl, pers. communication).

Hatter Barn is located at the southern boundary, i.e. sea urchins find suitable conditions only at greater depths under normal stratification conditions. Under strong lateral or vertical mixing conditions where water of salinities above 24 PSU enters the surface layer. Such mixing events, where the saltier water is mixed with less saline surface waters would provide favorable conditions to allow sea urchins to move up the water column and feed from macro algae growing at shallower depths on top of boulder reefs. The observations at Hatter Barn indicate that such conditions are frequently found at the shallower levels of the HB1 and HB2 stations (Figure 42).

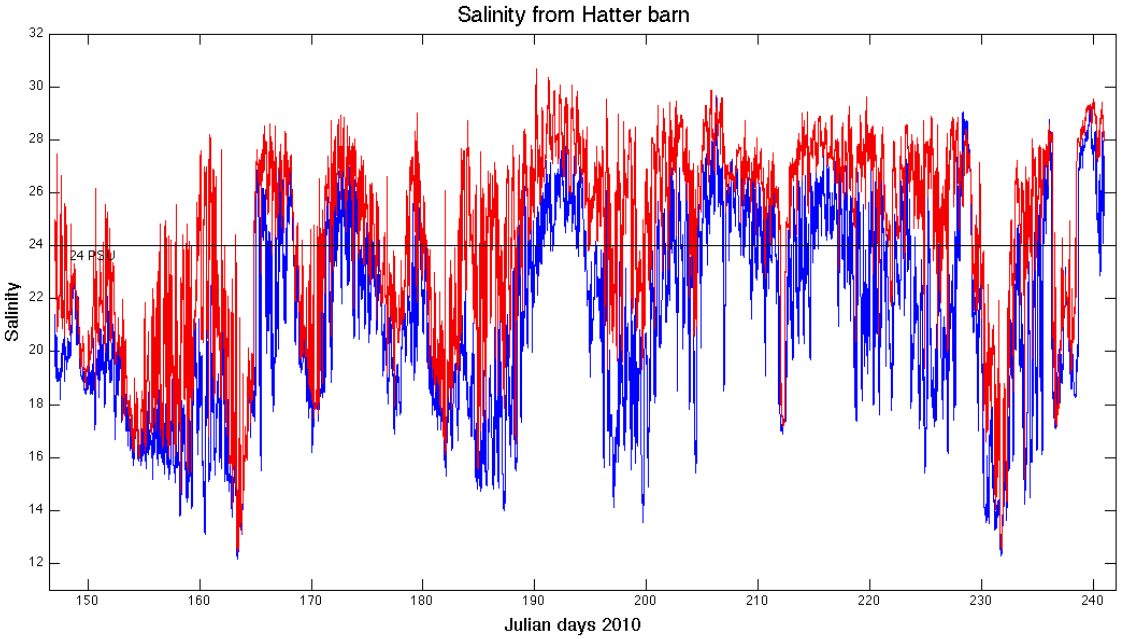

Figure 42: Salinity time series from the two Hatter Barn stations. The critical 24 PSU salinity level is marked by the black horizontal line.

6 Conclusion

The large-scale and long-term time series analysis provided a comprehensive picture of the waters surrounding the area of interest, the boulder reef Hatter Barn. The analysis clearly showed the stratification separating the two water layers from the North Sea and the Baltic Sea. It also showed how the thickness of these water layers changes with location throughout the Kattegat and Belt Sea. The long-term analysis also revealed a linear trend with increasing temperatures of approximately 1.46^{o}C over the observed 20 years in bottom water less affected by atmospheric variability. This warming trend is also confirmed by other studies. Not all atmospheric events are represented in the temperature distribution, mainly because of the large data gaps especially from 1997 onwards. More data are needed to close these gaps and to obtain a more robust picture of temperature variability and long-term trends.

The three month salinity and temperature observations from the boulder reef Hatter Barn showed some interesting signals. There are large fluctuations over different time scales from minutes to days. These fluctuations are caused by semi-diurnal tidal oscillations, vertical mixing or lateral advection due to wind. The observed high-frequency variability at periods less than one hour is most likely created by man-made forcing, although a more detailed analysis is necessary to support this conclusion. A visual examination of underwater noise data from the same periods indicates that ship-generated wave action in the shipping routes at either side of the reef is the most likely source. In the context of the blue corridor concept, the observed variability can be expected to also have an influence on both, the entrainment of biological particles to the reef and the residence time of biological particles at the reef. Further research is needed to investigate, how short-term variability might affect the stability of long-term particle pathways.

The model data proved a useful addition to the observations, although the comparison was limited by the model resolution and restriction of available depth levels in the model. The temporal resolution of one hour in the model was not enough to resolve time scales in the order of several tens of minutes. But given the possible anthropogenic character of the observed high frequency variability in temperature and salinity, it would have been surprising to find these signals in the output of an ocean circulation model without the appropriate forcing.

References

[Aarup (1994)] Thorkild Aarup, *Satellite imagery of Danish and neighboring waters*, Havforskning fra Miljøstyrelsen Nr. 52 1994.

[Bendtsen et al. (2007)] Jørgen Bendtsen, Johan Soderkvist, Karsten Dahl, Jørgen L.S. Hansen & Johnny Reker (2007), *Model simulations of blue corridors in the Baltic Sea*, BALANCE Interim Report No. 9, 2007.

[Berg et al. (2008)] Mark de Berg, Otfried Cheong, Marc van Kreveld, Mark Overmars, (2008), *Computational Geometry: Algorithms and Applications, Third Edition*, published by Springer-Verlag.

[Bergström (1992)] Bergström, S. (1992), *The HBV model - its structure and applications*, SMHI Reports RH, No. 4.

[Bergström et al. (2001)] Bergström, S., Alexandersson, H., Carlsson, B., Josefsson, W., Karlsson, K.G., & Westring, G., 2001. *Climate and hydrology of the Baltic Sea.* In: F. Wulff et al. (eds.), A System Analaysis of the Baltic Sea (Ecological Study No. 455, pp. 75-112). Springer Verlag, Berlin.

[Cushman-Roisin (1994)] Benoit Cushman-Roisin(1994), *Introduction to Geophysical Fluid Dynamics*, Print, Prentice Hall, Englewood Cliffs, New Jersey.

[Dahl et al. (2003)] Karsten Dahl, Steffen Lundsteen & Stig Asger Helmig(2003), *Stenrev – havbundens oaser*, 1. udgave, 1. oplag 2003, Gads Forlag, København K, Danmark.

[Dahl et al. (2012)] Karsten Dahl, Cordula Goke, Steffen Lundsteen, Jacob Carstensen, Zyad Al-Hamdani, Jørgen Overgard Leth, Charlotte Wiin Havesteen & Sussie von Qualen (2012), *Seabed and habitat mapping in the Hatter Barn area – a high risk area for shipping in the Danish Straits*, BaltSeaPlan Report 27, www.baltseaplan.eu, 2012.

[Dahl & Kofoed-Hansen (2003)] Karsten Dahl & Henrik Kofoed-Hansen (2003), *Effekter på havbunden ved passage af højhastighedsfærger*, Faglig rapport fra DMU, nr. 451, Danmarks Miljøundersøgelser, Miljøministeriet, 2003.

[DaMSA] DaMSA *Tide tables for Danish waters 2010*, Danish Maritime Safety Administration (DaMSA), `http://frv.dk/Maalinger/Farvandsmaalinger/Documents/tidevand/Tide10_DK.pdf`, (2011-02-17).

[Danielssen et al. (1997)] Danielssen, D. S., L. Edler, S. Fonselius, L. Hernroth, M. Ostrowski, E. Svendsen, & L. Talpsepp (1997), *Oceanographic variability in the Skagerrak and Northern Kattegat*, May– June, 1990, ICES Journal of Marine Science, 54, 753– 773.

[Davis et al. (2009)] Stephen E. Davis, III, John Bryan Allison, Matthew J. Driffill & Saijin Zhang (2009). *Influence of Vessel Passages on Tidal Creek Hydrodynamics at Aransas Wildlife Refuge (Texas, United States): Implications on Material Exchange.* Journal of Coastal Research, 25, No. 2, 359 – 365.

[DMI - a] `http://www.dmi.dk/dmi/danmarks_daarligste_somre`, Klima- og Energiministeriet, Danish Meteorological Institute, (2010-09-30).

[DMI - b] John Cappelen (2009) *Storm og ekstrem vind i Danmark- opgørelser og analyser september 2009*, Klima- og Energiministeriet, Danish Meteorological Institute, Teknisk rapport 09-12, `http://www.dmi.dk/dmi/tr09-12.pdf`, (2010-10-05).

[DMI - c] DMI *Arhundredets vejr i Danmark 1900 - 1999*, Klima- og Energiministeriet, Danish Meteorological Institute, `http://www.dmi.dk/dmi/vejr-top10.pdf`, (2010-12-08).

[DMI - d] DMI *Vintervejret 2001-2002 i Danmark*, Klima- og Energiministeriet, Danish Meteorological Institute, `http://www.dmi.dk/dmi/vintervejret_2001-2002_i_danmark`, (2010-12-14).

[DMI - e] DMI *Temperaturen i Danmark*, Klima- og Energiministeriet, Danish Meteorological Institute, `http://www.dmi.dk/dmi/index/klima/klimaet_indtil_nu/temperaturen_i_danmark.htm`, (2010-12-14).

[Fonselius et al. (2003)] Stig Fonselius & Jorge Valderrama, *One hundred years of hydrographic measurements in the Baltic Sea*, Journal of Sea Research Volume 49, Issue 4, Pages 229–241, June 2003.

[Funkquist & Kleine (2007)] Lennart Funkquist & Eckhard Kleine, 2007. *HIROMB - An introduction to HIROMB, an operational baroclinic model for the Baltic Sea.* SMHI report on oceanography No. 37, 48 pp.

[Giovanni database] *Ocean Color Radiometry Online Visualization and Analysis*, `http://gdata1.sci.gsfc.nasa.gov/daac-bin/G3/gui.cgi?instance_id=ocean_month`, National aeronautics and space administration, (2010-03-11).

[Guihen et al. (2012)] Damien Guihen, Martin White & Tomas Lundalv, *Temperature Shocks And Ecological Implications At A Cold- Water Coral Reef* , Submitted to journal: Marine Biodiversity Records, Cambridge University Press, 2012.

[HELCOM] Danish Martime Safety Administration, Danish Maritime Authority & Navy Admiral Danish Fleet `http://www.helcom.dk/`.

[Houmark-Nielsen et al. (2005)] Michael Houmark-Nielsen, Johannes Kruger & Kurt Henrik Kjær (2005), *De seneste 150.000 år i Danmark* , Geoviden, Geologi og geografi nr. 2, 2005.

[Knauss (1997)] John A. Knauss(1997), *Introduction to Physical oceanography*, Print, Waveland press, inc. Long Grove, Illinois.

[Leppäranta & Myrberg (2009)] Matti Leppäranta & Kai Myrberg, *Physical oceanography of the Baltic Sea*, Printed in Germany, Praxis publishing Lth, Chichester, UK, 2009.

[Luening (1990)] Luening, K., *Seaweeds - Their Environment, Biogeography, and Ecophysiology*, In: Yarish, C. and H. Kirkman (eds.), Edited Transl. of the German language ed. Meeresbotanik: Verbreitung, Okophysiologie und Nutzung der Marinen Makroalgen by Klaus Luening. John Wiley & Sons, Inc. NY, 1990.

[Lund-Hansen et al. (1994)] Lars Chresten Lund-Hansen, Christian Christiansen, Carsten Jürgensen, Katherina Richardson & Poul Skyum, *Basisbog i fysiske-biologisk Oceanografi*, Print, AKA-PRINT A/S, Gads forlag1994.

[MADS database - a] Den nationale database for marin Data (MADS), `http://www.dmu.dk/vand/havmiljoe/mads/ctd/data/`, Department of Bioscience, Aarhus University, (2010-09-10).

[MADS database - b] Den nationale database for marin Data (MADS), `http://www.dmu.dk/vand/havmiljoe/mads/vandkemi/data/`, Department of Bioscience, Aarhus University, (2010-09-10).

[Madsen & Højerslev (2009)] Kristine S. Madsen & Niels K. Højerslev, *Long-term temperature and salinity records from the Baltic Sea transition zone*, Boreal Environment Research 14: 125–13, 2009.

[Martin et al. (2006)] Georg Martin, Anita Makinen, Åsa Andersson, Grete E. Dinesen, Jonne Kotta, Jørgen Hansen, Kristjan Herkül, Kurt W. Ockelmann, Per Nilsson & Samuli Korpinen (2006). *Literature review of the "Blue Corridors" concept and it´s applicability to the Baltic Sea*. BALANCE Interim Report No. 4, 72 pp.

[Matlab Central 2012] MATLAB Central, `http://www.mathworks.com/matlabcentral/fileexchange/10113`, (2012-03-29).

[MathWorks 2012] MathWorks, `http://www.mathworks.se/help/techdoc/ref/fft.html`, (2012-03-29).

[MicroCAT 2011] MicroCAT C-T (P optional) Recorder SBE 37-SM, `http://www.seabird.com/products/spec_sheets/37smdata.htm`, (2012-02-09).

[Mortensen et al. (2011)] Lars O. Mortensen, Jakob Tougaard and Jonas Teilmann, *Effects of underwater noise on harbour porpoises around major shipping lanes*, BaltSeaPlan Report 21, 2011.

[MyOcean] MyOcean, http://www.myocean.eu/web/69-myocean-interactive-catalogue.php?option=com_csw&task=results&referenced_area%5B%5D=my-ocean-areas%23baltic&ocean_variable%5B%5D=cf-standard-name%23temperature&ocean_variable%5B%5D=cf-standard-name%23salinity&product_type%5B%5D=forecasting, (2012-02-09).

[Naturstyrelsen] Miljøministeriet, Naturstyrelsen, *Natura 2000 omrade nr. 198 Hatter Barn* http://www.naturstyrelsen.dk/NR/rdonlyres/0E87E08E-DCE8-4E6B-9898-8E7AD4DD97F6/113006/198_HatterBarn_resume.pdf, (2011-03-02).

[Nielsen (1999)] Mads Hvid Nielsen, *Den jyske kyststøm*, Speciale i fysisk og dynamisk oceanografi, April 1999, Københavns Universitet.

[Norderhaug & Christie (2009)] Kjell Magnus Norderhaug & Hartvig C. Christie (2009). *Sea urchin grazing and kelp re-vegetation in the NE Atlantic*. Marine Biology Research, 5, 515 – 528.

[OSPAR] Quality status report 2010, Impacts of climate change on the North-East Atlantic ecosystem, http://qsr2010.ospar.org/media/assessments/P00463_supplements/01_increased_sea_temperature.pdf,OSPAR commission, (2012-04-18).

[Rodhe (1998)] Johan Rodhe, *The baltic and North Seas: A process-oriented review af the physical oceanography*, The Sea, Volume 11, edited by Allan R. Robinson & Kenneth H. Birk, John Wiley & sons, inc. 1998

[Sameoto & Metaxas (2008)] Jessica A. Sameoto, Anna Metaxas (2008), *Interactive effects of haloclines and food patches on the vertical distribution of 3 species of temperate invertebrate larvae.* Journal of Experimental Marine Biology and Ecology, 367, 131-141.

[Sørensen (2010)] Lea K. D. Sørensen (2010), *An introduction to oceanography*, http://dl.dropbox.com/u/1143633/An%20introduction%20to%20oceanography.pdf.

[Tomczak et al. (1994)] Matthias Tomczak and J. Stuart Godfrey (1994), *Regional oceanography: An Introduction*, Print, Butler & Tanner Ltd, Frome and London.

[Tomczak et al. (2003)] Matthias Tomczak and J. Stuart Godfrey (2003), *Regional oceanography: An Introduction 2nd edn*, online colored version: http://www.es.flinders.edu.au/~mattom/regoc/pdfversion.html .

[Vejret (1993)] Dansk Meteorologiske selskab, *Vejret 57, november 1993* http://dams.risoe.dk/blad/pdf/Vejret57.pdf (2010-12-14).

Appendix

A Power spectra of the 365 day running mean

A.1 Temperature

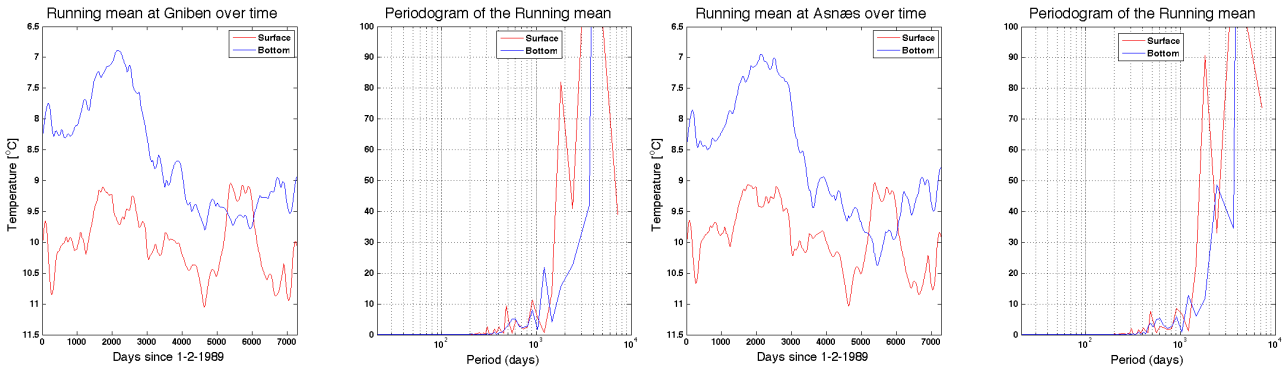

(a) Gniben

(b) Asnæs

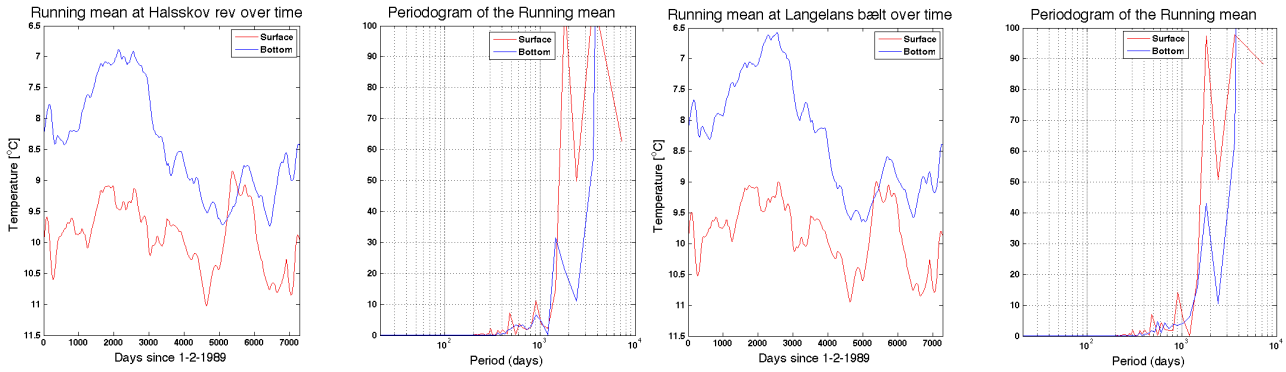

(c) Halsskov Rev

(d) Langelands bælt

Figure 43: The running mean of the temperature of the top (red) and bottom (blue) layer of the four stations and their corresponding power spectra.

A.2 Salinity

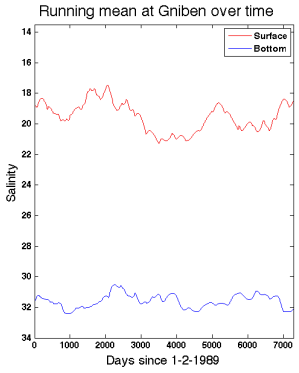

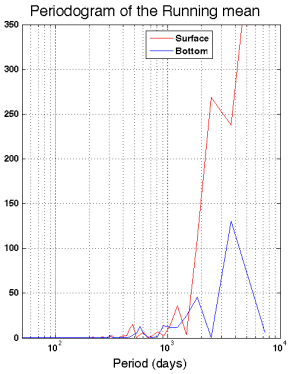

(a) Gniben

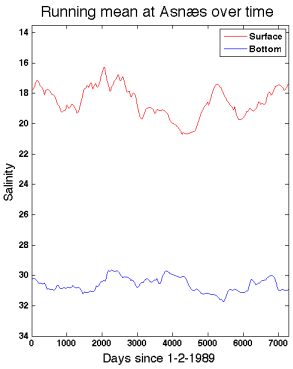

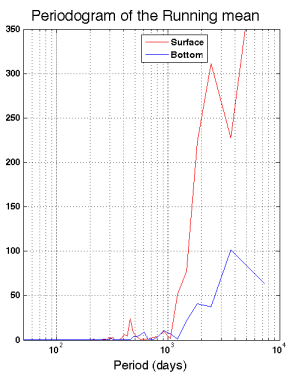

(b) Asnæs

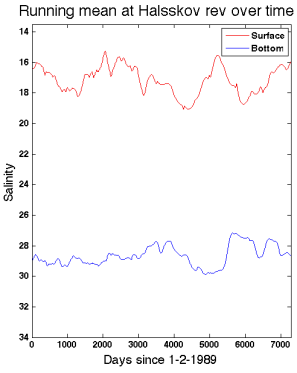

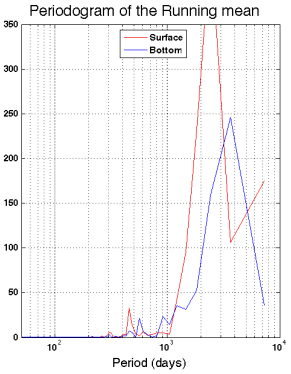

(c) Halsskov Rev

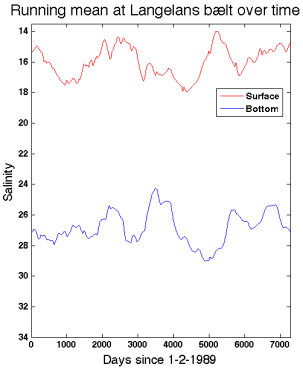

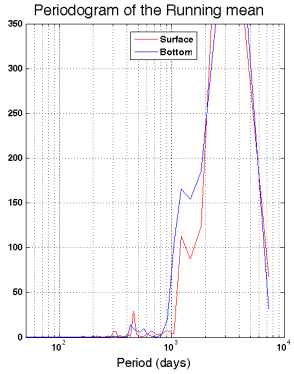

(d) Langelands bælt

Figure 44: The running mean of the salinity of the top (red) and bottom (blue) layer of the four stations and their corresponding power spectra.

B Contour plots of salinity and depth of the halocline

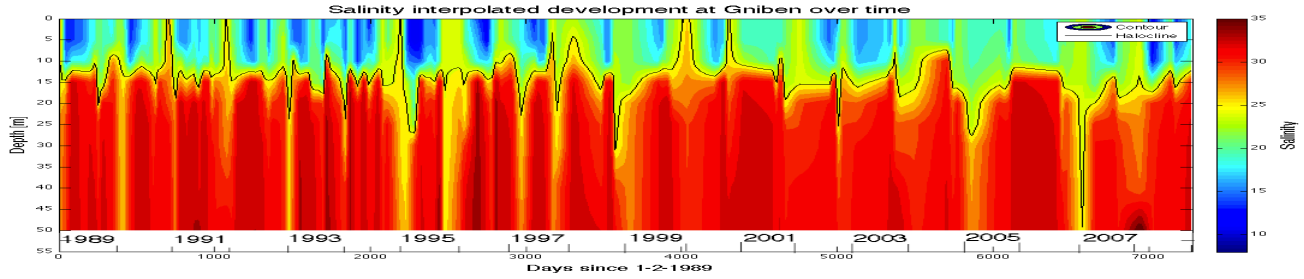

(a) Gniben

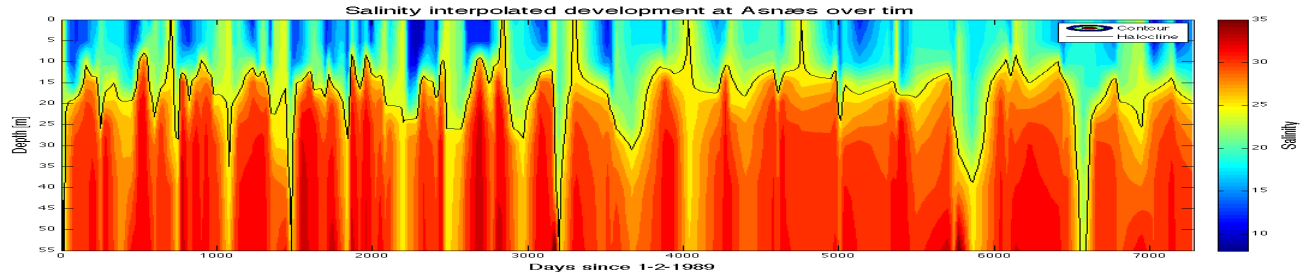

(b) Asnæs

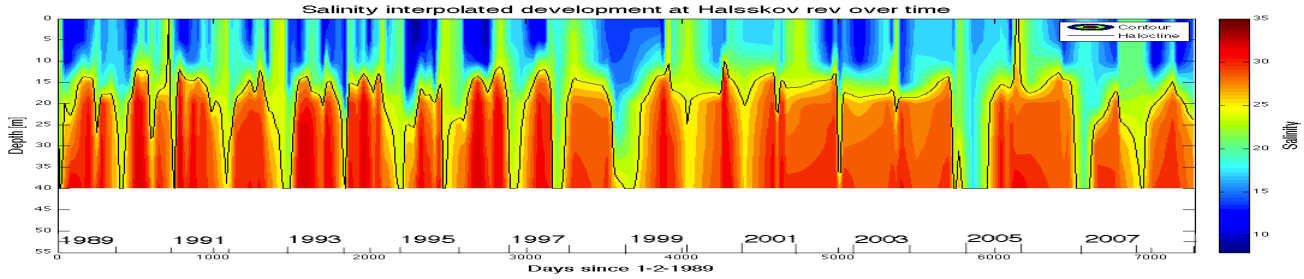

(c) Halsskov Rev

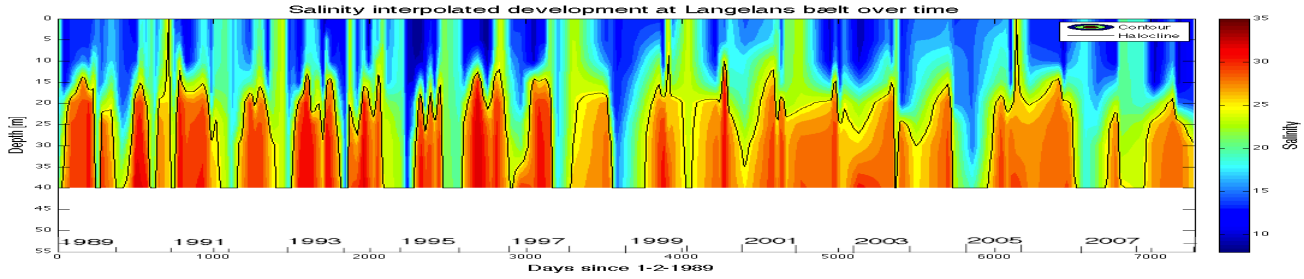

(d) Langelands bælt

Figure 45: : Contour plot from interpolated salinity data of all four stations with the corresponding depth of the halocline.

C Tidal oscillations at Hatter Barn observations and MyOcean model data

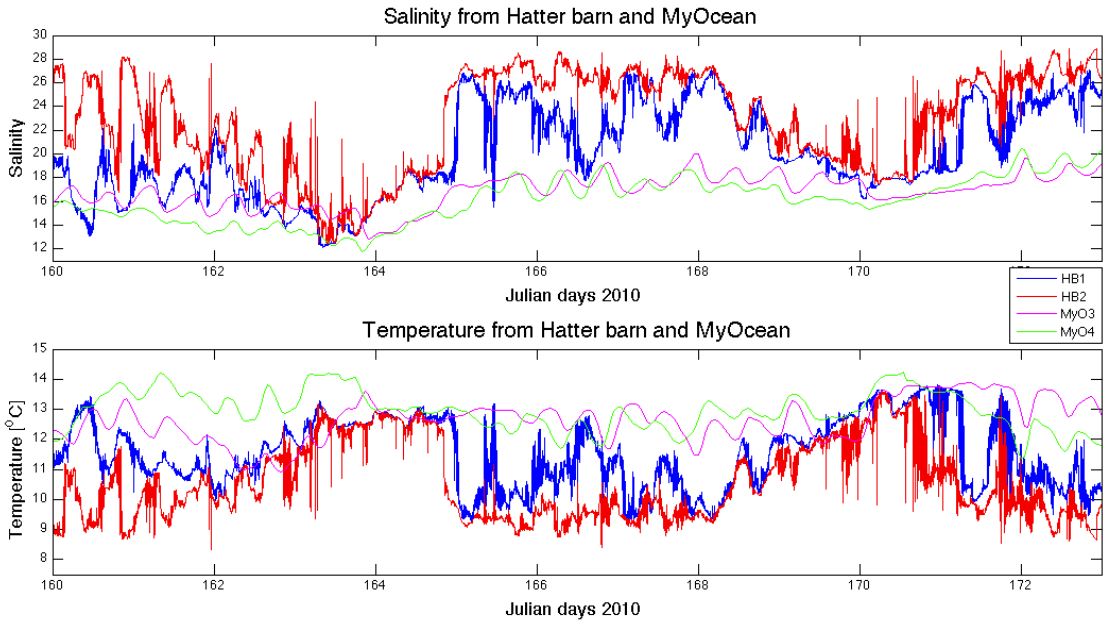

Figure 46: Salinity and temperature time series from Hatter Barn observations and MyOcean model data. The extracted period is from Julian day 160 to 172. Two events with no or small tidal oscillations are visible from Julian day 164 to 166 and 170 to172.

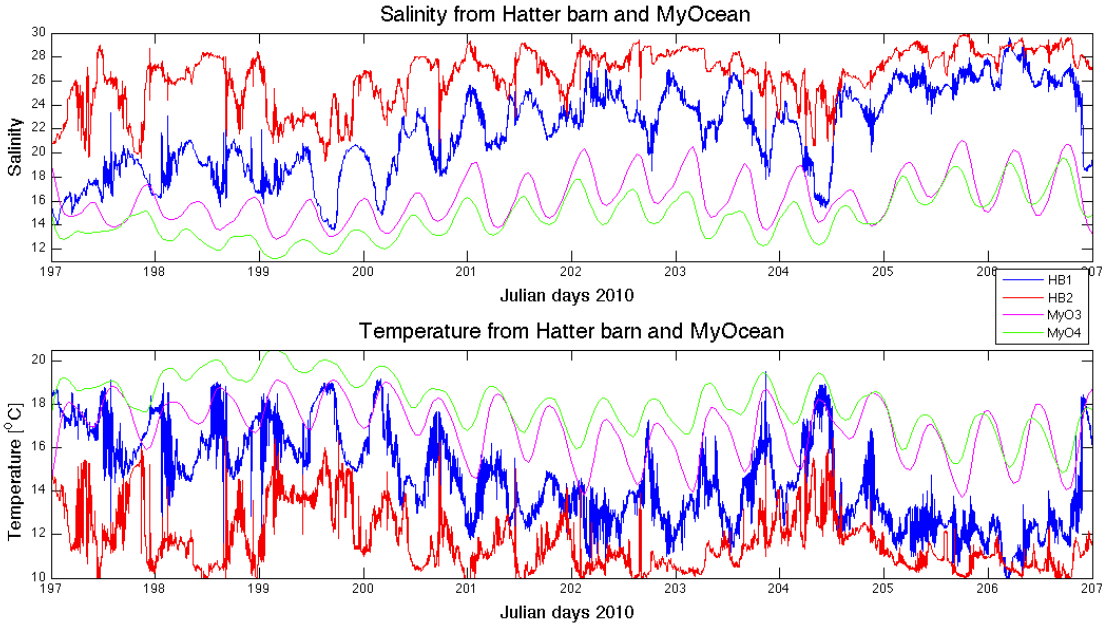

Figure 47: Salinity and temperature time series from Hatter Barn observations and MyOcean model data. The extracted period is from Julian day 197 to 207 showing large tidal oscillations with changes in the temperature and salinity of up to 7^{o}C and 7.5 PSU.

D Sound observations

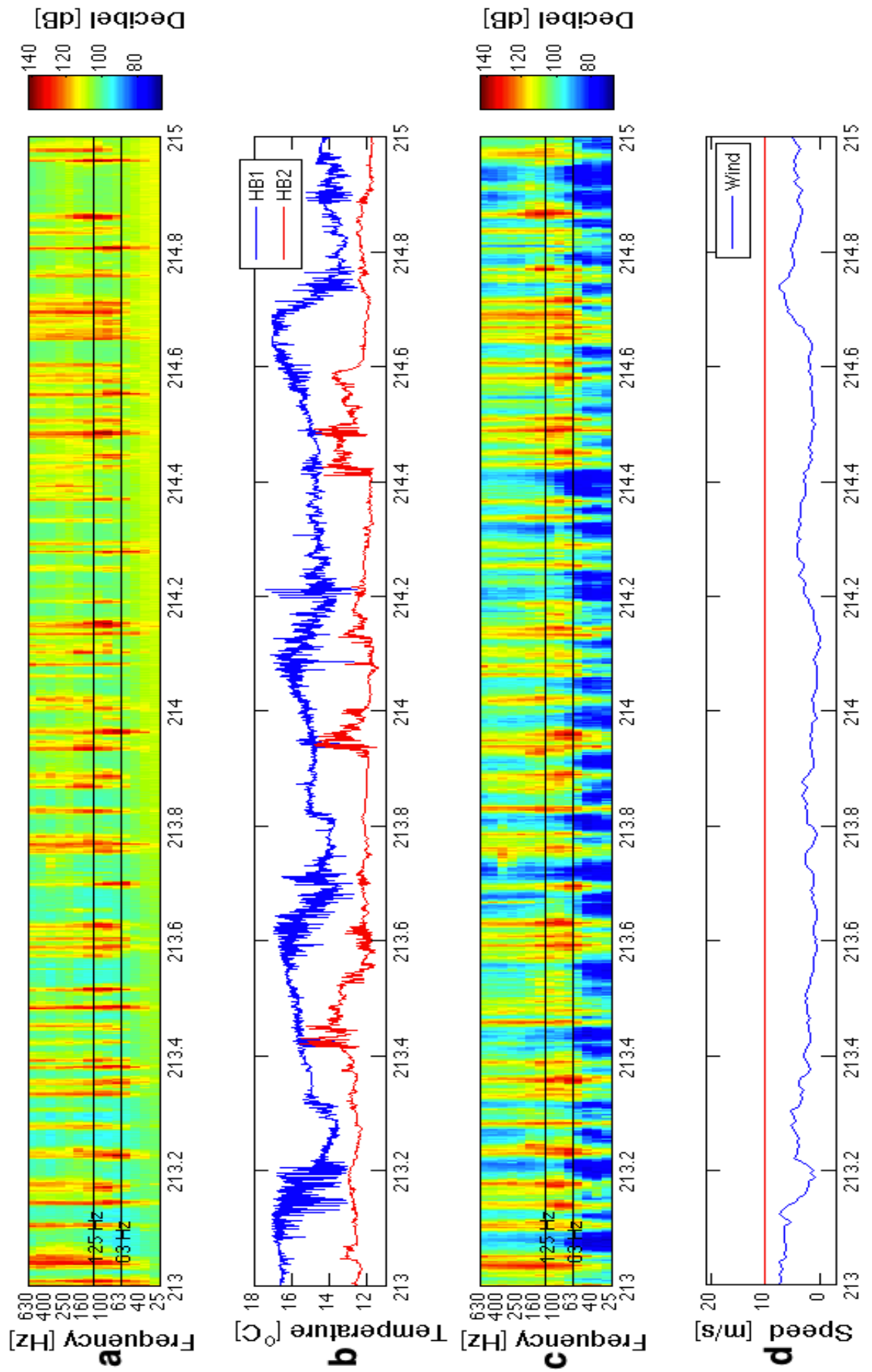

Figure 48: Observations from Julian day 213-215: (a) Sound station N0, (b) Temperature from Hatter Barn, (c) Sound station N2 and (d) wind observations from Gniben.

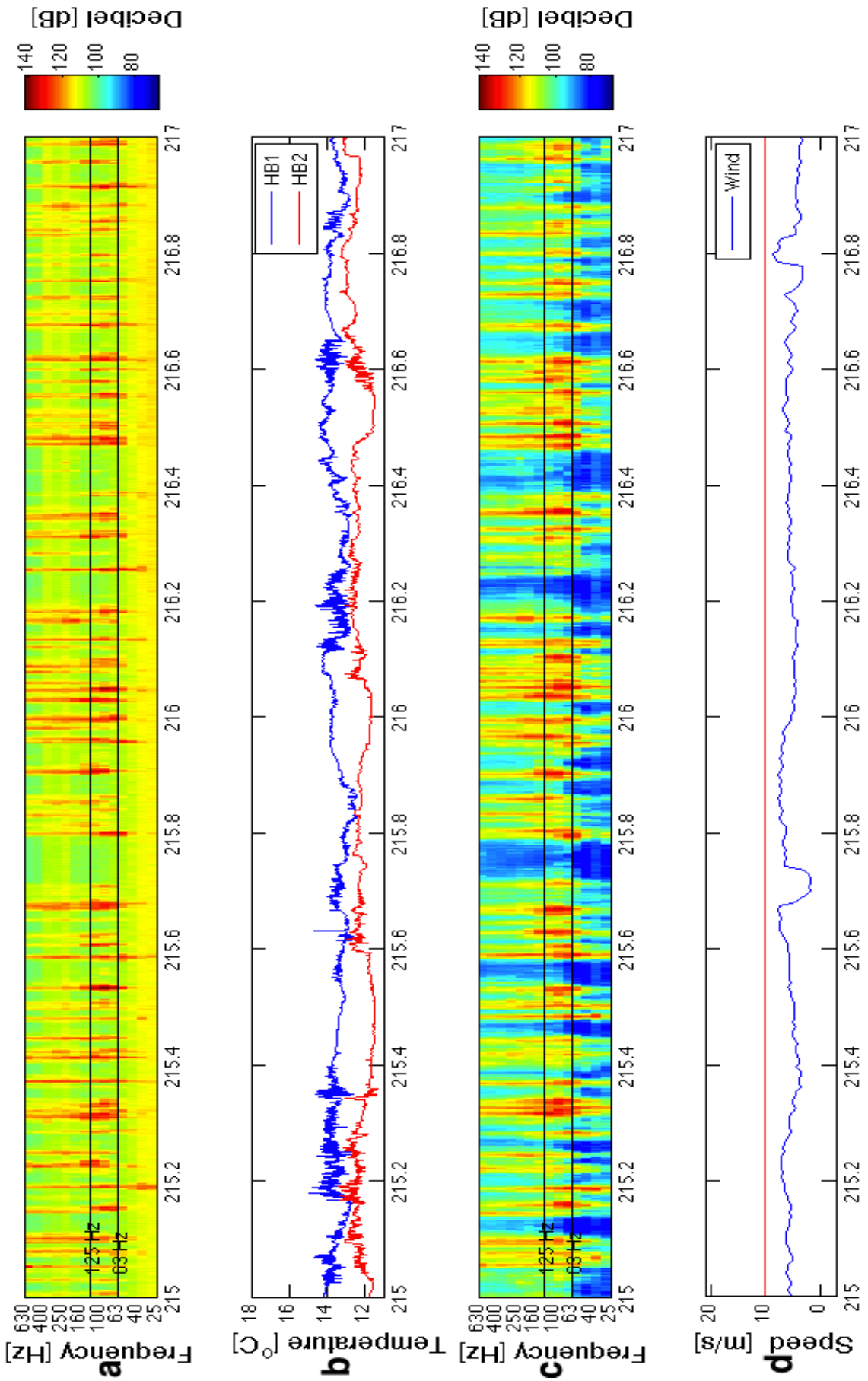

Figure 49: Observations from Julian day 215-217: (a) Sound station N0, (b) Temperature from Hatter Barn, (c) Sound station N2 and (d) wind observations from Gniben.

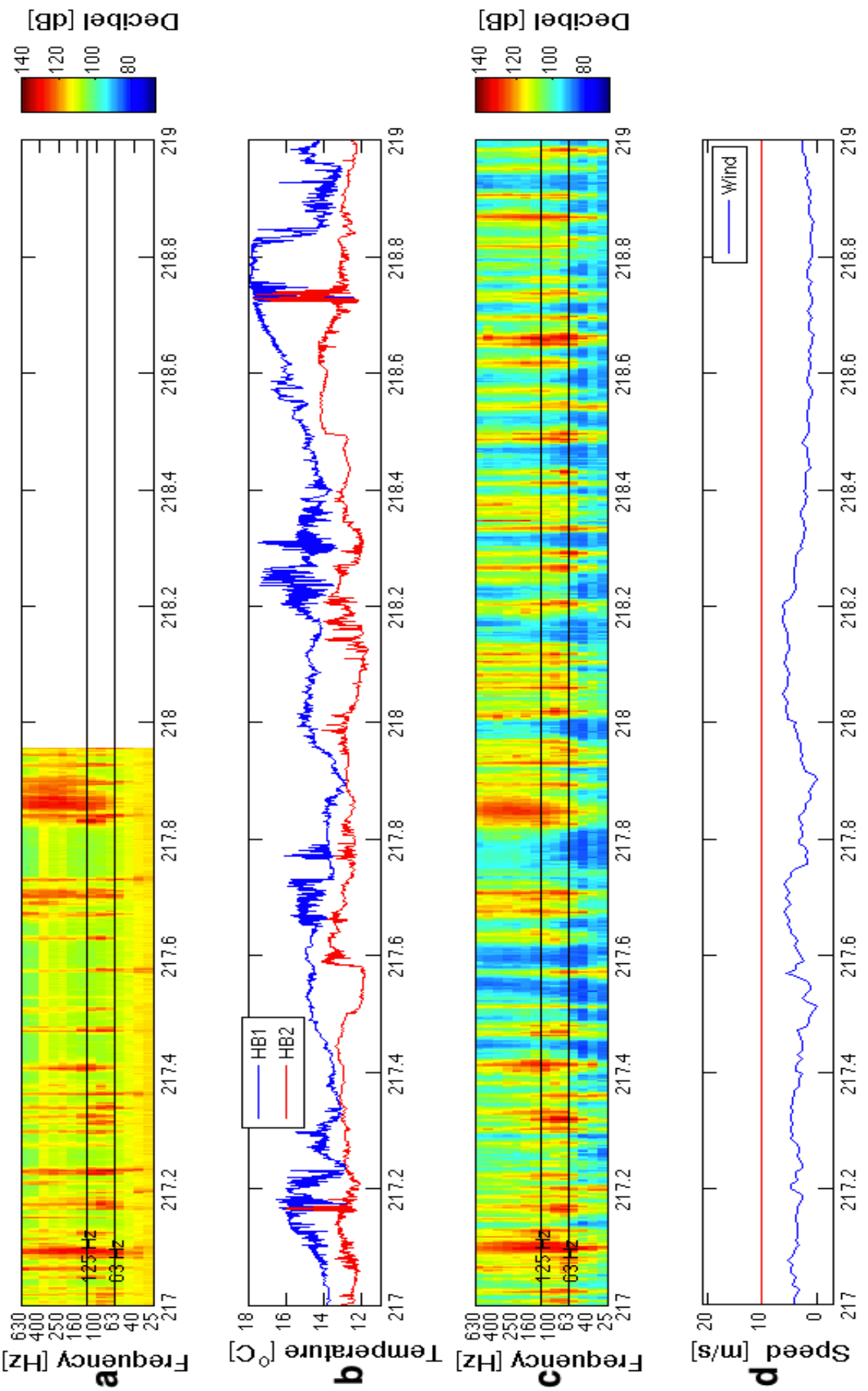

Figure 50: Observations from Julian day 217-219: (a) Sound station N0, (b) Temperature from Hatter Barn, (c) Sound station N2 and (d) wind observations from Gniben.

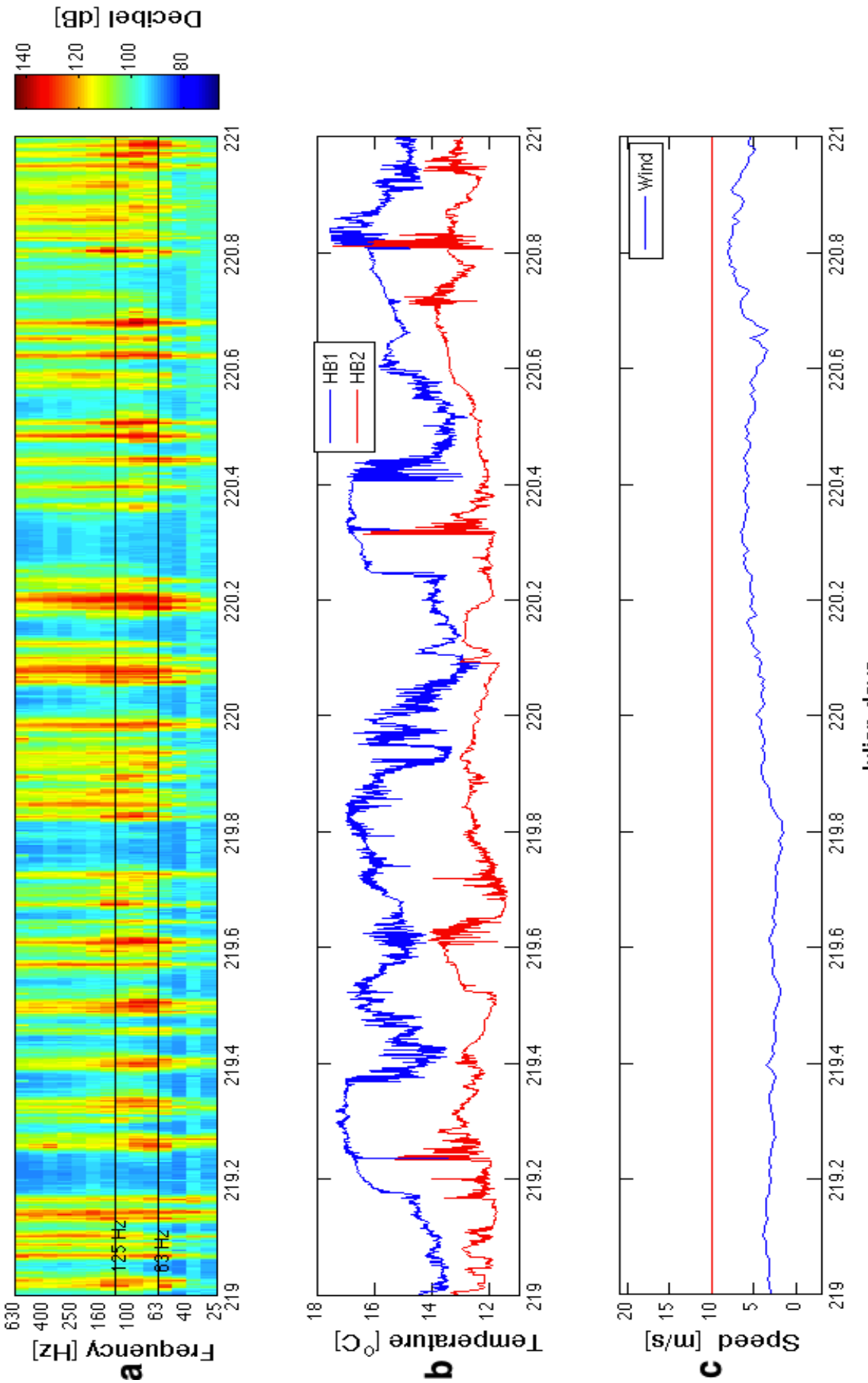

Figure 51: Observations from Julian day 219-221: (a) Sound station N2, (b) Temperature from Hatter Barn, (c) wind observations from Gniben.

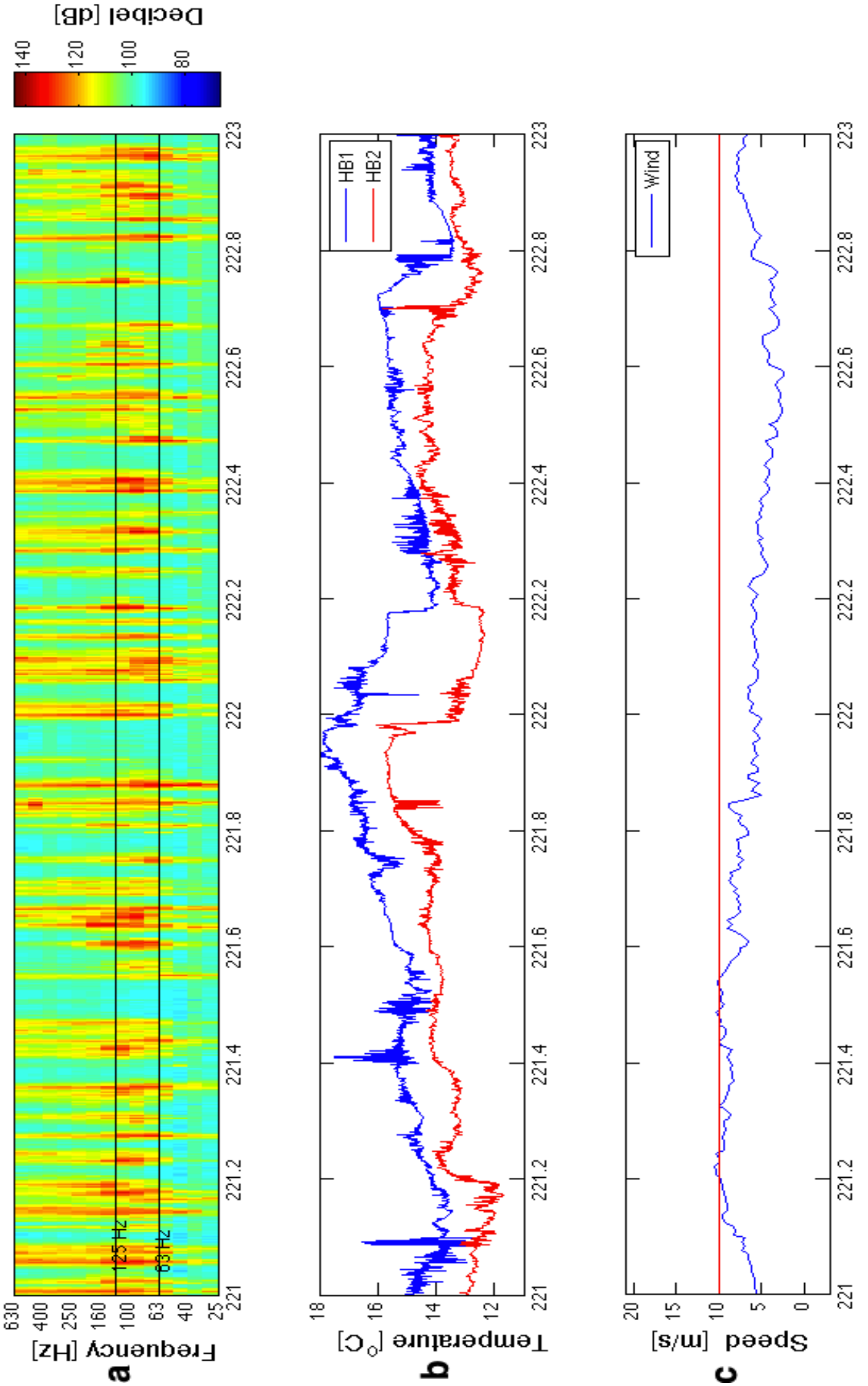

Figure 52: Observations from Julian day 221-223: (a) Sound station N2, (b) Temperature from Hatter Barn, (c) wind observations from Gniben.

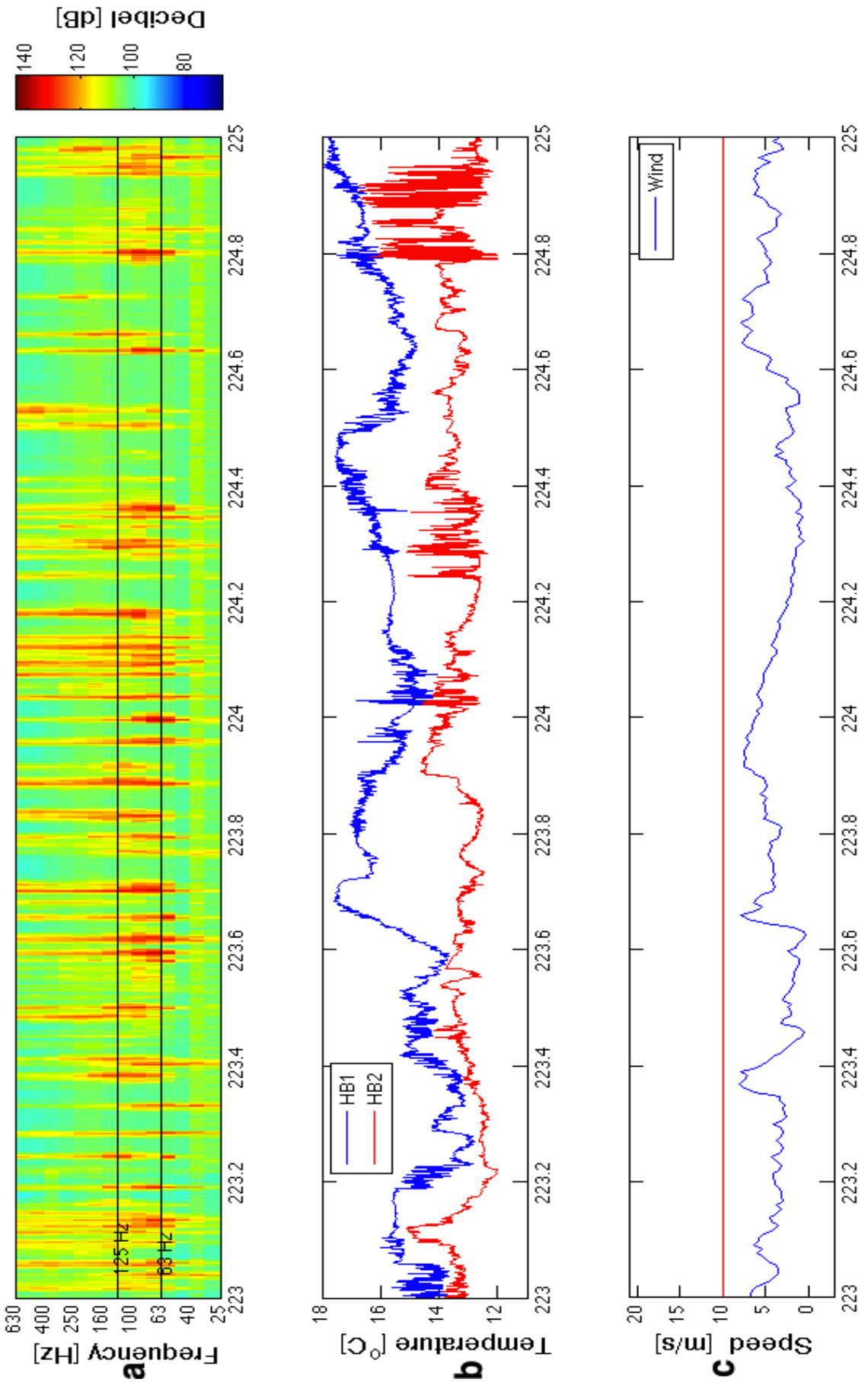

Figure 53: Observations from Julian day 223-225: (a) Sound station N2, (b) Temperature from Hatter Barn, (c) wind observations from Gniben.

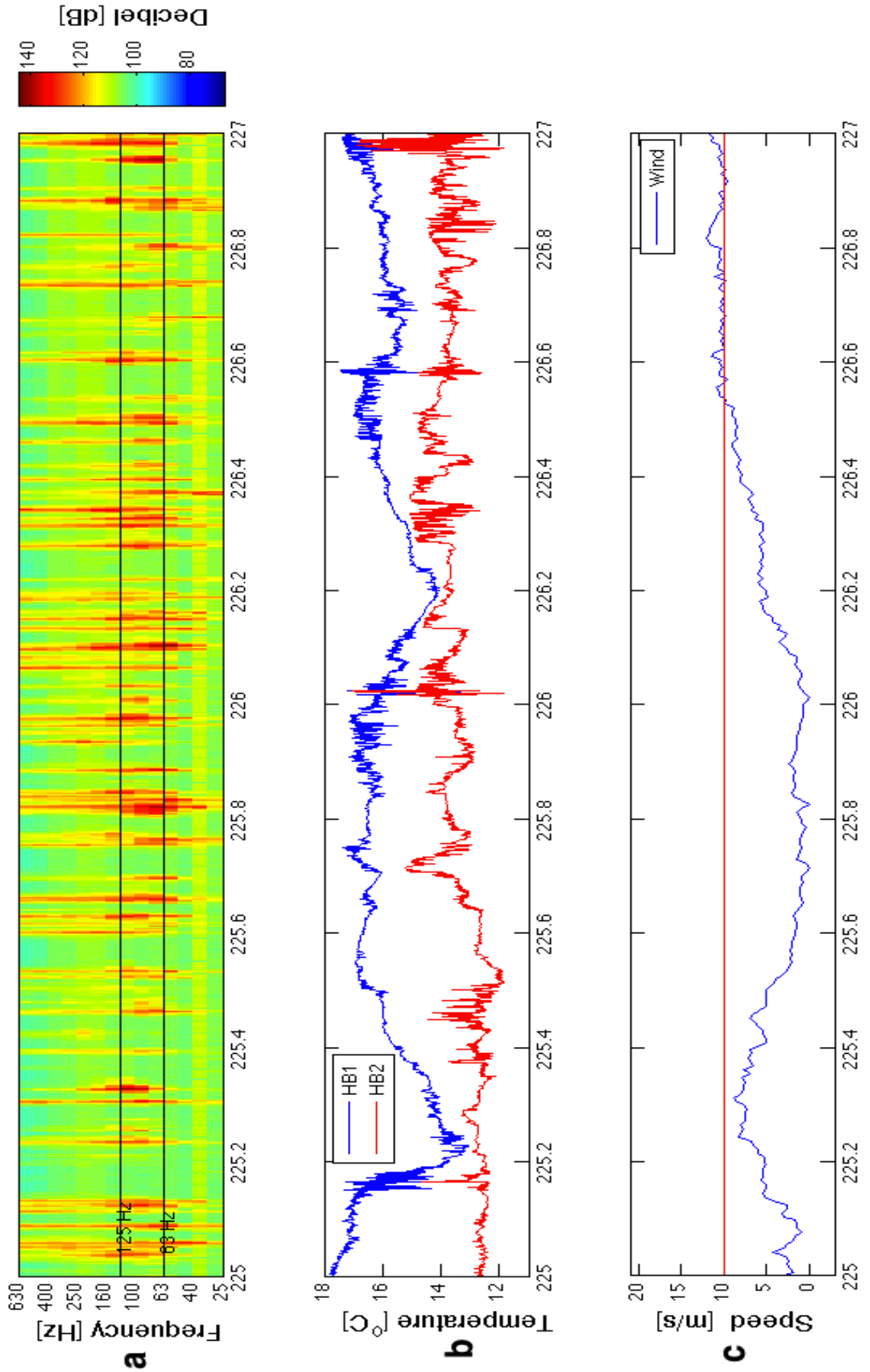

Figure 54: Observations from Julian day 225-227: (a) Sound station N2, (b) Temperature from Hatter Barn, (c) wind observations from Gniben.

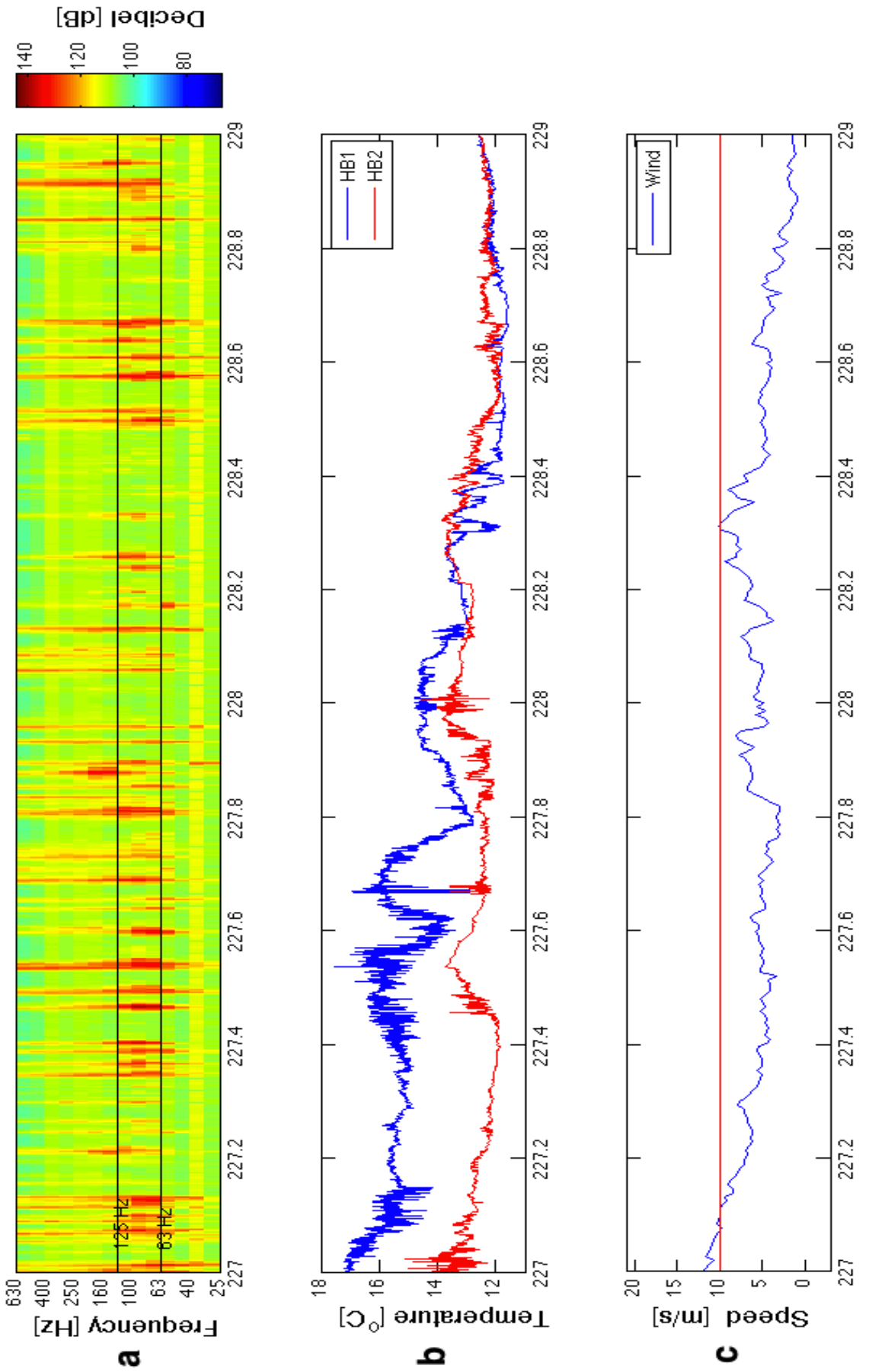

Figure 55: Observations from Julian day 227-229: (a) Sound station N2, (b) Temperature from Hatter Barn, (c) wind observations from Gniben.

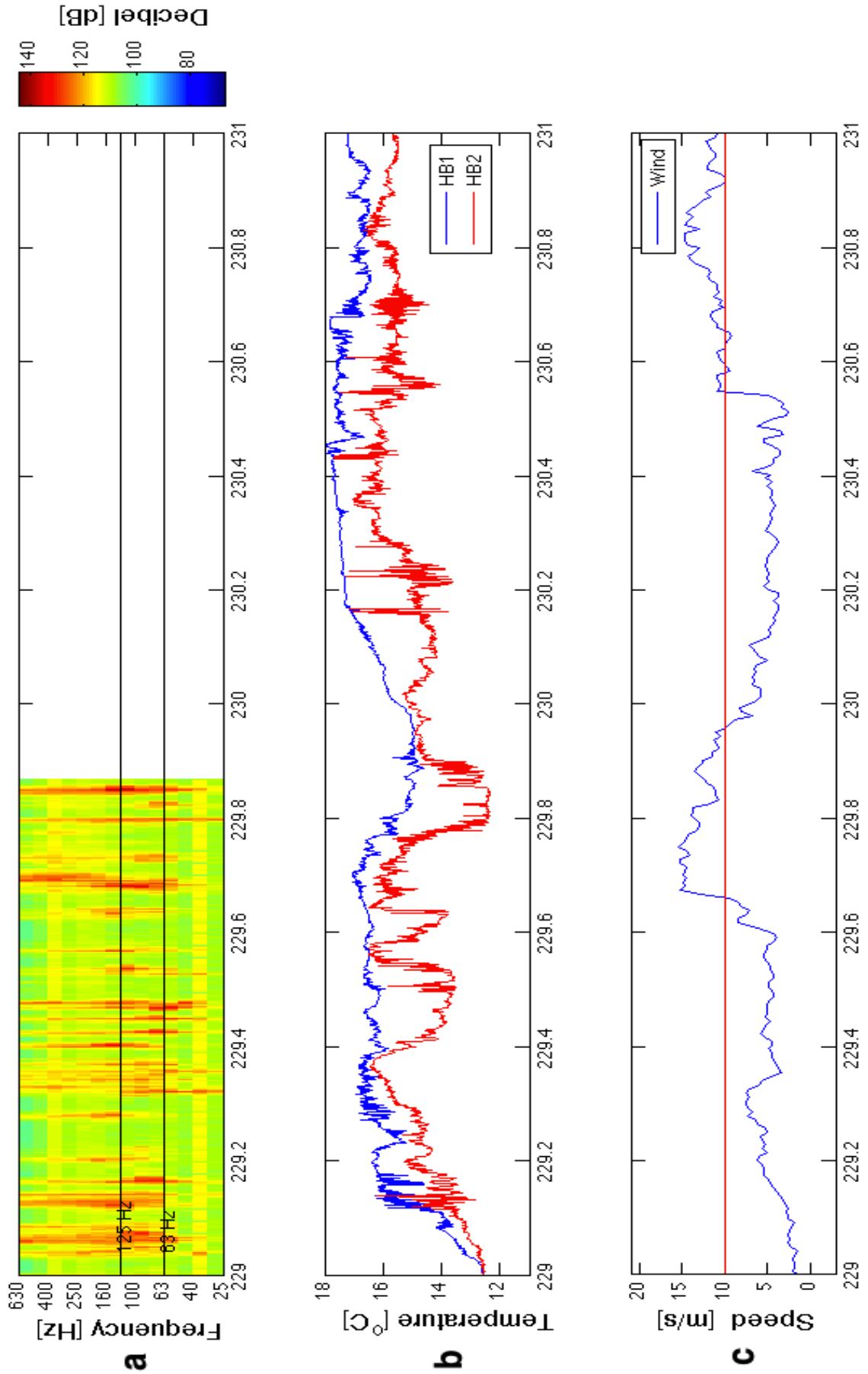

Figure 56: Observations from Julian day 229-231: (a) Sound station N2, (b) Temperature from Hatter Barn, (c) wind observations from Gniben.